คุณลักษณะของตัวเร่งปฏิกิริยาที่มีแพลทินัมเป็นพื้นฐานบนไทเทเนียมไดออกไซด์ที่เตรียมโดยวิธีเฟลมสเปรย์ไพโรไลซิสในปฏิกิริยาไฮโดรจิเนชันของ3-ไนโตรสไตรีน

นางสาวสุกัญญา พิศดวงดาว

วิทยานิพนธ์นี้เป็นส่วนหนึ่งของการศึกษาตามหลักสูตรปริญญาวิศวกรรมศาสตรดุษฎีบัณฑิต
สาขาวิชาวิศวกรรมเคมี ภาควิชาวิศวกรรมเคมี
คณะวิศวกรรมศาสตร์ จุฬาลงกรณ์มหาวิทยาลัย
ปีการศึกษา 2557

CHARACTERISTICS OF TiO_2 SUPPORTED PT-BASED CATALYSTS PREPARED BY FLAME SPRAY PYROLYSIS IN HYDROGENATION OF 3-NITROSTYRENE

Miss Sukanya Pisduangdaw

A Dissertation Submitted in Partial Fulfillment of the Requirements
for the Degree of Doctor of Engineering Program in Chemical Engineering
Department of Chemical Engineering
Faculty of Engineering
Chulalongkorn University
Academic Year 2014

Thesis Title	CHARACTERISTICS OF TiO_2 SUPPORTED PT-BASED CATALYSTS PREPARED BY FLAME SPRAY PYROLYSIS IN HYDROGENATION OF 3-NITROSTYRENE
By	Miss Sukanya Pisduangdaw
Field of Study	Chemical Engineering
Thesis Advisor	Associate Professor Joongjai Panpranot, Ph.D.

Accepted by the Faculty of Engineering, Chulalongkorn University in Partial Fulfillment of the Requirements for the Doctoral Degree

.....Dean of the Faculty of Engineering

(Professor BUNDHIT EUA-ARPORN)

THESIS COMMITTEE

.....Chairman

(Associate Professor Tawatchai Charinpanitkul, D.Eng.)

.....Thesis Advisor

(Associate Professor Joongjai Panpranot, Ph.D.)

.....Examiner

(Akawat Sirisuk, Ph.D.)

.....Examiner

(Chutimon Satirapipathkul, Ph.D.)

.....External Examiner

(Kajornsak Faungnawakij, D.Eng.)

CONTENTS

Page

Page

Page

Page

List of Tables

List of Figures

CHAPTER I

INTRODUCTION

Functionalized anilines are industrially important intermediates for pharmaceuticals, polymers, herbicides, and other substances in fine chemicals [1-3]. The selective reduction of a nitro group when other reducible groups are present in the same molecule is very challenging. In earlier studies, the selective hydrogenation of nitro compounds into amines in the presence of olefinic groups was based on cobalt and ruthenium sulfide catalysts [4], but the yields are low, and sulfur containing by-products are also formed that strongly limit the usefulness of these catalysts. Other catalytic systems including iron complexes [5] and doped Raney nickel [6] had practical drawbacks regarding the difficulty for reuse. Noble metal catalysts can activate both of nitro groups as well as carbonyl and double bonds, leading to unselective reduction [1, 7].

The most common method to increase aniline selectivity has been to modify the metal adsorption characteristics by means of surface modifiers. Blaser et al.[4] and Siegrist et al. [8] had shown that Pt/C modified by H_3PO_2 or other low valent phosphorous additives, together with soluble vanadium compounds could be highly selective in non-polar solvents. However, Pt-Pb/$CaCO_3$ catalysts, in the presence of $FeCl_2$ and tetramethylammonium chloride in solution, were shown to be adequate for polar solvents [4, 8]. Although these catalytic systems are effective, catalyst

preparation often remains critical, and the amount of the modifying agent must be precisely controlled. Recently, Makosch et al. [3] reported that 100% selectivity to 4-aminostyrene at high conversion was achieved over organic thiol modified Pt/TiO_2 catalysts in the liquid-phase selective hydrogenation of 4-nitrostyrene. Nevertheless, alternative heterogeneous catalysts for the chemoselective reduction of nitro groups that do not require soluble metal salts are more desirable and still state of the art research.

Fujita et al. [2] used pressurized CO_2 as the reaction medium and found that higher selectivity to VA was obtained than in its absence at any conversion level. The effect of dense phase CO_2 was ascribed to retardation on the hydrogenation of vinylanilene (VA) to ethylaniline (EA). Competitive adsorption of nitro and vinyl groups was suggested to determine the product selectivity. Furthermore, in a recent study by Beier et al. [7] , the presence of ionic liquid (IL), the support acidity/basicity, and the type of supports (carbon nanotube) were found to greatly influence the catalytic behavior of Pt nanoparticles in the selectivity hydrogenation of 3-nitrosyrene (NS). The presence of the IL was mandatory to achieve high selectivities for 3-aminostyrene.

From the literature, supported Pt catalyst is an interesting choice for the chemoselective nitrostyrene hydrogenation with the possibility for a large scale production because the build-up of hydroxylamine in reactor is minimized, making

the process much safer. However, Pt-based catalysts exhibited no preference in the selectivity for any of nitrostyrene hydrogenation products, hence surface modifications are required. TiO_2 is an interesting support for hydrogenation reactions because it exhibits the strong metal-support interaction (SMSI) effect under high temperature reduction. It has been reported that Pt/TiO_2 catalysts showed an improved selectivity in the hydrogenation of 3-nitrostyrene with increasing reduction temperature from 200 to 450°C due to the decoration Pt surface by the reducible TiO_x but their catalytic activity decreased [2]. The challenge is to increase the catalyst activity while preserving its high chemoselectivity of Pt/TiO_2 catalysts.

Moreover, there are many researchers studied about influence of second metals on catalytic performance for hydrogenation reactions such as Co-Pt [9], [10], [11] and [12], Fe-Pt [13], Ru-Pt [14] and [15], and Sn-Pt [16]. The addition of second metal influenced on both of electronic and geometric properties of the catalysts [16] and [13]. For examples, N. Mahata (2008) studied Pt-Fe and Pt-Zn catalyst in hydrogenation of cinnamaldehyde at 75°C and 16 bar of H_2. The addition of Fe and Zn enhanced the cinnamyl alcohol selectivity which was probable related to create electrophilic sites for the carbonyl group adsorption [13]. Among many additives, cerium is one of the most interesting promoters for Pt based catalysts in hydrogenation reaction due to the effect on electronic and geometric properties [17] and [18]. Ceria have been studied as catalysts, supports and promoters. So far, the

influence of promoting Pt with cerium in cinnamaldehyde hydrogenation has never been reported. However, there is a study on influence of Ce on ruthenium based catalysts used in gas phase crotonaldehyde hydrogenation. It is shown that the presence of new surface sites on the promoter activated the C=O bond of the aldehyde and favored its hydrogenation [19]. The presence of CeO_2 over Pt supported on CeO_2–ZrO_2 for hydrogenation of cinnaladehyde can increase the electronic density at Pt toward higher catalytic activity and the cinnamyl alcohol selectivity. The introduction of Ce on Pt-Sn/Al_2O_3 in propane dehydrogenation exhibited an increasing of active sites after loading with Ce and a modification of the structural and electronic properties over the Pt–Sn/Al_2O_3 catalysts [17]. In this work, TiO_2 supported nanocrystalline Pt-Co and Pt-Ce catalyst were tested in the nitrostyrene hydrogenation.

Cobalt is an interesting promoter for Pt-based catalysts in hydrogenation reactions because it can exhibit both electronic and geometric effects [11, 18]. The presence of Co over Pt-based catalysts led to improvement of catalytic performance compared to the Pt monometallic catalysts [9, 10, 20, 21]. Borgna et al. [11] prepared PtCo bimetallic catalysts supported on SiO_2 by spin-coating technique and tested in the hydrogenation of crotonaldehyde. The selectivity of crotylalcohol improved because of the electron transfer from Co to Pt metallic surface. To the best of our

knowledge, the influence of Co-promoted flame-made Pt supported catalysts in the hydrogenation of nitrostyrene has never been reported.

Flame spray pyrolysis (FSP) method is very flexible method to produce various nanoparticles with properties not easy accessible with another method and allow the use of a wide range of precursor, solvents, and process conditions [17, 22-28]. Flame-made nanomaterials find application in many catalytic reactions such as oxidation, photocatalytic degradation [29] lean-NO_x storage-reduction [30], hydrogenation [27, 28], and dehydrogenation [17, 22]. Interestingly, superior catalytic performances have been reported for the flame-made catalysts compared to those prepared by conventional impregnation method; for examples, Pt/Al_2O_3 in the dehydrogenation of propane [22], and Pd/TiO_2 in the liquid-phase selective hydrogenation of enantionselective hydrogenation [27]. The structural differences of the flame-made and conventionally prepared catalysts have often been explained as the reasons for the differences in their catalytic behavior.

In this work, Pt/TiO_2 catalysts were synthesized by using FSP method and employed in the chemoselective hydrogenation of 3-nitrostyrene. The effects of preparation methods (FSP and impregnation), reduction temperature, and second metal (Co and Ce) on the physiochemical and catalytic properties were investigated by means of several characterization techniques such as N_2 physisorption, X-ray diffraction (XRD), CO pulse chemisorption, H_2-temperature programmed reduction

(H_2-TPR), infrared spectroscopy of adsorbed CO (CO-IR), and transmission electron spectroscopy (TEM).

1.1 Objectives of the Research

The objective of this research is to investigate the characteristics and catalytic properties of Pt/TiO_2, $Pt\text{-}Co/TiO_2$ and $Pt\text{-}Ce/TiO_2$ catalysts prepared by flame spray pyrolysis in 3-nitrostyrene hydrogenation in terms of 3-nitrostyrene conversion and selectivity to vinylaniline.

1.2 Scopes of the Research

- Preparation of Pt/TiO_2 catalysts by flame spray pyrolysis and co-impregnation and evaluation of the catalytic performance of the flame- and impregnation-made catalysts after reduction at various temperatures (200-700 $^{\circ}C$) in the hydrogenation of 3-nitrostyrene in a batch reactor at constant temperature and pressure 50$^{\circ}C$ and 40 bar in hydrogen.

- Preparation of Pt/TiO_2 by impregnation method on a FSP-made TiO_2 and a sol-gel. Evaluation of the catalytic performances of the impregnation-made catalyst

- Preparation of nanocrystalline Pt-Co on TiO_2 catalysts by flame spray pyrolysis method with Pt content 0.5 wt% and Co loading 0-0.5 wt% and evaluation of the catalytic performance of the flame-made $Pt\text{-}Co/TiO_2$ catalysts with in hydrogenation of 3-nitrostyrene in batch reactor at constant temperature and pressure 50$^{\circ}C$ and 40 bar in hydrogen.

- Preparation of Pt-Ce on TiO_2 by flame spray pyrolysis with Pt content 0.5 wt% and Ce loadings 0-1.5 wt% and evaluation of the catalytic performance of the flame-made Pt-Co/TiO_2 catalysts with in hydrogenation of 3-nitrostyrene in batch reactor at constant temperature and pressure 50^{o}C and 40 bar in hydrogen.

-Characterization of the prepared catalysts by various methods including X-ray diffraction, CO pulse chemisorption, N_2 physisorption, H_2-temperature programmed reduction (H_2-TPR), infrared spectroscopy of adsorbed CO (CO-IR), and transmission electron spectroscopy (TEM).

CHAPTER II

Background

2.1 Heterogeneous catalyst

Heterogeneous catalysts are a fundamental importance for the worldwide production such as chemicals, both bulk and fine chemicals. It has been became interestingly importance due to the world population is growing and then the worldwide demand of energy and feedstock are increasing. Most all chemicals are produced with catalysts. Catalysis has been favorably operated in the chemical industry for more than 100 years. Catalytic process drives petrochemistry. There are many organic intermediates using in the manufacture of pharmaceuticals, dyes, plastics, fibers, pigments and crop protecting agent that can be produced by catalytic process. The term catalysis has already been introduced by Berzelious in 1836 and its definition is a catalyst accelerates a chemical reaction without affecting the position of the equilibrium by Ostwald in 1895. Moreover, catalysts are importance in controlling environmental pollution, which reduces emission from car engines. Normally, catalysts have two major groups as homogeneous and heterogeneous (solid- state) catalyst. For homogeneous catalysis, the reactant and catalyst are same phase. Homogeneous catalysts are usually coordination complex. For heterogeneous

catalysis, reactant and catalyst are different phase. Generally, the reactants are gas and/or liquid, and the catalysts are solid.

The advantage of heterogeneous catalysts are easy separation from the product, facilitate recyclability and high stability compare to homogeneous catalysts. The simple separation can be completed by filtration or directly such as the gas phase in fixed bed reactors. The separation of homogeneous catalysts is normally complicated process such as ion-exchange, distillation, and liquid-liquid extraction. For examples of heterogeneous catalyst are metals, oxides, zeolites, the active metal is finely dispersed on a support (silica, alumina and carbon). Heterogeneous catalysts are mostly used in industry. Commonly, a heterogeneous catalytic has three steps. At the beginning, reactants adsorb on the surface of catalyst, the adsorbed species react on the surface of catalyst and finally, the product desorb from the surface of catalyst. An energetically favorable reaction pathway is provided by catalyst and the activation energy of all intermediate steps is lower than the activation energy of the uncatalyzed reaction. Catalyst also influence on activity and selectivity of chemical reactions. The various products are obtained by modifying catalyst as same starting reactants. The determination of catalysis performance is activity, selectivity and stability. At present, raw material and energy are efficiently utilized and high selective catalysts for producing the desired products become interestingly important.

2.2 Properties of platinum

Platinum is a chemical and an atomic number as 78. The chemical symbol of platinum is Pt. It is named from Spanish term platina and a solid, malleable, ductile, precious, high unreactive and gray-white transition metal. Platinum is one of group 10 of the periodic table of elements and also one of the platinum group metals. There are six isotopes of Pt in natural. Platinum is the least reactive metal and can resist to corrosion at high temperatures so it is considered to be a noble metal. Use of platinum is widely in several applications such as catalytic converters, electrical contract, electrodes platinum resistance thermometers and jewelry.

Platinum has been used as hydrogenation catalyst. Platinum is the first transition metal using as catalytic hydrogenation. Methylamine production by mixing with hydrogen over black platinum was found by Debus [31]. Since the beginning of history of catalytic hydrogenation, platinum has been widely used catalysts. Platinum catalyst has a good characteristic feature that it has been favorably used in liquid-phase hydrogenation due to it is active under mild condition. Platinum catalyst has been operated on unsupported fine metal particle and supported on porous or nonporous material. Unsupported Pt catalyst is used in small-scale laboratory hydrogenation. However, the advantage of supported Pt catalysts is more than unsupported Pt catalyst because the expensive metals are efficiently used by obtaining a larger active surface area and supported Pt catalysts have more stable

and a better resistance to poisoning. The performance of the supported Pt relies on their physical and chemical properties.

2.3 Hydrogenation of nitro group over platinum metal group

Platinum or palladium catalysts are mostly utilized in these reactions. Use of rhodium and ruthenium catalysts has found in only special. The reactions are operated under mild condition. However, the aliphatic nitro group is difficult to hydrogenate and the reduction rate is lower than the aromatic nitro group. Hydrogenation of both aliphatic and aromatic nitro compounds on platinum, palladium and rhodium catalyst has exhibited excellent results. The catalytic design for any particular nitro compounds hydrogenation relies on the product required. Taya et al studied the hydrogenation of various aromatic nitro groups over ruthenium dioxide. The hydrogenation of rate in aqueous dioxane increased with increasing the water content of the solvent. A study of platinum oxide exhibited that it cannot hydrogenate nitro groups but they are hydrogenated by only over the reduced metal surface. Hydrogenation of p-substituted nitrobenzene to amine was tested over colloidal rhodium and palladium catalysts. Surprisingly, the rate of reaction was influenced by the electron-shifting properties of the substituent and acid or base over rhodium catalyst while there was no any effect over palladium catalyst. These results were carefully reexamined and it was concluded that palladium or rhodium

catalysts can impact on the substituent of nitrobenzene reaction rate with only reaction as first-order at respect to the nitro groups.

2.4 Hydrogenation of nitrostyrene over heterogeneous catalyst

The selective hydrogenation of nitrostyrene (NS) to vinylaniline (VA) has been applied in many industries as important chemical transformation to gain functionalized anilines for pharmaceutical, polyurethanes, dyes and explosive. 3-nitrostyrene compound consists of two reducible groups as a nitro group and C=C double bond. Reaction pathway in hydrogenation of 3-nitrostyrene are shown in Figure 1. Nitrostyrene (NS) can be hydrogenated to be vinylaniline (VA) and ethylnitrobenzene (ENB) and then both of compounds are hydrogenated to be ethyaniline (EA). It is a difficult task to achieve high selectivity for either compound with high conversion. There are many attempts to solve this problem with using different metals, supports and solvents.

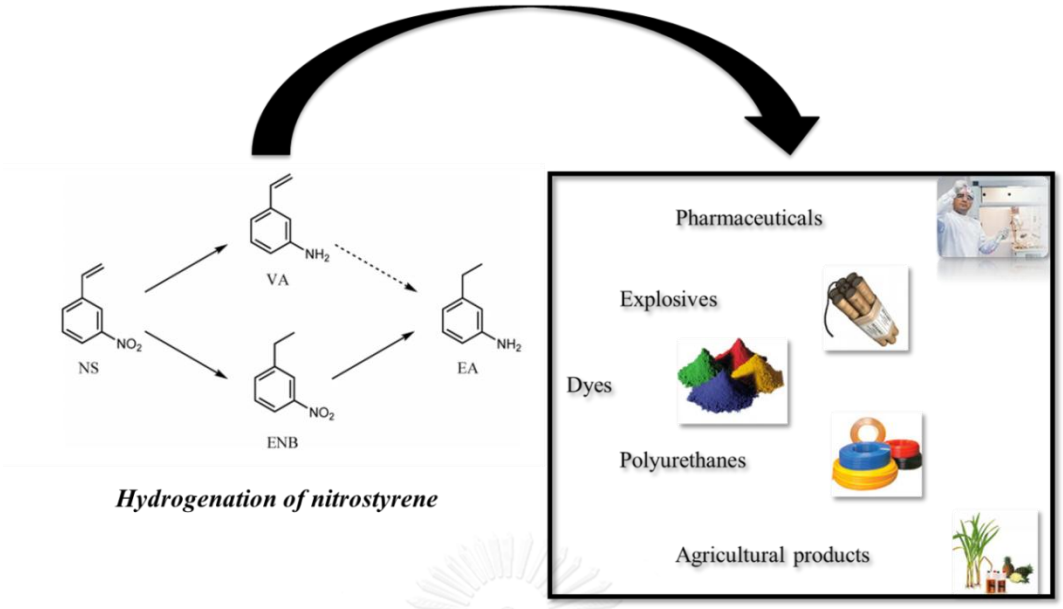

Figure 1 Schematic of nitrostyrene hydrogenation.

The metal catalysts are used in hydrogenation of nitrostyrene such as Pt, Pd, Ni, Ru, Ag and Au. These metals were supported on various materials such as CNT, Fe_2O_3, SiO_2, Al_2O_3 and TiO_2. Corma et al [1] reported that gold supported on TiO_2 and Fe_2O_3 exhibited a very high selectivity toward the nitro compound hydrogenation in nitrostyrene hydrogenation because of highly strong interaction between metal and support. The catalytic activity relied on the gold particle size and support oxides. The highest intrinsic activity in nitrostyrene hydrogenation could be achieved on small Au particle at 2.5 nm on Al_2O_3 [32]. However, the hydrogenation activity of gold catalyst was much lower than platinum catalyst and required more forcing reaction condition. The low activity of gold catalyst can be attributed to an intrinsic nobleness of gold for activation of H_2. Generally, Pt catalyst is not commercially used in

substituted nitrostyrene hydrogenation with H_2 [1]. The high catalytic activity can be obtained on Pt/TiO_2 catalyst but it is no prefer selectivity of possible any products from hydrogenation of nitrostyrene. There are many attempts to undertake this problem by studying Pt loading, reduction temperature, support and solvent. It has been suggested that the effect of Pt content on catalyst performance over Pt/TiO_2 and Pt/Al_2O_3 catalysts [1, 2]. Fujita et al. [2] studied varying Pt content from 0.5 to 2.0%wt in hydrogenation of 3-nitrostyrene hydrogenation and found that Pt crystallite size and catalytic activity increased with increasing Pt loading. At the high Pt loading, the Pt/TiO_2 catalyst exhibited low vinylaniline selectivity. This result can be concluded that the decreasing of Pt atoms on edge and corner sites over Pt/TiO_2 catalyst result from the increasing of Pt content. This obtained result is in agreement with Corma 's work who studied the effect of Pt loading on Al_2O_3 catalyst for selective hydrogenation of nitrostyrene to vinylaniline. A series of Pt/Al_2O_3 catalyst with various Pt loading was prepared and characterized by FTIR measurement to determine Pt spicy sites. Reaction test results indicated that the selectivity of vinylaniline over Pt catalyst increased with decreasing the metal crystalline size by preparing a catalyst at low Pt loading. From FTIR results, it is probably due to the nitro compound preferentially proceed on low-coordination Pt surface sites such as edge, corner and kink while the vinyl group would occur on the terrace sites. Corma et al [1] reported that decoration of Pt catalyst by increasing reduction temperature can enhance the selectivity of vinylaniline. $0.2\%Pt/TiO_2$ was prepared by

impregnation method and was reduced with various reduction temperatures from 473 to 723K. The results showed the improvement of vinylaniline selectivity and the Pt/TiO_2 catalyst should be reduced at 723 K instead of 473 K in order to increase Pt-TiO_x interface sites. These obtained information is in agreement with Fujita et al [2] 's study. They also found that 0.5%Pt/TiO_2 catalyst prepared by impregnation method exhibited higher vinylaniline selectivity at high reduction temperature. Due to the decoration of TiO_2 preferentially occurs over Pt crystalline terrace sites toward the high fraction of low- and high- coordination Pt sites. The enhancement of the selectivity in nitrostyrene hydrogenation on NPs with different (Al_2O_3, SiO_2, TiO_2 and CNT) support was studied. The highest selectivity of ENB was reported on SiO_2 support which might be due to the stabilizing effect of SiO_2 support. The other supports gave lower ENB selectivity that SiO_2 support because they are generally expected to interact stronger with metal. TiO_2 support shows highest selectivity to VA compared to the other supports. Table 2.2 shows the performance of various metals catalysts and condition reactions in hydrogenation of nitrostyrene. Hydrogenation of nitrostyrene was operated in batch reactor with various temperatures from 40 to 120°C and pressure from 3-40 bars.

Table 1Catalytic performance of nitrostyrene hydrogenation on various catalysts.

Researchers	**Catalyst**	**Reactant**	**Condition Rx.**	**Results**
Boronat et al. [33]	Au/TiO_2	3-NS[a]→VA[b]	RT=200 °C T = 120 °C P = 9 bar	Conv.=98.5% Selec.=96%
Fujita et al. [2]	Pt/TiO_2	3-NS[a]→VA[b]	RT=200 T = 50°C P = 40 bar H_2 under $scCO_2$	Conv.=64% Selec.=75%
Corma et al. [34]	1.Au/TiO_2 2.Au/Fe_2O_3 3.Pd/C 4.Pt/C	3-NS[a]→VA[b]	RT=450 °C T = 120°C P = 9 bar	Conv.=98.5% (1) Selec.=95.9% (1)
Makosch et al. [3]	Pt/TiO_2	4-NS[a]→VA[b]	RT= n.d. T = 80°C P = 10 bar	A-lipoic acid Conv.=100% Selec.=100%
Yoshida et al. [35]	Pt/TiO_2	4-NS[a]→VA[b]	RT=200 T = 120°C P = 40 bar H_2 under $scCO_2$	Conv.=50% Selec.=85% At CO_2 10 bar
Corma et al. [1] 2008	1. Pt/TiO_2 2. Pt/C	3-NS[a]→VA[b]	RT=450 °C T = 40°C	Conv.=95.1% (1) Selec.=93.1%

	3. Ni/TiO_2 4. Ru/TiO_2 5. Au/TiO_2		P = 3 bar	
Shimizu et al. [32]	Ag/Al_2O_3	3-NS[a] → VA[b]	RT=300 °C T = 160 °C P = 30 bar	Conv.=100% Selec.=96%

a= Nitrostyrene, b= Vinylaniline

2.5 Effect of size and shape on catalytic performance in the hydrogenation reaction.

Normally, there are two reaction types which are sensitive structure and insensitive structure reactions. The structure-sensitive reaction is mainly found on isomerization and hydrocracking but hydrogenation and dehydrogenation are structure-insensitive. Figure 2 (terrace, kink, and corner) shows schematic of a metal surface including the terrace, step, kink as well as adatom. The Wulff 's theorem describe in term of the central distance proportionality and energy of surface that the metal form the face-centered cubic (fcc) and body-centered cubic (bcc), which are the optimal equilibrium shapes, in order to minimize the total surface energy. Face-centered cubic metal facet (111), (100) and (110) consist of 9-fold, 8-fold and 7-fold coordination, respectively. The free energy of surface increase from the (111) > (100) > (110) plane but the electronic density, which is determined by the surface

atoms density and metal work function, is opposite trend. The (111) metal plane is the highest stable surface compared to the other metal planes. The particle shape can be controlled by preparation method, pretreatment, and the interaction with support. The influence of size and shape on catalytic performance relies on metal and reaction types [36]. For examples, the catalytic activity on hydrogenolysis reaction over Ni/SiO_2 catalyst depends on the fraction of (111) and (100) planes on the surface of catalyst [37]. It was reported that the formation of hexagonal morphology of Ni metal on graphite can increase the catalytic selectivity in hydrogenation of 1,3 butadiene to 1-butene. The influence of metal particle structure on Pt based catalyst in hydrogenation of crotonaldehyde was conclude that the increasing of selectivity of unsaturated alcohol relied on Pt (111), Pt (100) and Pt (110) terraces[11]. The catalytic activity of nitrostyrene hydrogenation over Pt/Al_2O_3 catalyst increased with decreasing of Pt particle size and was highest at 0.2%wt Pt loading [1]. Additionally, the fraction of terrace to corner of Pt sites also affected on the catalytic selectivity over Pt based catalyst in hydrogenation of nitrostyrene [1, 2] which it preferred the low fraction of Pt terrace/corner site as determined by FTIR characterization. It has been suggested that the hydrogenation of cinnamaldehyde and crotonaldehyde to cinnamyl alcohol favor the large metal particle sizes [15, 16]. These results were explain that enhancement of selectivity of unsaturated alcohol was facilitated on large particles, which is low index face of fcc,

Pt (111) sites. C=O hydrogenation actives on Pt (111) sites while both of C=O and C=C hydrogenation active on low coordination Pt (steps, kinks) sites [1, 11, 16].

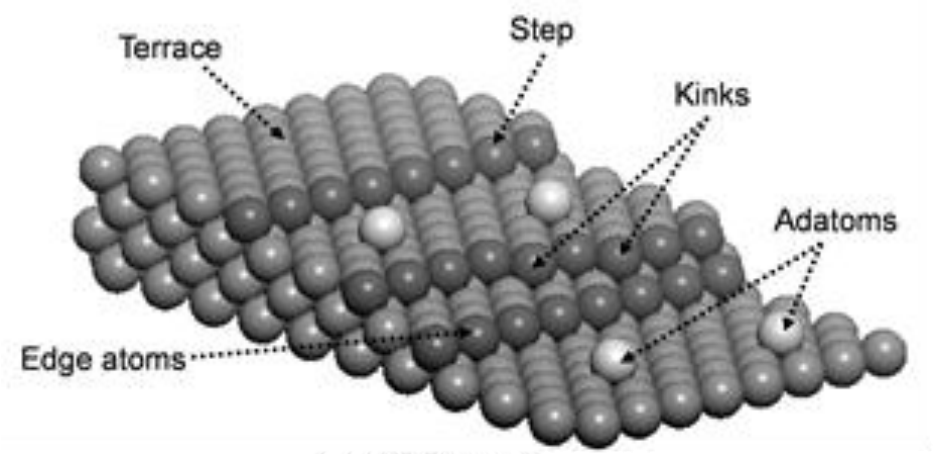

Figure 2 Schematic of a surface structure of a metal [38].

2.6 CO adsorption on Pt based catalyst

There are several researches on metal-support interaction during the past two decades [1, 2, 35, 39]. Reducible supported metal exhibit significant difference on catalytic performance of hydrogenation reactions with different reduction temperatures [1, 2]. These results were indicated the metal-support interaction in two parts. First, the influence of electronic density that transfers from the support to metal, which was noticed on the formation of Pt-Ti alloy. Therefore, the electronic density in platinum enhance toward a changing of catalytic selectivity in hydrogenation reactions [39]. Second, the influence of morphology of platinum was observed after reduced at high temperature. The crystalline lattice is expanded

because of partial reduction of TiO_2 to TiO_{2-x} species and that cause a support encapsulation on metal. It can explain on the reducing of metal adsorption on catalyst lead to variant catalytic performance. However, both effects of electronic and morphological are determined in many techniques such as FTIR, UV-vis, NMR, XPS, EXAFS-XANES in order to understand completely.

Fourier transform infrared (FTIR) spectroscopy of the CO adsorption is widely employed and a useful method for characterize the surface of catalyst. Carbon monoxide is an extremely proper probe molecular to characterize the nature (linear, bridge and multi-bond) of the adsorbed, which can explain the correlation of metal surface structure and catalytic performance. In a shot review, adsorption of CO on the metal is stronger than the metal oxide. Interaction of CO and the metal is reported as molecular adsorption and molecular dissociation of CO. The type of CO adsorption relies on the metal, metal structure surface and reaction condition. The investigation of the Co adsorption with various transition metals in gas-phase was studied. Figure 3 shows the adsorption of CO type with different transition metals. There are 14 transition metal were tested such as V, Y, Ta, W, Re, Fe, Ru, Co, Rh, Ni, Pd, Pt, Ag, and Au. The adsorption of CO as the molecular adsorption is show in the blue shade (V, Nb and Ta) and the molecular dissociation is shown in the brown shade (Re, Fe, Ru, Co, Rh, Ni, Pd, Pt, Ag, and Au). The interaction of Co with W metal exhibits both CO adsorption behaviors as adsorption and dissociation molecules.

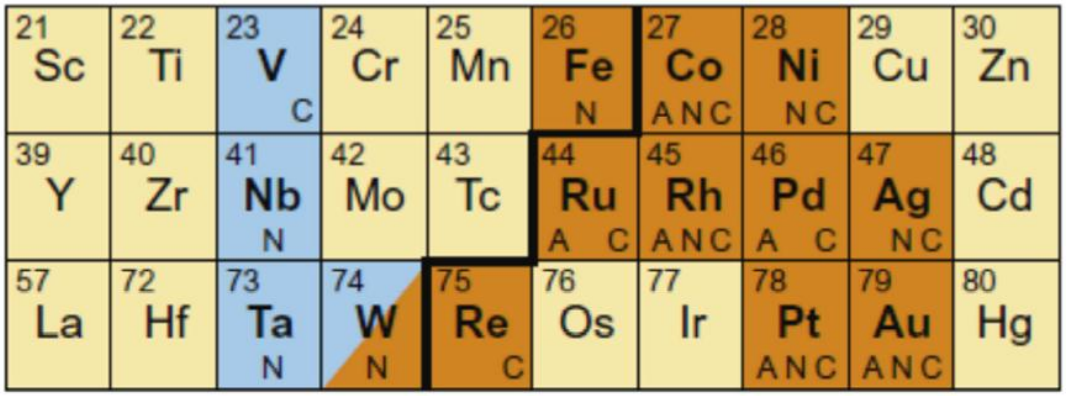

Figure 3 Interaction behavior of Co with various the transition metals.

Adsorption of CO on Pt catalysts is used for characterizing the Pt surface structure in various hydrogenation reactions [1, 2, 35, 40, 41]. The vibrational frequencies of C-O bond stretching depend on the different CO adsorption sites on Pt metal. Figure 4 shows CO adsorption behaviors on Pt clusters as linear CO adsorption, bridge CO adsorption and hollow CO adsorption (Multi-bonded CO adsorption). CO adsorbed on linear sites exhibits stretching frequencies approximately from 1900 to 2100 cm^{-1} and bridge sites exhibits stretching frequencies approximately from 1780-1985 cm^{-1}.

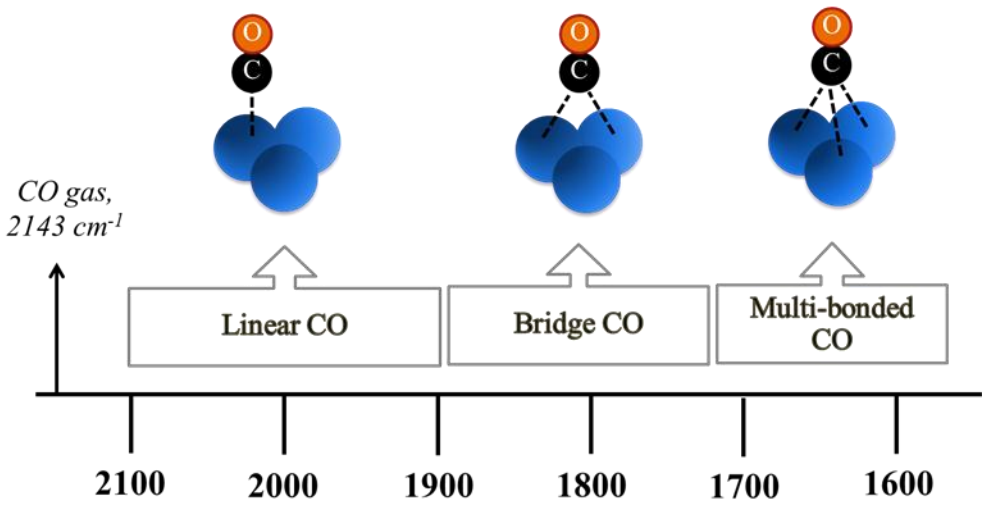

Figure 4 CO adsorption sites on Pt based catalyst [41]

Dulaurent et.at [41] studied the adsorption of Co on 2.9%Pt/Al_2O_3 catalyst prepared by impregnation method by using FTIR spectroscopy. They found that there were two major IR bands at 2073 and 1845 cm-1 which can attribute to linear CO specie and bridge CO specie, respectively, as show in Figure 5. It has reported that the bridge CO adsorption occurs on large Pt particles but linear CO adsorption occurs on small Pt particles. Corma et al. [1] studied Pt structure on 0.2%wtPt/Al_2O_3 catalyst by CO-IR and STEM characterizations. They suggested that there is a high adsorption band at 2056 cm-1 relating to CO linearly adsorbed and a low intensity of IR band at 1823 cm-1 attributing to CO bridged adsorbed. This obtained result can indicate that the Pt particle is very small and it was confirmed by STEM measurement around 2 nm.

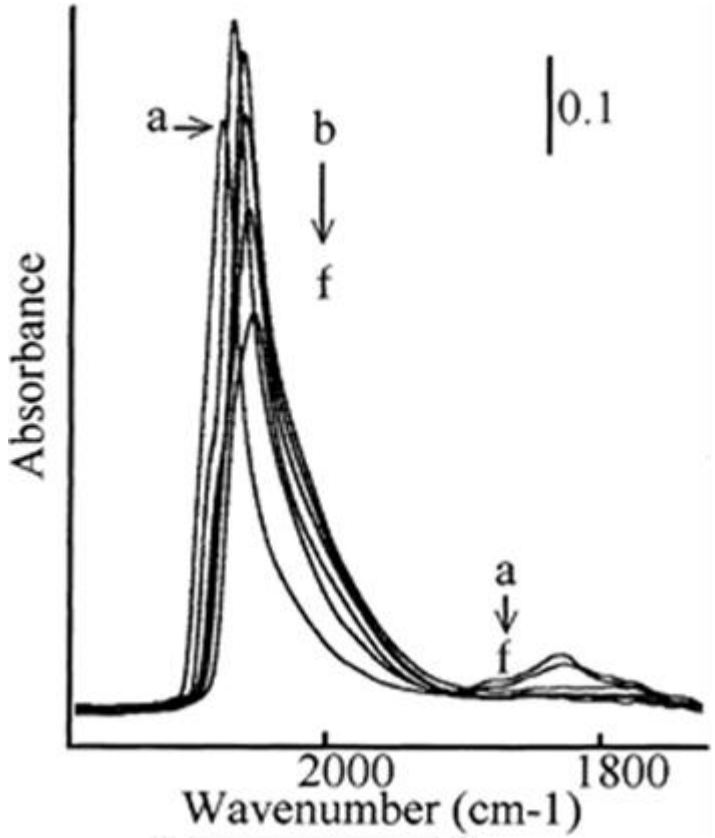

Figure 5 CO-FTIR spectra of 2.9%Pt/Al_2O_3 at different temperature [41]

2.7 Flame process

Nanotechnology has been a popular research in the decade. There are many researches of applying heterogeneous catalyst to develop in nanotechnology. Heterogeneous catalyst is defined on nano scale to control the nanostructure for achieving good catalytic performance. Nanoparticle can be controlled easily by single-step flame synthesis. Schematic of preparation of Pt/Al_2O_3 catalyst by wet impregnation and flame methods are shown in Figure 6. Flame synthesis is a new

single-step continuous production method for catalyst. Wet impregnation method exhibits many steps more than flame process, which consists of many post-treatment steps such as filtration, washing, drying and calcination [42, 43].

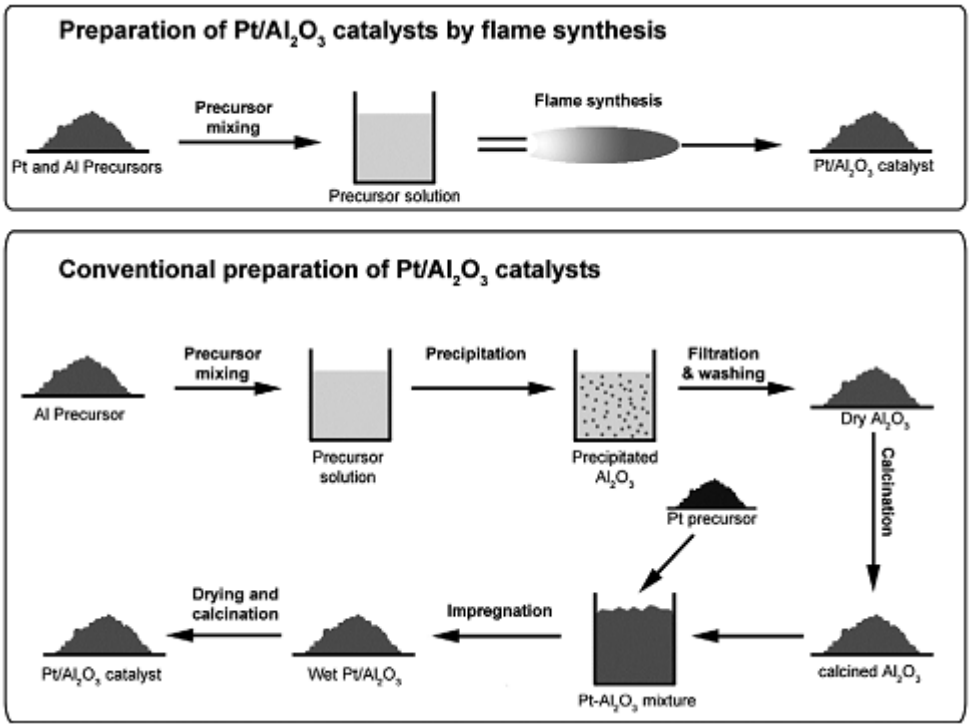

Figure 6 Comparison of conventional wet-phase and flame methods for the synthesis of Pt/Al_2O_3 catalyst [42].

There are three types of flame process classified by the precursor state feed. Additional, the cluster formation occurs during flame synthesis and then grows by coagulation and sintering in the hot flame environmental to nanoparticles. Three primary types of the flame process are illustrated in Figure 7.

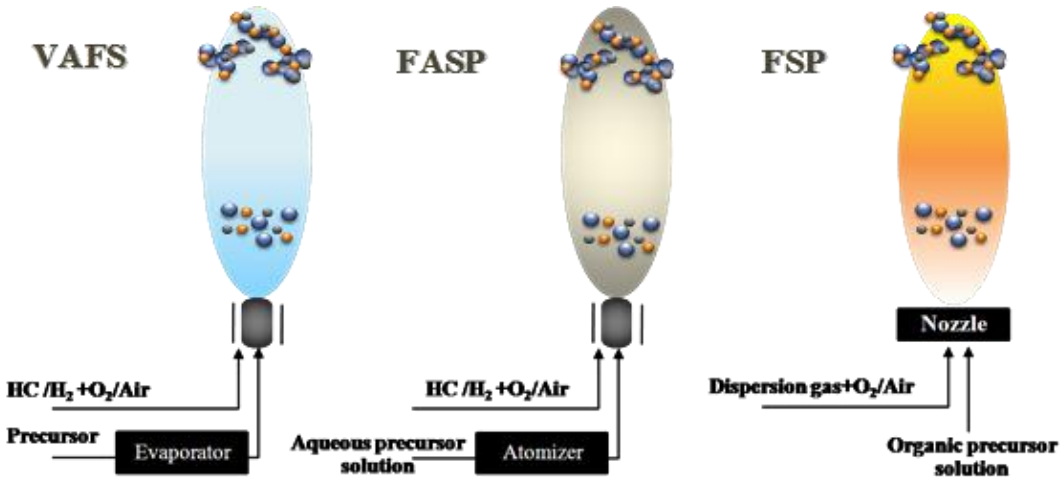

Figure 7 Schematic of flame reactors [44].

One is the most common industrial process to produce several ceramic commodities such as fumed silica, alumina and pigment titania [38, 44-49] that is called as flame aerosol vapor synthesis (VAFS). This process requires the use of volatile precursors to be evaporated and fed into a flame. The precursor is converted to be metal oxide and the particle formation occurs from the gas phase. However, in this process volatile precursor is highly requires for high product rate and the VAFS process allows the generation of ultrapure materials. Synthesis of high-purity volatile precursors is complicated and expensive that is a drawback of the process. There are many metals and heterogeneous catalyst produced by VAFS process such as SiO_2, TiO_2, V_2O_5, TiO_2/V_2O_5, Pt/TiO_2 and $Cu/ZnO/Al_2O_3$. The other flame process is a flame assisted liquid-to-particle conversion process which is called as flame assisted spray pyrolysis (FASP) and flame spray pyrolysis (FSP). In FASP process aqueous precursor is injected into atomizer and then is evaporated and

pyrolyzed on a flame. The energy source of this process is hydrogen or hydrocarbon. The metal precursor converts to product when the aqueous solution is sprayed and evaporated as show in Figure 8. Products of FASP process are mainly perovskite and spinel structure. FSP process is a process of dispersed organic solution to be fine droplet by gas convection though a nozzle that is ignited by supporting flame (Figure 7). The feature of FSP process is shot residence time and high maximum process temperature. The major advantage of FSP process is the formation of nanoparticles though controlling precursor solvent composition. FSP has been used for producing many metal and metal oxide catalysts such as Pt/Al_2O_3 [17, 22], Pd/TiO_2 [50, 51] , Pt/ZnO [52, 53]and various perovskites [24, 25, 54, 55].

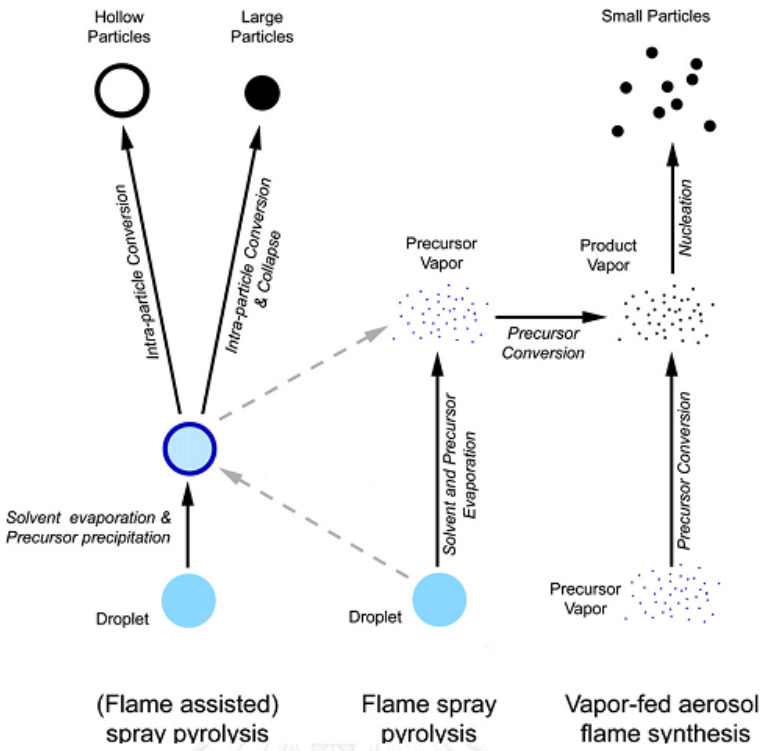

Figure 8 Schematic of particle formation occurs during spray pyrolysis [44].

2.8 Flame spray pyrolysis

Sokolowski et al [44] develop flame spray pyrolysis as early 1977 to synthesize Al_2O_3. A wide array of precursor can be used in FSP process compares to conventional of vapor-fed reactor. FSP process is very interesting and can produce particles with a broad range of size, phase compositions and morphologies. Flame-made material can be applied as heterogeneous catalyst in various reactions such as photocatalysis, dehydrogenation and hydrogenation due to accomplishable precision of product properties can be controlled during flame synthesis with flame condition.

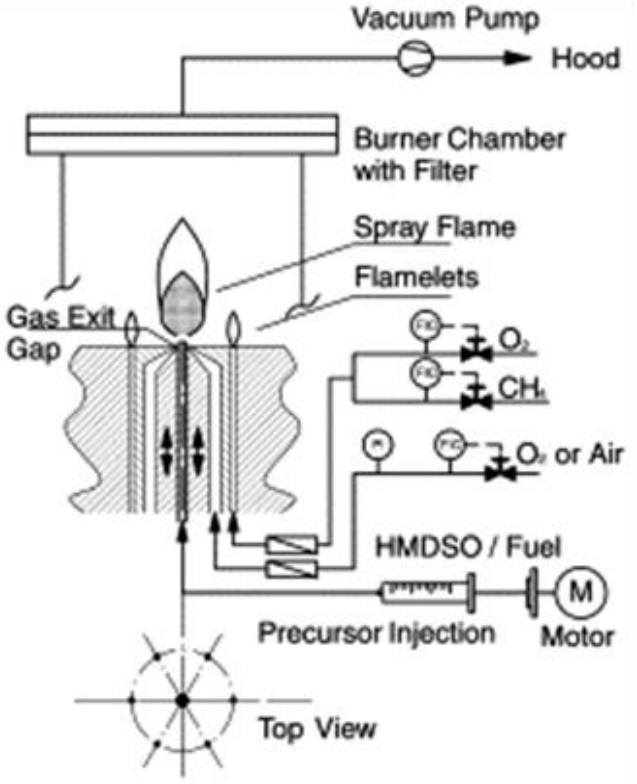

Figure 9 Schematic of Flame spray pyrolysis (FSP) [44]

A schematic of experimental set-up of FSP is shown in Figure 9. The apparatus consists of an external-mixing gas nozzle made from a tube of outer diameter 0.91 mm (inner diameter 0.6 mm). It is settled in an opening of 1.2 mm in diameter making an annular gab of 48 mm2 maximum area. Precursor and fuel flow through the tube while dispersion gas flow though the annular gab. The droplet size can be controlled by adjustment by dispersion gas or liquid flow rate. The products are corrected on a glass fiber filter and then the gas flow though the filter which is maintain by vacuum pump.

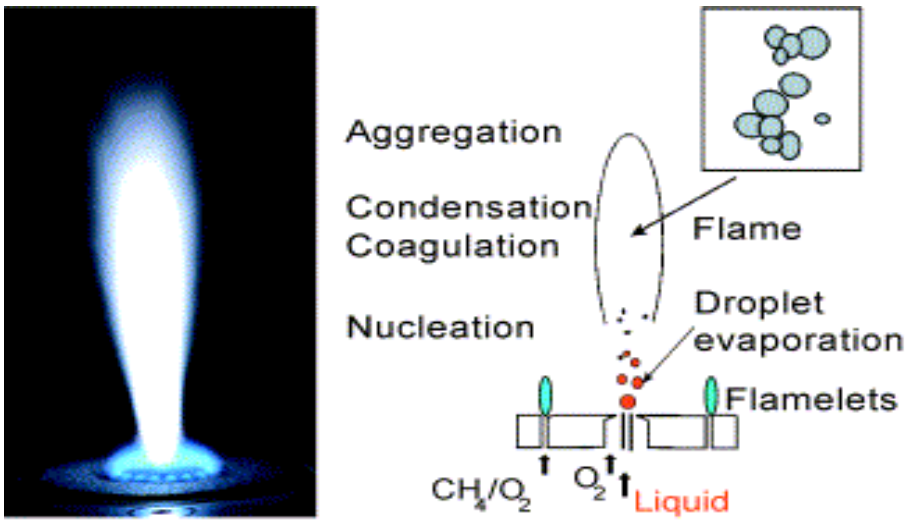

Figure 10 Particle formation during flame spray pyrolysis synthesis [56] .

Formation of particle during flame spray pyrolysis is shown in Figure 10. The mechanism of flame-made formation is explained as follow: A liquid precursor was injected in the flame though a two-phase nozzle and dispersed to be fine droplets by dispersion gas. Then the fine droplets were evaporated and combusted when the met the flame. Afterward subsequent, nucleation and growing particle by coagulation and condensation were occurred along the axial direction of the flame. The various properties of the FSP product have a large range and can be change by selecting precursor condensation, feed rate and dispersion gas flow rate.

One of significance flame condition for adjusting physical properties is the dispersion gas flow rate. Glassman et al [56] reported that the mixing and accelerates combustion is intensified by increasing of the dispersion gas flow rate and then the flame height decrease. As show in Figure 11, the spray flame height is as a function

of dispersion gas (air and O_2) at an SiO_2 production rate of 300 g/h with using 1.26 M HMDSO in Ethanol. It was found that the spray flame height decrease when the dispersion gases (air and O_2) increase. Moreover, Madier et al [56] suggested that the droplet concentration of spray flame decrease with increasing of the local fuel vapor function lead to shorter gaseous diffusion flames surrounding the droplets. Obviously, air spray flame is longer than oxygen spray flame because of faster combustion by pure O_2

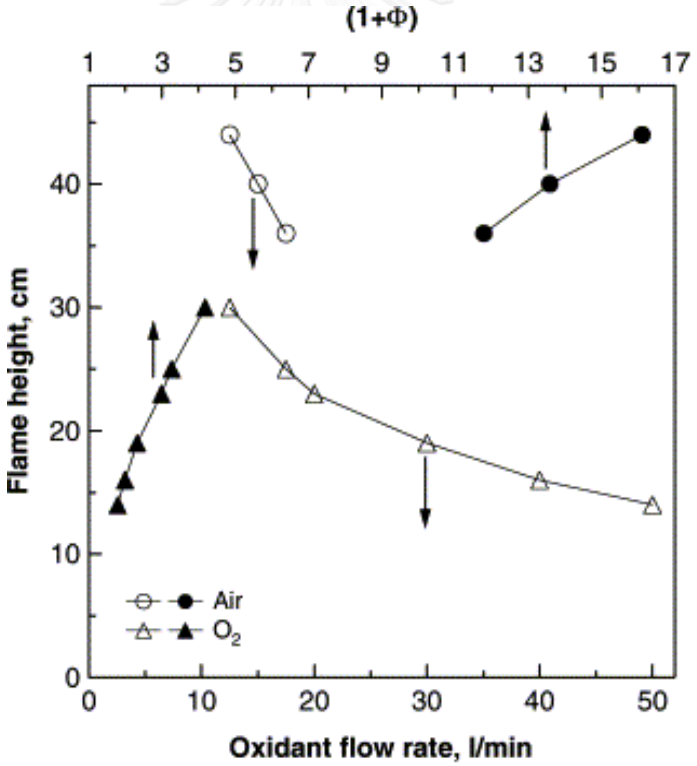

Figure 11 Spray flame height as a function of air (circles) and O_2 (triangles) flow rate (open symbols) or fuel equivalence ratio (1+Φ) (filled symbols) for a SiO_2 production rate of 300 g/h using 1.26 M HMDSO in EtOH [56].

Effect of dispersion gas flow rate on primary particle size at SiO_2 production rate of 300g/h is show in Figure 12. The increasing dispersion gas flow rate can decrease the particle size. This effect was described by Fourier transform infrared (FTIR) spectroscopy. Madler et al [56] studied the effect of electrical field on the flame-made TiO_2 and found that the maximum temperature of flame is lowered significantly when the dispersion gas flow rate increases. This result is in agreement at low production rates [57] but not at production rate of 9 g/h in the flame-made silica study. This observation is also in agreement with Kammler et al [58]'s research. It was reported that the average primary particle size is smaller from 25 to 17 nm with increasing of air flow rate from 68 to 154 l/min in vapor-fed flame aerosol reactor. The obtained primary particle size for both vapor-and liquid-fed flame reactors are similar. This exhibits that the adjustment of dispersion gas flow rate can control the primary particle size at a constant production rate. Increasing the oxidant flow rate increases the gas liquid mass ratio (GLMR) as indicated.

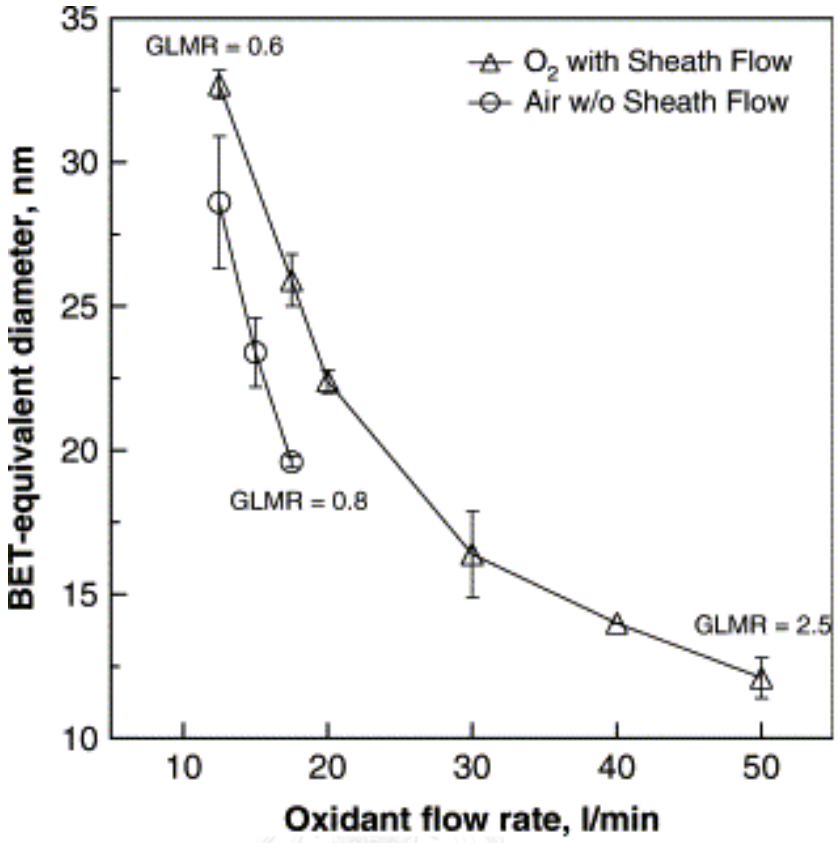

Figure 12 BET-equivalent diameter as a function of air (circles) or O_2 (triangles) dispersion gas flow rate at silica production rate of 300 g/h using 1.26 M HMDSO in ethanol [56].

It is known that the properties of the FSP product can be varied by precursor feed rate. Figure 13 exhibits spray flame of 1.26 M HMDSO in ethanol solutions with difference silica feed rate (a-c) at a constant dispersion gas feed rate. Air or O_2 are used as dispersion gas as 12.5 l/min without (d-f) and with (g-i) a constant sheath O_2. The spray flame is higher from 17 to 44 cm with increasing silica production feed rate from 100 to 300 g/h. The spray flame is larger because of the extension of time for fuel combustion.

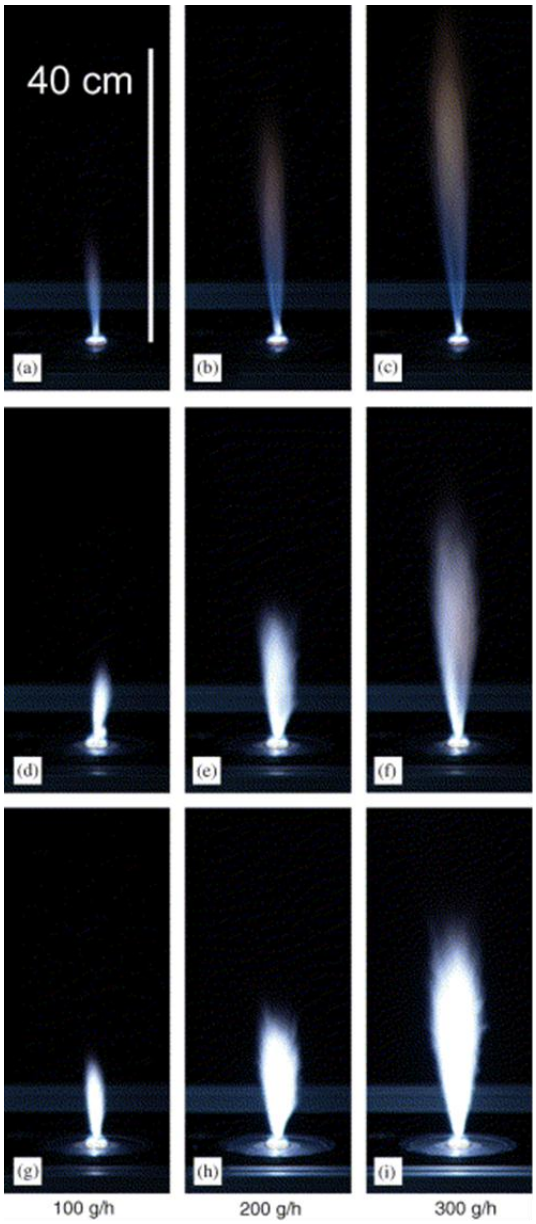

Figure 13 Spray flames (1.26 M HMDSO in ethanol) producing 100, 200 and 300 g/h of silica using 12.5 l/min air (a–c) or O_2 as dispersion gas without (d–f) and with (g–i) additional 25 l/min of O_2 sheath flow at 1 bar pressure drop across the nozzle tip [56].

Flame-made silica particle size is bigger or equal when using O_2 instead of air as dispersion gas. The particle size increases with increasing feed rate as show in Figure 14. The primary particle size is 18 nm by using air and is 18 or 19 nm by using O_2 as dispersion gas with or without sheath O_2, respectively. When the feed rate is up to 300 g/h, the particle size is 29 nm by using air and 33 or 41 nm by using O_2 as dispersion gas with or without sheath O_2, respectively. The using O_2 as dispersion gas accelerate fuel combustion toward higher flame temperature. Then, the obtained product particles are larger due to sintering is accelerate by high flame temperature. Producing silica nanoparticle by supplying sheath O_2 gas can decrease the particle diameter. Introducing sheath O_2 in the spray flame can accelerate combustion of fuel and precursor and prevent air diffusion into the spray flame. Therefore, the nanoparticles form rapidly and give the characteristic bright light-emission of silica formation (Figure 13). This additional O_2 can dilute the spray flame toward consequently less particle collisions and reduced growth (Figure 14)

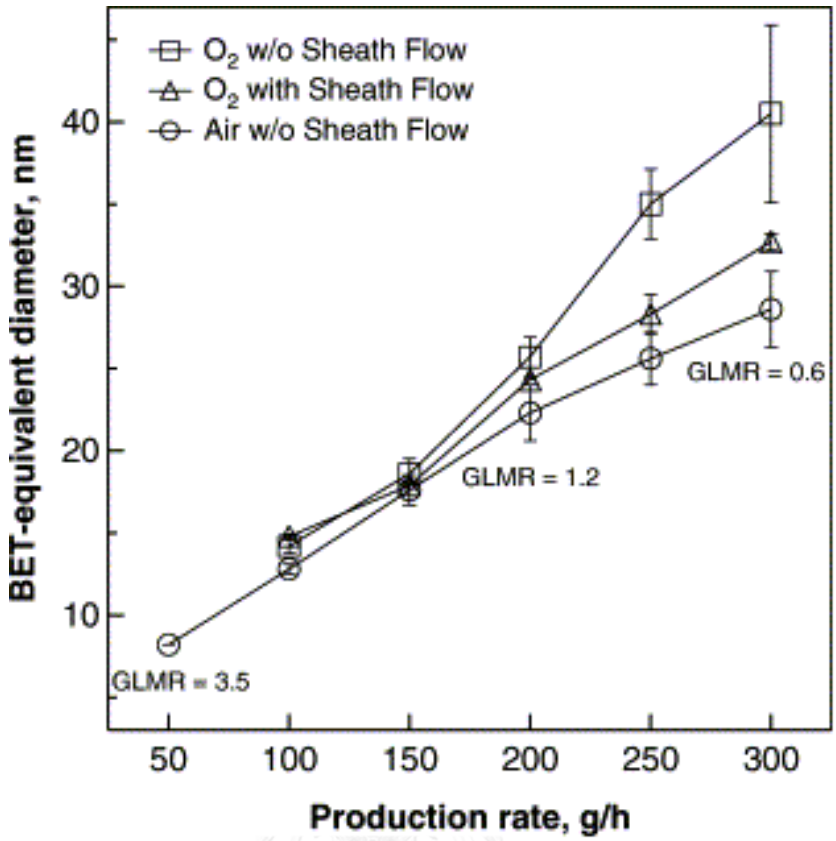

Figure 14 BET-equivalent diameter of silica nanoparticles is as a function of powder production rate (1.26 M HMDSO in ethanol) by using 12.5 l/min air or O_2 as dispersion gas without and with additional 25 l/min of O_2 sheath flow [56].

The dilution by sheath O_2 is dominant at low GLMR but has a minimal effect at GLMR. The images of flame-made silica nanoparticles with different feed rate from 150 to 300 g/h by using air (a,b) and O_2 dispersion gas with no (c,d) and with (e,f) sheath O_2 at a constant precursor concentration are shown in Figure 15. Using air instead of O_2 is to be dispersion gas decrease flame temperature and particle sintering rates toward decreasing particle size as show in Figure 15 (b) and (d). This increasing is in agreement with BET characterization (Figure 14). The morphology of

the particle is strongly influenced by the residence time. It is found that the small particles agglomerate nevertheless of the dispersion gas composition at a feed rate of 150 g/h. The enthalpy of the flame spray is increased with higher feed rate resulting in longer residence time, higher flame temperature and shorter particle residence time. The both reasons lead to the larger particle size formation. The product morphology seems not to be influence by sheath O_2.

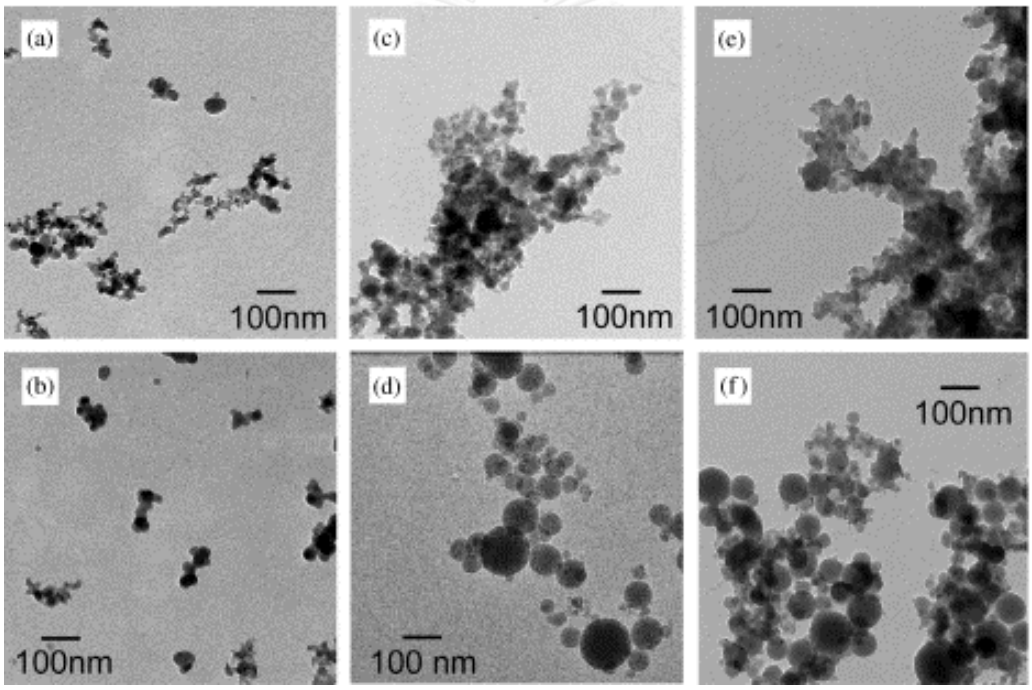

Figure 15 TEM images of silica nanoparticles at production rates of 150 g/h (top row) and 300 g/h (bottom row) by using 12.5 l/min air (a,b) or O_2 as dispersion gas without (c,d) and with (e,f) additional 25 l/min of O_2 sheath flow using 1.26 M HMDSO in ethanol [56].

The effect of concentration on SiO_2 particle size using O_2 as dispersion gas and additional sheath O_2 is shown in Figure 16. The precursor was increased from

1.26 to 3.0 M HMDSO in ethanol and to 4.7 M for pure HMDSO. The primary particle size increases from 15 to 33 nm with production rate from 100 to 300 g/h at 1.26 M HMDSO, from 24 to 56 nm with production rate from 244 to 733 g/h at 3.0 M HMDSO and from 32 to 75 nm with production rate 377 to 1132 g/h with 4.7 M of pure HMDSO. The increasing of HMDSO concentration with a constant feed rate increases the production particle size because of increasing the particle concentration and residence time at high temperature. It was reported by Madler et al [58] that the temperature of spray flame is high enough for aggregation of the particle to coalesce to solid particles (Figure 16).

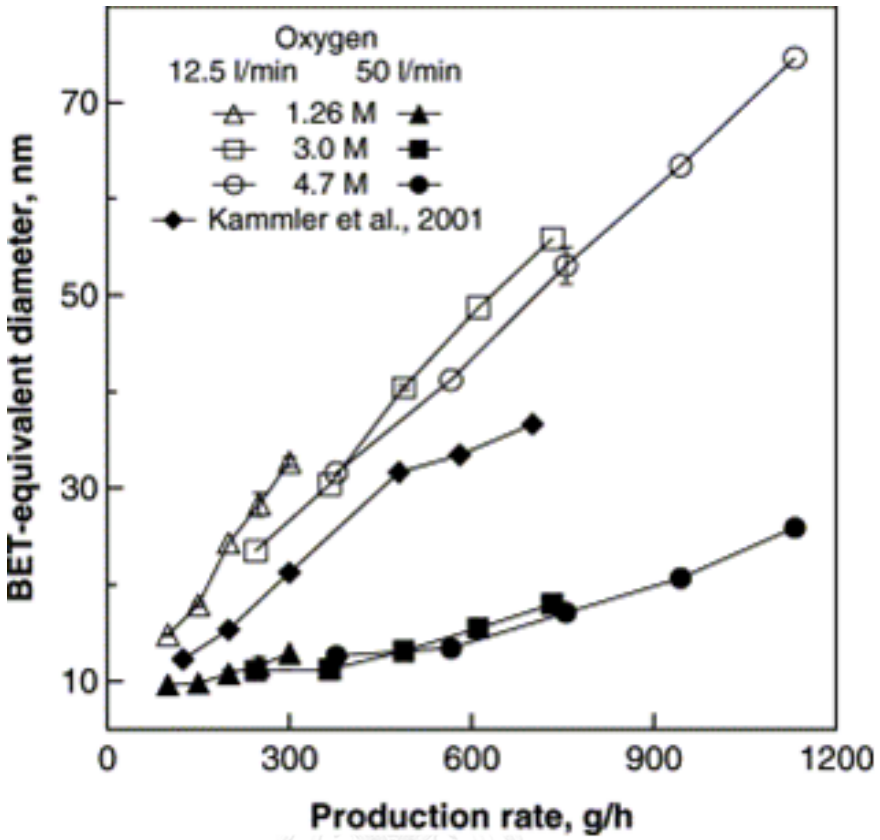

Figure 16 BET-equivalent average diameters are as a function of silica production rate and precursor concentration (1.26 M HMDSO in ethanol (triangles), 3.0 M HMDSO in ethanol (squares) and 4.7 M HMDSO (pure HMDSO: circles) (Kammler, H.K 2001b) [59].

For all flame spray conditions can produce perfect white silica powder. The indication on carbon-free powder is confirm by thermogravimetic analysis (TGA) coupled with a mass spectrometer (MS) [59, 60]. This characterization exhibits that there is no remaining of carbonaceous species in the silica powders. At high production rate, the adaptable FSP is similar to vapor-fed flame aerosol reactor used for large-scale production in industry (Ulrich 1984).

FSP method is very useful for producing nanopowder in a single-step. A problem of nanopowder production is to use expensive raw materials, which include metal chloride precursor. Protective construction of equipment is needed because of highly corrosive by using chloride precursors in FSP. Furthermore, the pollution of byproduct is also need to arrange. FSP process does not require protective equipment and dispose toxic byproduct due to the use of organometallic materials, which are non-corrosive precursor. Therefore, the using organometallic precursors are low cost and easy to produce. The controlling the size, size distribution and agglomeration of particles is another problem in nanopowder synthesis. There are many conventional methods used for particle size reduction such as milling, grinding, jet milling crushing and micronization. However, no particle size can reach the nanoscale and same uniform. FSP process can produce nanoparticles in uniform particle size distribution which are not possible grinding. Producing high purity and narrow size distribution by FSP process is much easier the alternative processes. FSP method can be used to produce nanopowder at high production rate. For example, hydrothermal process of nanoparticles on supercritical water with a rate 10-15 g/h. normally, coated nanoparticle are mainly obtained from solution phase method and sol-gel processing, which have many steps of pretreatment. These methods are not efficient in time, cost and purity of the fine product because of multi-step production. However, FSP method has the potential to provide efficient and simple routed for coated nanoparticles production. Synthesis of nanoparticle by FSP

method can be applied in several applications such as laser, composite, military, self-cleaning and catalyst.

Flame-made nanoparticles have been applied in various types of catalytic reactions as shows in Table 2. Many researchers have suggested the preparation catalysts by FSP and showed significant physiochemical properties and their good catalytic performance in different reactions. For examples, Lui et al [61] suggested that synthesis of 12.5%wt Ce-Mn oxide by FSP and compared to other Ce-Mn oxides with varying cerium/magnesium ratios. They found that flame-made Ce-Mn oxide showed high catalytic activity in oxidation of benzene due to the strong interaction between cerium and magnesium oxides were formed during the high temperature flame process. Vegton et al [62] studied spirel-kike oxides with the general formula $MgAl_{2x}M_xO_4$ (M=Mn,Fe and Co) synthesized by FSP for methane combustion. The flame-made nanoparticles exhibited high surface area and resistance to sintering leaded to good thermal stability and activity in the catalytic combustion of methane. Schimmoeller et al [63] reported that effect of vanadia loading on V_2O_5/TiO_2 catalysts were prepared by FSP method and wet-impregnation for oxidation of chlorobenzene. The flame-made V_2O_5/TiO_2 catalysts with varying vanadia loading showed no crystallite V_2O_5 species and high VO_x species dispersion. The catalytic activity increased when vanadia content increased and was independent of preparation method. Hoxha et al [64] researched the flame-made Au-Pd/TiO_2 catalyst which were tested in hydrogenation of acetophenone and compared to other preparation

methods such as co-impregnation and deposition methods. They also reported that Au-Pd alloy particle on the surface of flame-made catalyst were smaller and more uniform that the catalysts obtained by co-impregnation and deposition methods. In term of catalytic activity, The DP catalysts showed higher activity than FSP catalysts. Channei et al. [65] recommended that flame-made Fe-doped CeO_2 nanoparticles can be applied in photocatalytic. All flame-made samples exhibited the absence of any impurity phases that were determined by X-ray diffraction characterization. For photocatalytic performance, introducing Fe over CeO_2 nanoparticales can increase degradation of the carbon from formic and oxalic acids

Table 2 Application of FSP-made catalyst in various reactions

Heterogeneous catalyst	**Reaction**	**Reference**
Pt-Sn/Al_2O_3	Propane dehydrogenation	[22]
CuO	Photoelectrochemical water splitting	[66]
Perovskites	Methane catalytic combustion	[24]
Au–ZnO and Pt–ZnO	Photocatalytic degradation of dyes	[53]
Pd/Al_2O_3	Hydrogenation of ethyl pyruvate	[28]
Pt–Ba/Al_2O_3	Lean-NOx storage-reduction	[67]
Pd-Rh and Pd-Pt on Al_2O_3	Partial oxidation of methane	[68]
Pd/SiO_2–Al_2O_3	Hydrogenation of acetophenone	[69]

V/SiO_2	Oxidative dehydrogenation of propane	[70]
Co/ZrO_2	CO hydrogenation	[23]
Pd/TiO_2	Hydrogenation of phenylacetylene	[71]

CHAPTER III

Experimental

This chapter exhibits the detail of experimental of this research in three parts. They are the catalyst preparation of Pt based catalysts, characterization of physiochemical properties of catalysts several techniques such as N_2 physisorption, X-ray diffraction (XRD), CO pulse chemisorption, H_2-temperature programmed reduction (H_2-TPR), infrared spectroscopy of adsorbed CO (CO-IR), and transmission electron spectroscopy (TEM) and evaluation of catalytic performance on 3-nitrostyrene hydrogenation.

3.1 Catalyst preparation

3.1.1 Materials

Table 3 shows the chemicals using as precursors for catalyst preparation (impregnation and flame spray pyrolysis methods) in this research. There are six precursors for Pt (1and 2), Co (3), Ce (4 and 5) and TiO_2 (6) and order 7 is used as solvent, xylene.

Table 3 Chemicals used in catalyst preparation

Order	Chemical	Supplier
1	Chloroplatinic acid 99.99%	Aldrich
2	Platinum(II)acetyl-acetonate 99.99%	Aldrich
3	Cobalt naphthenate, 10 wt% in mineral spirits	Aldrich
4	Cerium actetylacetonate	Aldrich
5	Cerium nitrate 99.99%	Aldrich
6	Titanium(IV) butoxide reagent grade, 97%	Aldrich
7	Xylene 99.8%	Merck

3.1.2 Preparation of monomrtallic Pt /TiO_2 catalyst

The flame-made Pt/TiO_2 catalysts were carried out using a spray flame reactor similar to our previous studies [19, 20, and 23]. Platinum actetylacetonate and titanium (IV) butoxide reagent grade from Aldrich were used as platinum and titanium precursors, respectively. Precursors were prepared by dissolving the designed amounts of metal precursor in xylene (MERCK; 99.8 vol %). The total metal concentration was maintained at 0.3 M. The platinum concentration was fixed at 0.5 wt%. Using a syringe pump, 5 ml/min of precursor solution was dispersed into fine droplets by a gas-assist nozzle fed by 5 l/min of oxygen (Thai Industrial Gas Limited; purity > 99%). The pressure drop at the capillary tip was maintained at 1.5 bars by

adjusting the orifice gap area at the nozzle. The spray was ignited by supporting flamelets fed with oxygen (3 l/min) and methane (1.5 l/min) which are positioned in a ring around the nozzle outlet. A sintered metal plate ring (8 mm wide, starting at a radius of 8 mm) provided additional 10 l/min of oxygen as sheath for the supporting flame. The product particles were formed by passing through the flame at a temperature of approximately 2,000°C in milliseconds and collected on a glass fiber filter (Whatman GF/C, 15 cm in diameter) with the aid of a vacuum pump as shown in Figure 17.

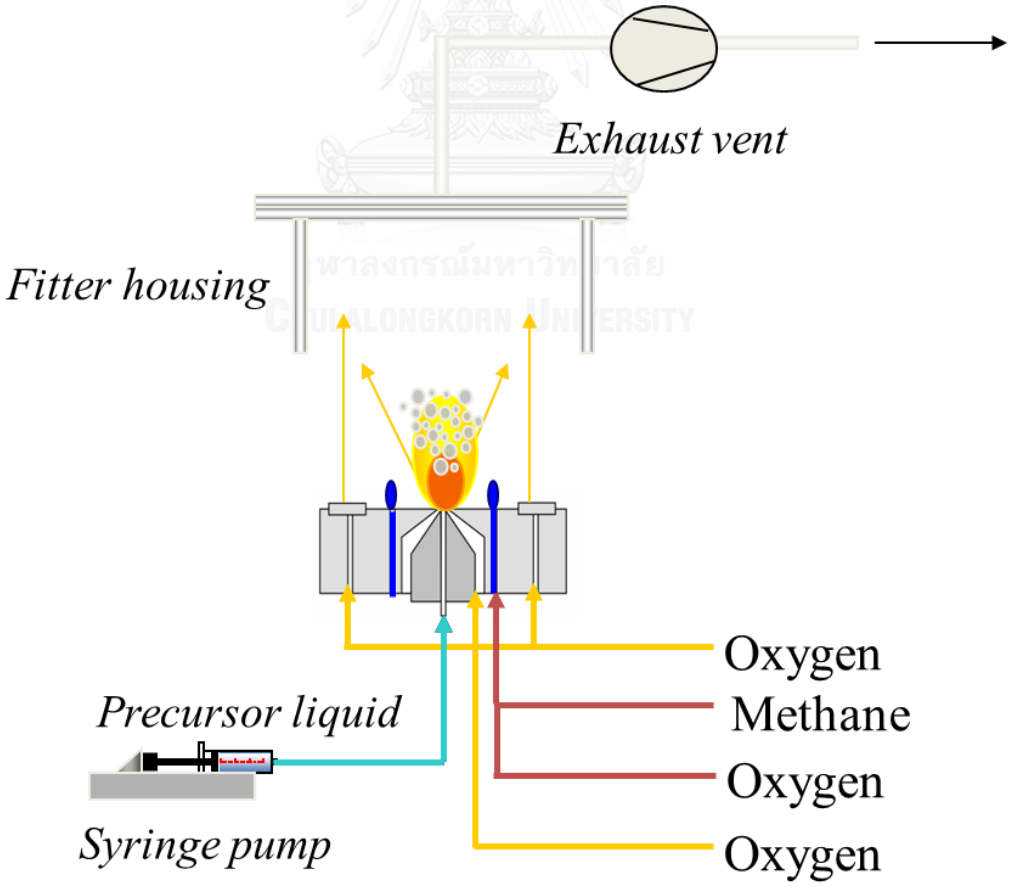

Figure 17 Diagram of flame spray pyrolysis

For comparison purposes, Pt/TiO_2 catalysts were also prepared by impregnation method using a sol-gel TiO_2 support [24] and an aqueous solution of $H_2PtCl_6.6H_2O$. The sol-get TiO_2 support was prepared by using 83.5 cm^3 of titanium isopropoxide (Aldrich Chemical Ltd.), 7.33 cm^3 of 70 vol.% nitric acid (Asia Pacific Specialty Chemical Limited), and 1000 cm^3 of distilled water. 70 vol.% nitric acid was mixed distilled water and the solution was continually stirred using a magnetic stirrer. Titanium isopropoxide was added slowly during the solution was stirred and then the mixture was stirred continually until it become homogenous mixture at room temperature. The obtained mixture was put in dialysis tubing and then submerged in distilled water. The pH of obtained mixture was adjusted by DI water until reached 3.5 from the initial pH at 1.1. The mixture was removed and then dried at 110 ℃ overnight. It were calcined in air at 350 ℃ for 2 h. The catalysts were dried in an oven at 100 ^{o}C for 24 h. The prepared catalysts were calcined in oxygen at 500 ^{o}C for 2 h, and reduced in H_2 at 200-700 ^{o}C.

3.1.3 Preparation of bi-metallic PtCo and PtCe catalysts by FSP

Syntheses of mono and bi-metallic catalysts were carried out using a spray flame reactor similar to that of Ref. [1]. For $PtCo/TiO_2$ catalysts, platinum actetylacetonate, cobalt naphthenate 10 wt% in mineral spirits, and titanium (IV) butoxide reagent grade from Aldrich were used as platinum, cobalt, and titanium precursors, respectively. Precursors were prepared by dissolving the designed

amounts of metal precursor in xylene (MERCK; 99.8 vol %). The total metal concentration was maintained at 0.3 M. The platinum concentration was fixed at 0.5 wt%, while the cobalt contents were varied between 0.1 and 0.5 wt%. For $PtCe/TiO_2$ catalysts, platinum actetylacetonate, cerium actetylacetonate, and titanium (IV) butoxide reagent grade from Aldrich were used as platinum, cerium, and titanium precursors, respectively. The platinum content was also fixed at 0.5 wt%, while cerium and were varied between 0.5 and 2 wt% and then, they were dissolved with xylene. Using a syringe pump, 5 cm^3/min of the precursor solutions were dispersed into fine droplets by a gas-assist nozzle fed by 5 l/min of oxygen (Thai Industrial Gas Limited; purity > 99%). The pressure drop at the capillary tip was maintained at 1.5 bars by adjusting the orifice gap area at the nozzle. The spray was ignited by supporting flamelets fed with oxygen (3 l/min) and methane (1.5 l/min) which are positioned in a ring around the nozzle outlet. A sintered metal plate ring (8 mm wide, starting at a radius of 8 mm) provided additional 10 l/min of oxygen as sheath for the supporting flame. The product particles were collected on a glass fiber filter (Whatman GF/C, 15 cm in diameter) with the aid of a vacuum pump (Figure 3.1).

3.1.4 Preparation of $PtCe/TiO_2$ by co-impregnation method

0.5 wt% of Pt/TiO_2 catalysts were prepared by wet-impregnation of the titanium oxide supports with a solution of $H_2PtCl_6.6H_2O$ in distillated water. Cerium modifications of platinum catalysts with varying 0.1-2 wt % were prepared by co-

impregnation of titanium oxide supports with a solution of cerium nitrate. After agitation at room temperature for 24 h and evaporation of the excess water solvent, the catalysts were put in a vacuum oven at 80 $^{\circ}$C for 24h. The prepared catalysts were decomposed in argon at 500 $^{\circ}$C for 2 hr, calcined in O_2 at 350 $^{\circ}$C for 2 hr, and reduced in H_2 at 500 $^{\circ}$C for 2 hr. Figure 18 shows diagram of the catalyst preparation.

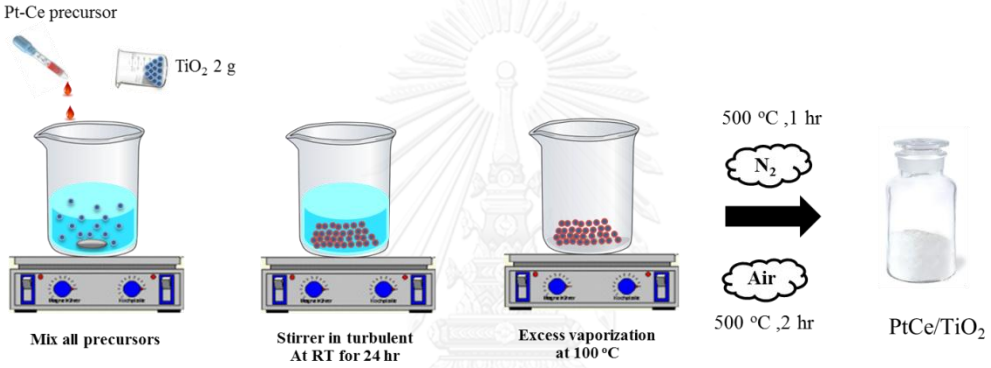

Figure 18 Diagram of catalyst preparation by wet-impregnation

3.2 Catalyst characterization

To investigate the physiochemical properties of catalysts, fresh catalysts was characterized by several techniques.

Inductively Coupled Plasma Emission Spectrometry (ICP)

The actual Pt loading was analyzed by ICP-AES technique after digestion of the powder and they were analysed at Iron and Steel Institute of Thailand.

X-ray diffraction (XRD)

XRD patterns were determined using a Siemens D5000 using nickel filtered CuK α radiation. The crystallite size (d_{XRD}) was calculated using the Scherrer equation and α -alumina as the external standard.

N_2-Physorption

The BET surface area, average pore size diameters, and pore size distribution were determined by physisorption of N_2 using a BEL-SORP automated system.

Transmission electron microscopy (TEM)

The morphology and particle size of powders were observed using a JEOL-JEM 200CX TEM operated at 100 kV. Transmission electron microscope operated at 100 kV. Up to 150 individual metal particles were counted for each Pt/TiO_2 catalysts with different reduction temperature and average Pt diameter (dp) was calculated from

$$dp = \frac{\sum n_i d_i^3}{\sum n_i d_i^2}$$

Where n_i is number of Pt particle of diameter d_i.

CO-Chemisorption

The relative percentages of platinum dispersion were determined by CO pulse chemisorption at 40°C using a BEL-METAL-1 system. Approximately 0.1 g of catalyst was reduced under hydrogen flow at 40°C for 2 h, and then helium was purged. The CO was pulsed over the reduced catalyst until the TCD signal from the pulse was constant.

H_2-Temperature Program Reduction (H_2-TPR)

The H_2-TPR measurements were carried out in a quartz U-tube reactor. Prior to these measurements, all the catalyst samples were pretreated with a N_2 flow (30 mL/min, 1 h, 150 ^{o}C). The TPR profiles were obtained by passing carrier gas (10% H_2 in nitrogen) through the catalyst samples (30 mL/min, ramping from 30 to 600 ^{o}C at 10 ^{o}C/min) using a Micromeritics AutochemiSorb 2910 system attached with ChemiSoft TPx software.

Fourier Transform Infrared spectroscopy (FTIR)

The CO adsorbed species on the Pt/TiO_2, $PtCo/TiO_2$ and $PtCe/TiO_2$ catalysts were measured using FTIR-620 spectrometer (JASCO) with a MCT detector at a wavenumber resolution of 2 cm^{-1} at Hokkaido University. He gas was introduced into the sample cell in order to remove the remaining air. The system was switched to hydrogen and heated to 200-500 °C. The temperature was kept constant for 60 min and then cooled down to the room temperature with Helium gas. After that, carbon monoxide was flow to the system for 15 min. The IR spectrum of CO adsorbed onto the catalyst was recorded in the 1800-2200 cm^{-1} range after the gaseous CO had been removed from the cell by Helium flow.

3.3 Evaluation of catalytic performance in hydrogenation of 3-nitrostyrene

The hydrogenation of 3-nitrostyrene was carried out in a 50 cm^3 autoclave. The reactor was loaded with approximately 10 mg of catalyst and 0.5 cm^3 of nitrostyrene

(3.6 mmol), purged with hydrogen to remove the air for three times. The reaction was carried out isothermally at 323 K at 40 bar of H_2 with a high-pressure liquid pump. Prior to the experiments the reaction mixture was stirred with a magnetic stirrer. After the reaction, the reactor was cooled below room temperature by ice-water and carefully depressurized. The obtained-products were mixed with decane 10 ml and then analysed by a gas chromatograph attached with a flame ionization detector using decane as an internal standard. Figure 19 shows schematic of liquid-phase hydrogenation of 3-nitrostyrene.

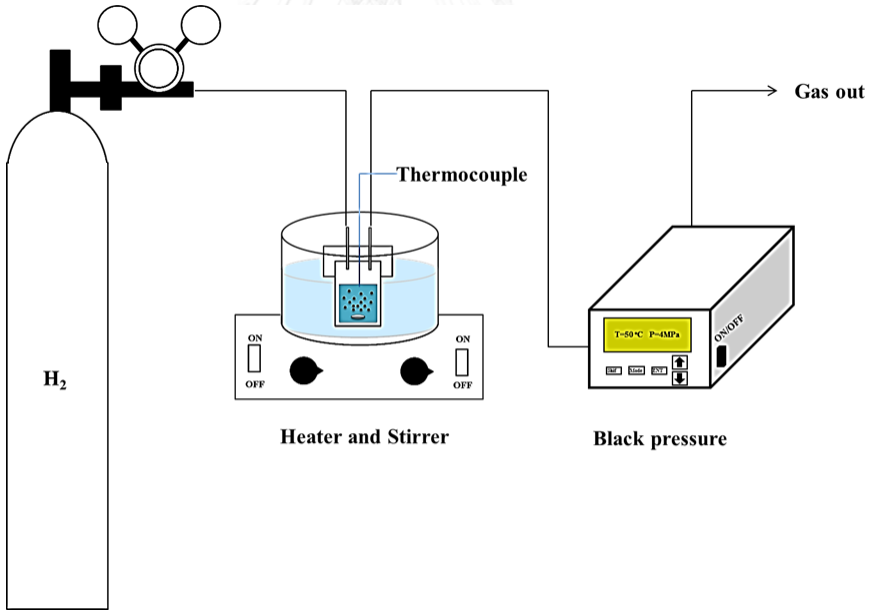

Figure 19 Schematic of liquid-phase line reaction of 3-nitristyrene hydrogenation

CHAPTER IV

Results and discussion

In this Chapter, the investigation of the physiochemical and catalytic properties over flame-made and impregnated Pt/TiO_2 catalysts are discussed. The results and discussion are described and divided into three major parts. First, influence of Pt/TiO_2 preparation for liquid-phase selective hydrogenation of 3-nitrostyrene, influence of reduction temperature on flame-made Pt/TiO_2 and impregnated catalysts for the liquid-phase selective hydrogenation of 3-nitrostyrene, Influence of Co loading on Pt/TiO_2 catalyst synthesized by flame spray pyrolysis for the liquid-phase selective hydrogenation of 3-nitrostyrene and Effect of cerium loading on catalytic performance of flame-made Pt/TiO_2 catalysts.

4.1 Influence of Pt/TiO_2 preparation for liquid-phase selective hydrogenation of 3-nitrostyrene

The effects of preparation methods on the physicochemical and catalytic properties were investigated and discussed in this section by means of several characterization techniques such as X-ray diffraction (XRD), CO pulse chemisorption, infrared spectroscopy of adsorbed CO (CO-IR), and transmission electron spectroscopy (TEM). The Pt/TiO_2 catalyst prepared by flame spray pyrolysis method is given symbol as F-Pt/Ti, prepared by impregnation method on a flame-made TiO_2

is given symbol as I-Pt/FTi and those prepared by impregnation method on a sol-gel TiO_2 is given symbol as I-Pt/STi.

4.1.1 XRD

The XRD patterns of the Pt/TiO_2 catalysts prepared by one-step FSP method (F-Pt/Ti) conventional impregnation on a flame-made TiO_2 (I-Pt/STi) and conventional impregnation on a sol-gel made TiO_2 (I-Pt/STi) are shown in Figure 20. The characteristic peaks corresponding to both anatase and rutile phases TiO_2 were observed on all samples. Bookite phase TiO_2 was observed only on I-Pt/Ti catalyst at 2Θ degrees 31. Those of Pt/PtO species were not detected due probably to a low metal loading and/or high Pt dispersion.

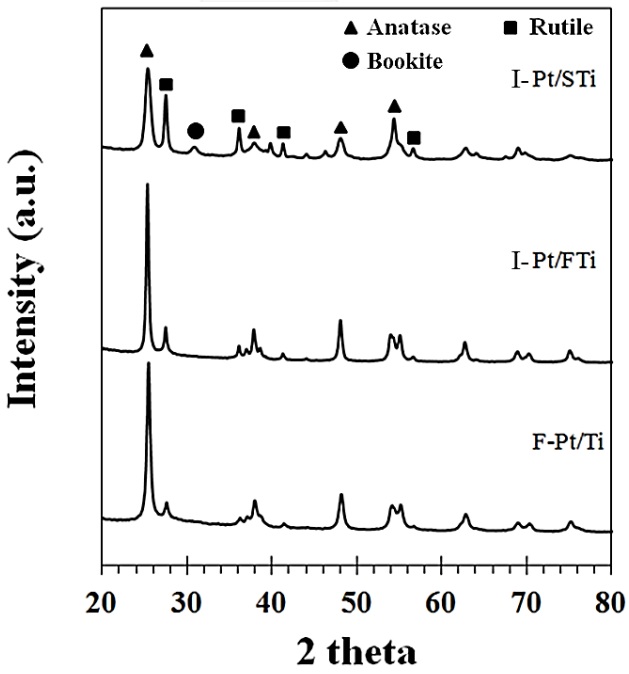

Figure 20 XRD patterns of I-Pt/Ti and F-Pt/Ti catalysts

The XRD patterns of bare TiO_2 and F-Pt/Ti catalyst are shown in Figure 21. The addition of Pt on TiO_2 support prepared by FSP exhibits little effect on the phase transformation of anatase to rutile TiO_2. The bare TiO_2 produced under similar flame conditions composed of 90.3% anatase TiO_2 whereas the flame-made Pt/TiO_2 contained 91.2% anatase TiO_2.

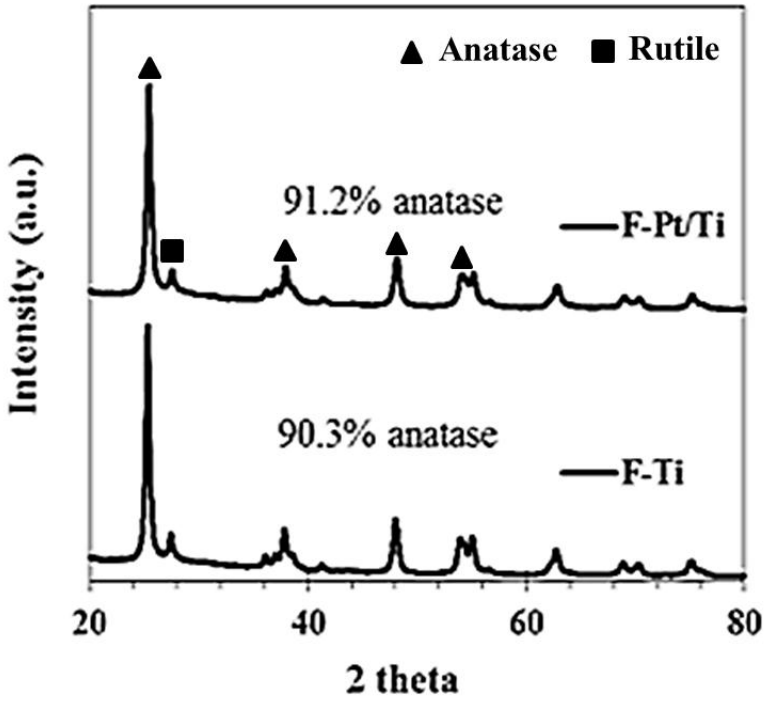

Figure 21 XRD patterns of F-Ti and F-Pt/Ti catalyst

4.1.2 N_2 physisorption

The N_2 physisorption isotherms of F-Pt/Ti, I-Pt/FTi and I-Pt/STi catalysts are shown in Figure22. The F-Pt/Ti and I-Pt/FTi catalysts were macroporous material that contained interparticle pores with relatively large pore diameter. On the other hands,

the I-Pt/Ti possessed much lower pore volume, smaller pore size, and the characteristic hysteresis loop of an opened cylindrical pore structure with various diameters of mesoporous structure. BET surface area, pore volume and average pore size diameter of the catalysts, which were calculated from BTH model, are summarized in Table 4. The BET surface areas of all catalysts, however, were not significantly different ranging between 48-67 m^2/g.

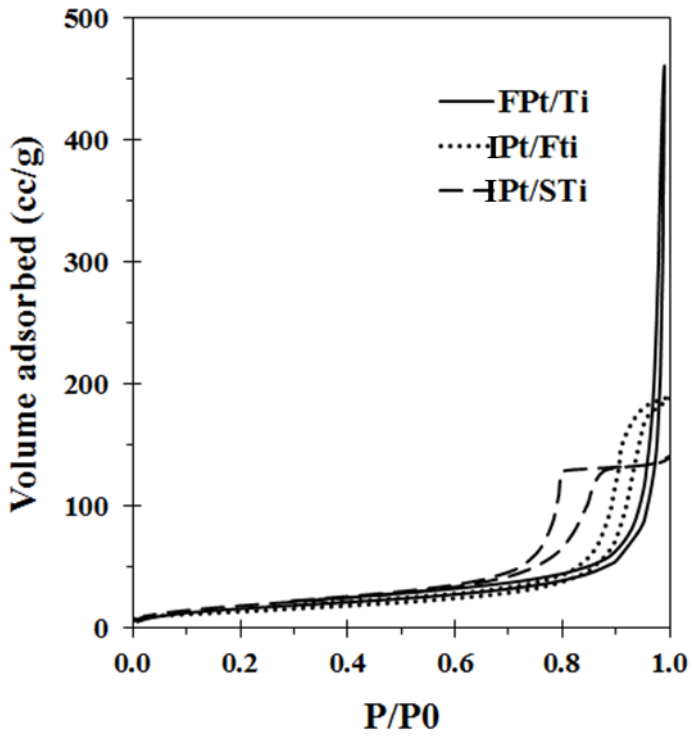

Figure 22 N_2 adsorption-desorption isotherms of F-Pt/Ti, I-Pt/FTi and I-Pt/STi catalysts

Table 4 Physical properties of the I-Pt/STi , I-Pt/FTi and F-Pt/Ti catalysts

Catalyst	Crystallite size (nm)	% Phase Composition		BET Surface Areas (m^2/g)	Average Pore Diameter (nm)	Pore Volume (cm^3(STP)/g)
		Anatase	Rutile			
F-Pt/Ti	20.4	91.2	8.8	58.7	192.4	0.695
I-Pt/FTi	21.4	84.8	15.2	48.0	28.6	0.286
I-Pt/STi	14.3	45.8	54.2	67	13.9	0.217

*I-Pt/STi contains bookite phase TiO_2 but was not use for calculation of phase composition

4.2.3 TEM

The morphology of the TiO_2 supports in Figure 23. The nearly spherical shape particles were found on both TiO_2 supports but the average particle size of sol-gel made TiO_2 was smaller and was found to be more agglomerated than the flame-made one. The morphology of the all samples is shown in Figure 24. The nearly spherical shape particles were found on all catalyst. The Pt particle sizes were quite similar on both supports. The Pt particles were not observed at reduction temperature as 200 ^{o}C. The average size of Pt particles of all sample at reduced 500 ^{o}C are around 0.7 -1.7 nm.

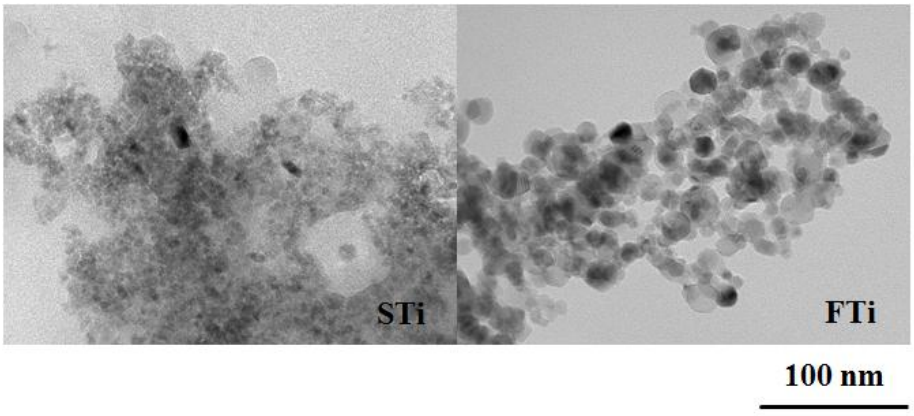

Figure 23 TEM images of TiO_2 supports

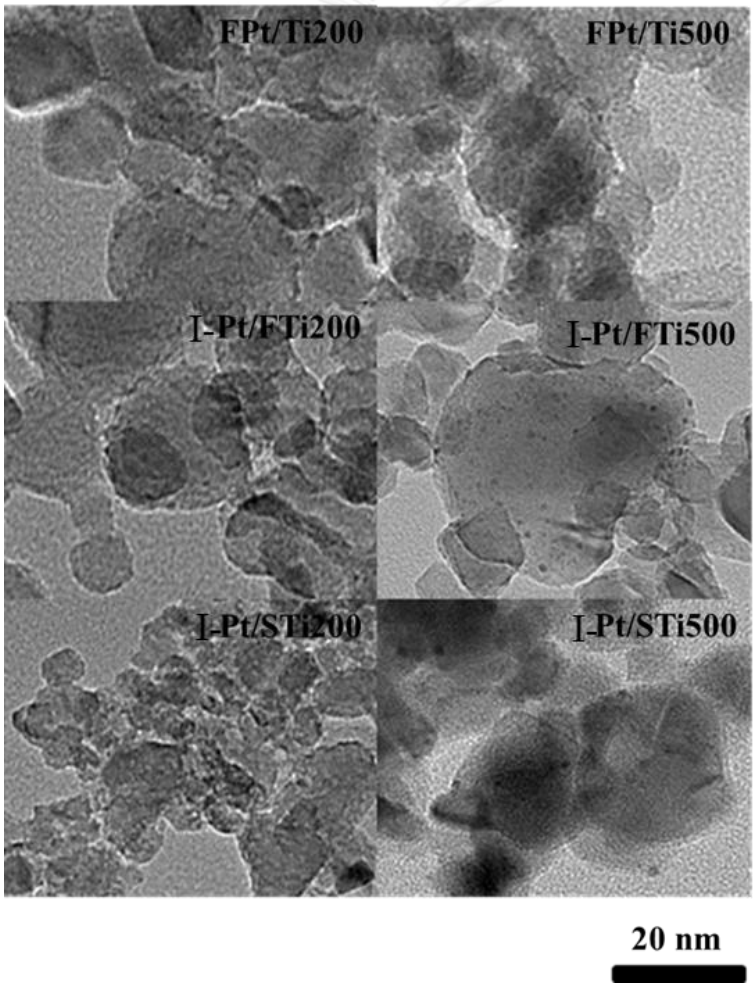

Figure 24 TEM images of the F-Pt/Ti, I-Pt/STi and I-Pt/STi catalyst with reduction temperatures as 200-500 $^{\circ}C$

4.1.4 CO-IR

Figure 25 shows CO adsorption behavior on Pt catalyst which consists of linear, Bridge and hollow CO adsorptions. Adsorption of CO on Pt catalysts can use for characterizing the Pt surface structure in nitrostyrene hydrogenation [1, 2, 35].

Figure 25 Model of CO adsorption behaviors

The FT-IR spectra of adsorbed CO on the Pt/TiO_2 catalysts reduced at reduction temperatures as 200-500 ^{o}C are shown in Figure 26. The CO linearly adsorbed on low-coordination Pt atom on edge sites and bridged-type adsorbed CO were characterized by adsorption bands at 2056 and 1825 cm^{-1}, respectively. It has been reported that bridge-type adsorbed CO formed mainly on large Pt particles while linear-type adsorbed CO dominated on small Pt particles [1]. In this study, the ratio of Pt on corner to terrace was high due to the presence of very small Pt particle size (≤ 2 nm). In addition, the fraction of Pt terrace was decreased by reduction at high temperature, while the number of Pt-TiO_x sites increased. However, the IR spectra could not be detected on the I-Pt/STi catalyst when they were reduced at

500 °C and higher, due probably to the excessive decoration of TiO_x on Pt surface. The CO adsorbed band was observed over I-Pt/FTi catalyst at reduction temperature as 500°C.

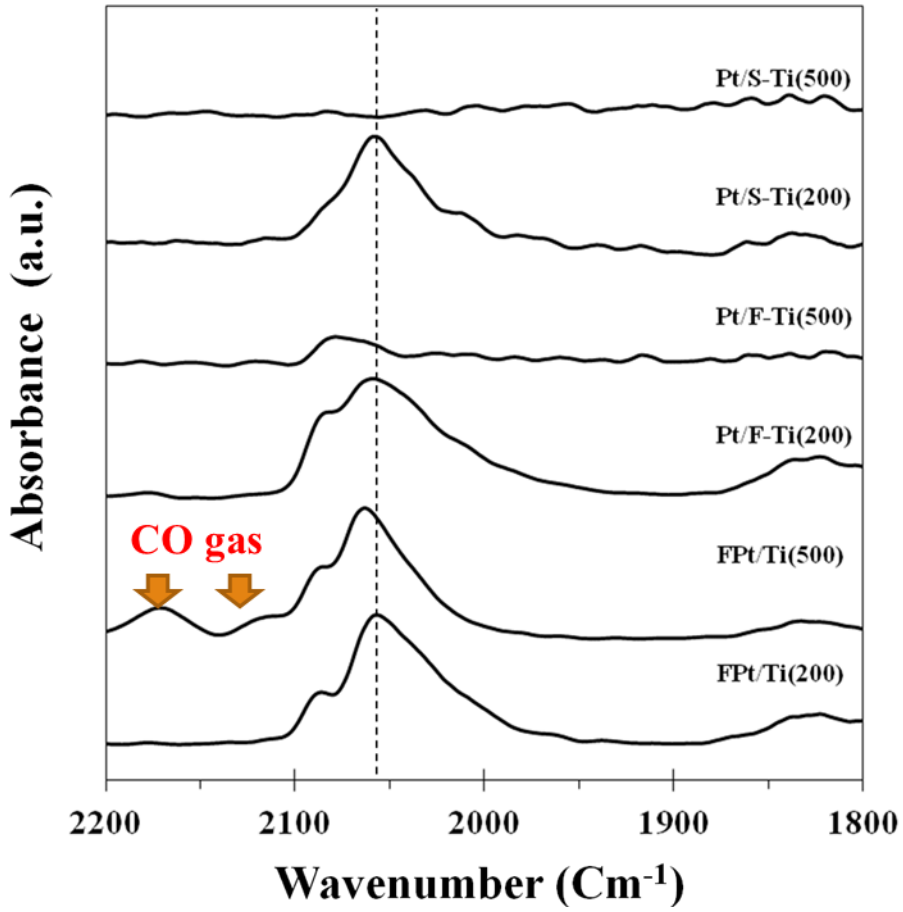

Figure 26 CO-IR results of the F-Pt/Ti, I-Pt/FTi and I-Pt/STi catalysts

4.1.5 Evaluation of 3-nitrostyrene hydrogenation

The schematic of 3-nitrostyrene hydrogenation is shown in Figure 1. Under reaction conditions used, nitrostyrene (NS) hydrogenation is an quite complex reaction, which has two main reaction pathways occurring from a hydrogenation of

C=C double bond and a nitrogroup N=O. Hydrogenation of C=C double bond provides ethylnitrobenzene (ENB) and hydrogenation of a nitro group provides vinylaniline (VA). The both of hydrogenated products can be hydrogenated to be ethylaniline (EA). The catalytic behaviors of all the flame-made catalysts in the hydrogenation of 3-nitrostyrene are summarized in Table 5.

The catalytic performance of all catalysts exhibited in table 5. For any reduction temperature used, the F-Pt/Ti catalysts exhibited much higher catalytic activity than the other catalysts, which could be attributed to the higher anatase phase TiO_2. However, for low reduction temperature, all Pt/TiO_2 catalysts had no favored selectivity for the possible product of the hydrogenation. The major hydrogenation products were ENB and VA without formation of intermediates hydrogenation products such as the hydroxylamine. The selectivity of VA on IPt/STi catalyst was higher than IPt/FTi catalyst while the activity exhibited lower at reduction temperature as 500 ^{o}C

.

Table 5 reaction results of the Pt/TiO_2 catalysts with difference preparation method

Catalyst	Red.	Time	Conv.	Selectivity [%]		
	[°C]	[min]	[%]	VA	ENB	EA
FPt/Ti	200	20	61.2	39.7	47.6	12.7
		40	89.1	43.0	34.2	22.8
	500	20	66.1	60.0	28.2	11.8
		30	99.4	53.1	10.5	36.4
IPt/FTi	200	20	41.9	51.3	33.2	15.5
		40	84.2	53.6	25.9	20.5
	500	20	56.9	60.0	26.6	13.4
		40	96.5	64.7	0.8	34.5
IPt/STi	200	20	4.8	58.1	41.9	0.0
		120	20.3	50.0	46.6	3.4
	500	20	49.5	72.1	19.9	8.0
		60	97.1	77.5	4.6	17.9

Reaction (3.4 mmol NS in 10 ml of ethanol) at 50 ^{o}C with 10 mg catalyst under 40 bar H_2 after 20 min

4.2 Influence of reduction temperature on flame-made Pt/TiO_2 and impregnated catalysts for the liquid-phase selective hydrogenation of 3-nitrostyrene

The effects of reduction temperature on the physicochemical and catalytic properties were investigated and discussed in this section by means of several characterization techniques such as N_2 physisorption, X-ray diffraction (XRD), CO pulse chemisorption, H_2-temperature programmed reduction (H_2-TPR), infrared spectroscopy of adsorbed CO (CO-IR), and transmission electron spectroscopy (TEM).

The Pt/TiO_2 catalyst was prepared by flame spray pyrolysis method is given symbol as F-Pt/Ti and prepared by impregnation method is given symbol as I-Pt/Ti.

4.2.1 XRD

XRD patterns of the both Pt based catalysts with various reduction temperatures from 200-700 $^{\circ}C$ are exhibited in Figure 27-28. After reduced at 200-500 $^{\circ}C$, the XRD patterns exhibited only the characteristic peaks of anatase and rutile and no peak of Pt/PtO species. Transition temperature of anatase to rutile is in range 400-1200 $^{\circ}C$ which depends on transition temperature, preparation methods and raw materials. It has reported that pure bulk anatase transformed irreversibly to rutile under air treatment at approximately 600$^{\circ}C$. The transformation phase of I-Pt/Ti catalyst to pure rutile is completed at 600 $^{\circ}C$ while F-Pt/Ti catalyst exhibits the high intensity characteristic peaks of anatase. F-Pt/Ti catalyst exhibits the irreversible transformation to rutile phase at 700 $^{\circ}C$.

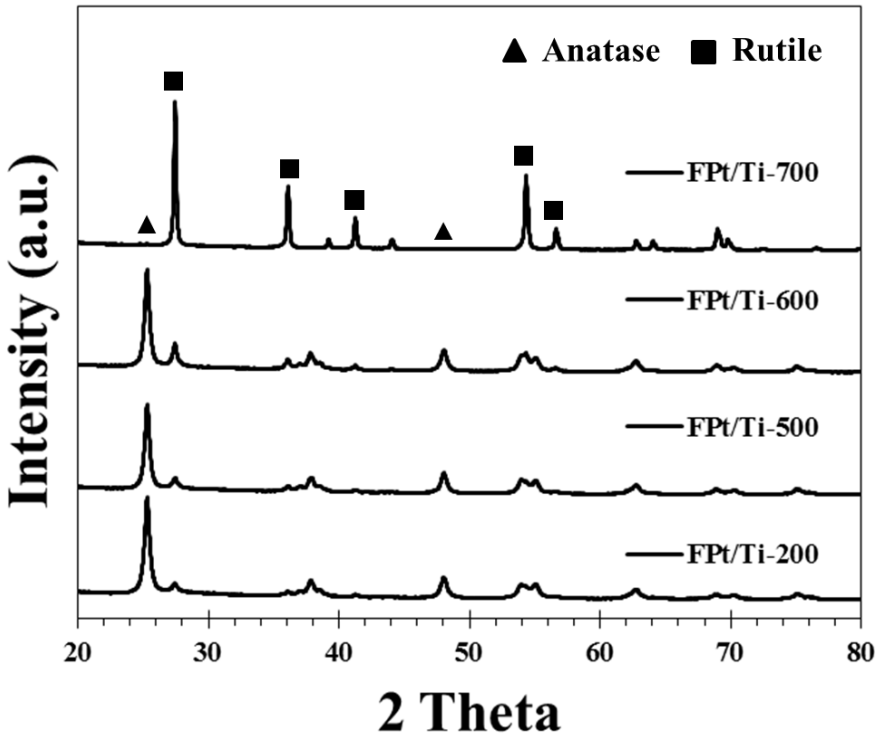

Figure 27 XRD pattern of F-Pt/Ti catalyst with different reduction temperature

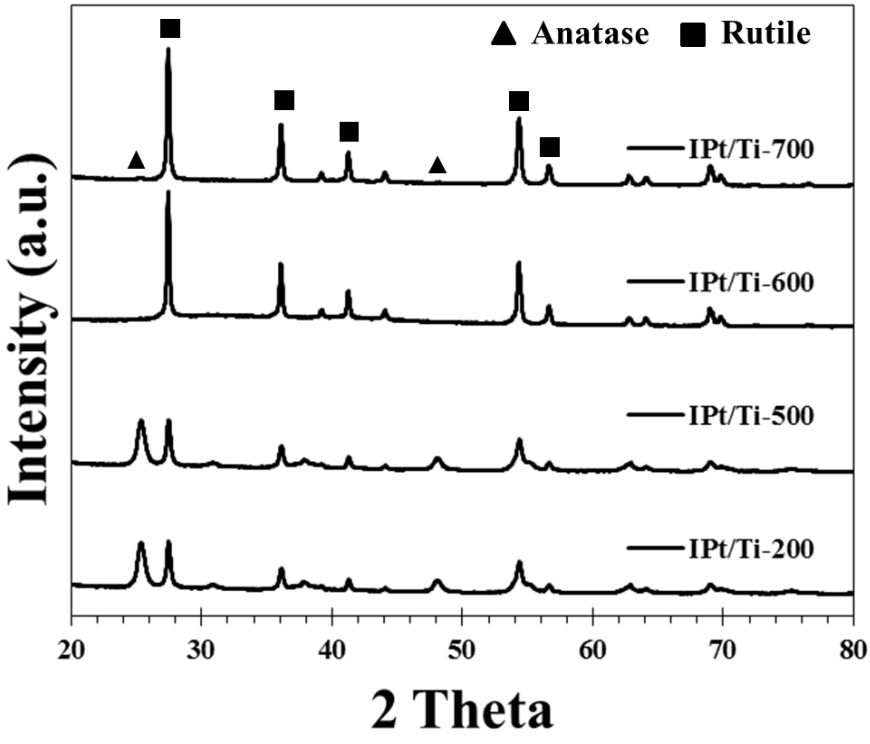

Figure 28 XRD pattern of I-Pt/Ti catalyst with different reduction temperature

The physical properties including the Pt metal content, average crystallite size, rutile and anatase phase composition of the catalysts are summarized in Table 6. Both Pt-supported catalysts were found to have a Pt-metal loading around 0.5 to 0.54 wt. %The F-Pt/Ti catalysts contained larger amount of anatase phase TiO_2 than the I-Pt/Ti. The crystallite size and %anatase phase of both catalysts after reduction at various temperatures are given in Table 4. The crystallite size of F-Pt/Ti was slightly increased from 20 to 22 nm while %anatase decreased from 91 to 73% after reduction at 200-600 ^{o}C. After reduction at 700 ^{o}C, the rutile phase transformation was completed and the crystallite size increased rapidly from 22 to 48 nm. In the case of I-Pt/Ti, reduction at 200 and 500 ^{o}C did not change the crystallite size and %anatase phase because the I-Pt/Ti was pretreated at 500 ^{o}C for 2 h before the reduction step. The rutile phase trans-formation of I-Pt/Ti was completed after reduction at 600 ^{o}C. Lower thermal stability of the I-Pt/Ti could be explained by the smaller crystallite size and lower crystallinity of the I-Pt/Ti before the reduction process. A smaller-sized anatase TiO_2 can be transformed to rutile more easily than a larger one [72].

4.2.2 TEM

The morphology of the Pt/TiO_2 catalysts is shown in Figure 29 and 30, respectively. The nearly spherical shape particles were found on both TiO_2 supports but the average particle size of sol-gel made TiO_2 was smaller and was found to be more agglomerated than the flame-made ones. The Pt particle sizes were quite similar on both supports. The average size of Pt particles was slightly increased from 1.2 nm to 2.2 nm when the reduction temperature increased from 200 to 700 $^{\circ}C$. A number of TEM micrographs have been analyzed in order to obtain a histogram of particle size distribution and the results is shown in Figure 4.7 and 4.8. The particle size distribution of F-Pt/Ti catalysts is narrow and approximately monodispersed giving an average Pt particle sizes for the catalysts reduced at 500, 600 and 700$^{\circ}C$ 0.76, 0.87, and 2.2 nm, respectively, and is wider when the reduction temperature reach up to 700 $^{\circ}C$. The I-Pt/Ti catalysts showed wider particle size distribution and larger average Pt particle sizes. The Pt particle size increased with increasing reduction temperature as 1.7, 2.3, and 2.6 nm for the I-Pt/Ti catalysts reduced at 500, 600, and 700$^{\circ}C$, respectively.

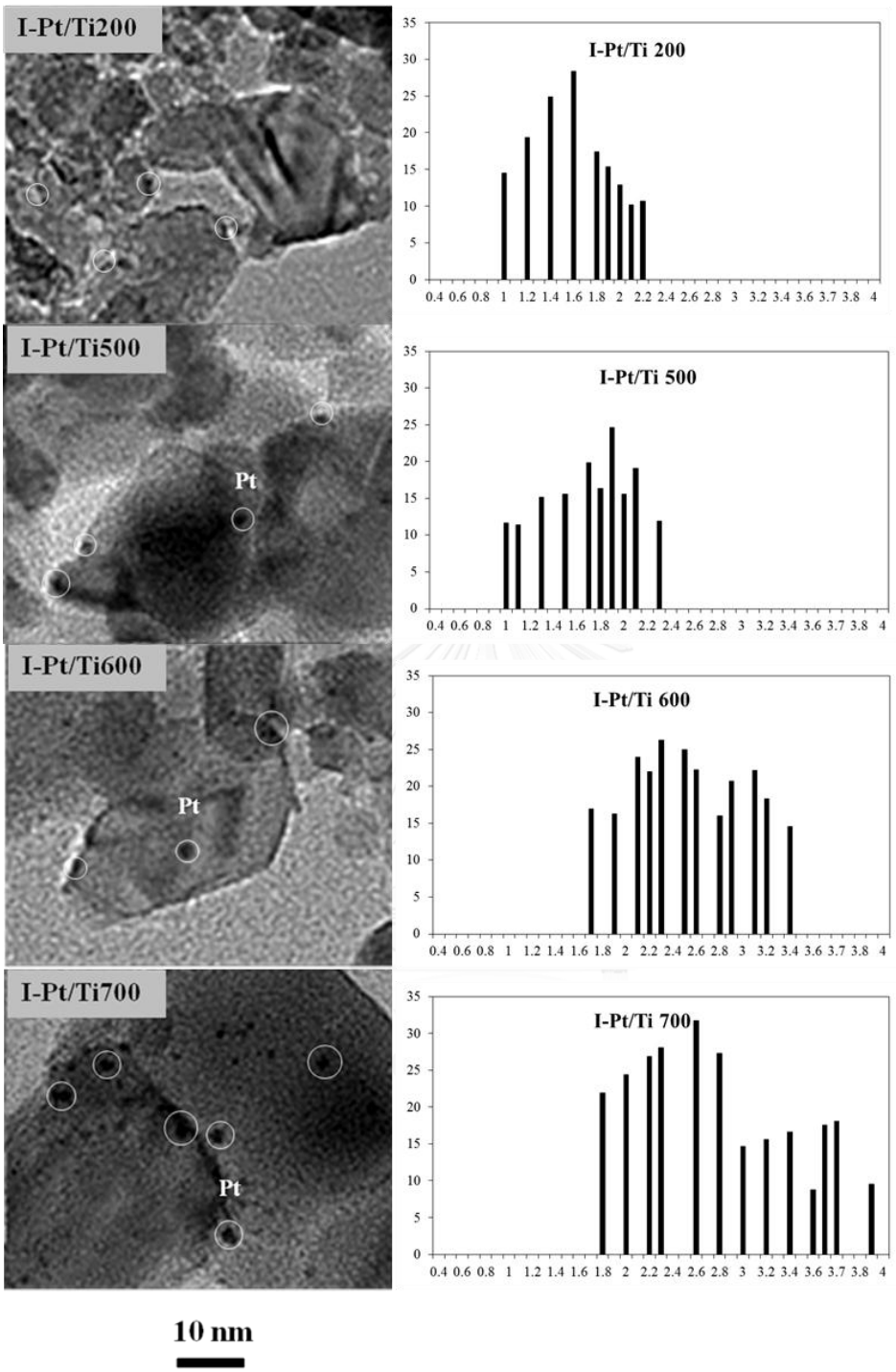

Figure 29 TEM images of the I-Pt/Ti catalyst with various reduction temperatures

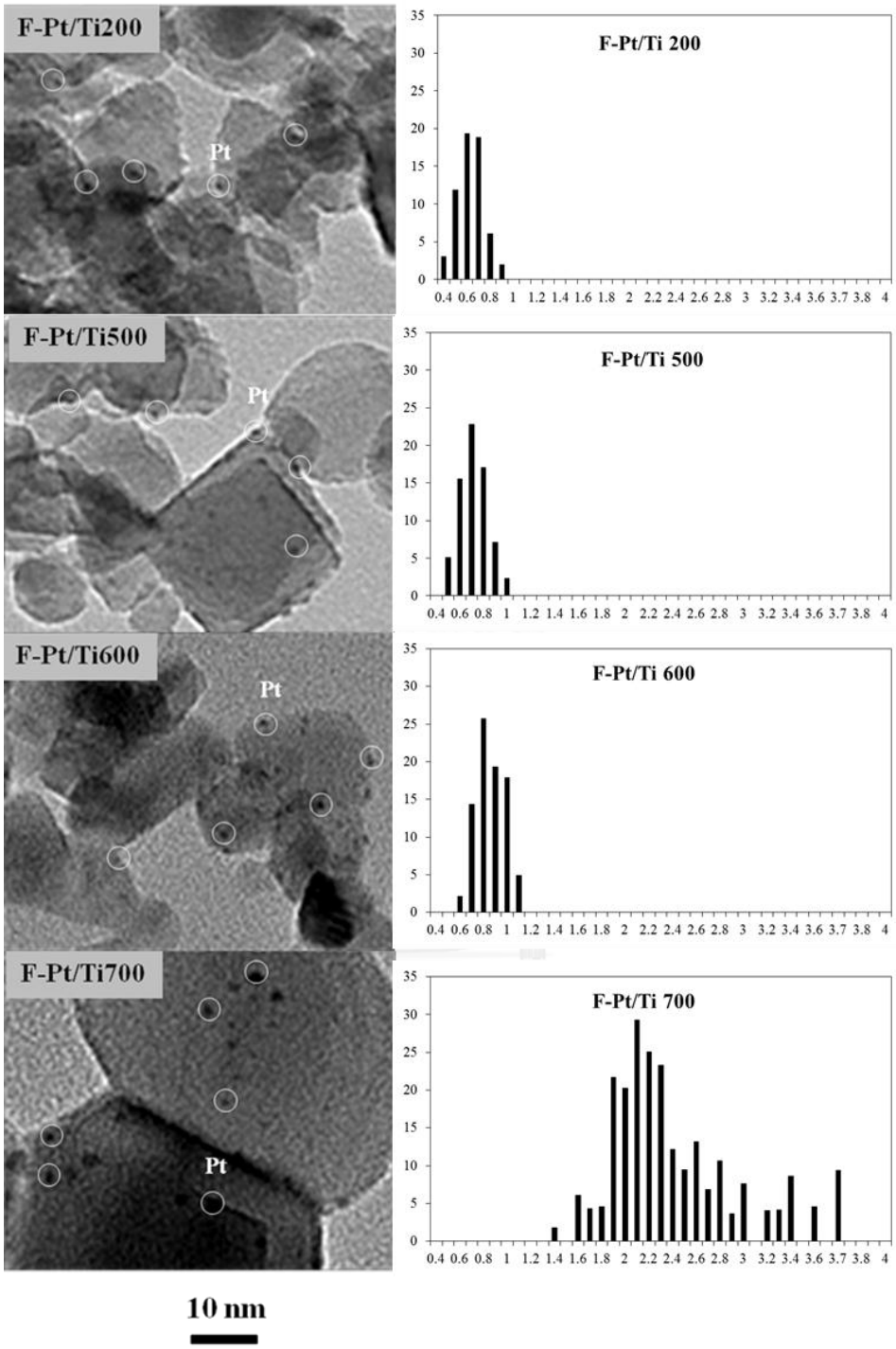

Figure 30 TEM images of the F-Pt/Ti catalyst with various reduction temperatures

4.2.3 CO chemisorption

The relative amounts of active Pt metal surface on the catalyst samples were calculated from CO chemisorption based on the assumption that one carbon monoxide molecule adsorbs on one Pt site and the results are shown in Table 6. It was found that Pt dispersion on the F-Pt/Ti catalysts were much higher than on the I-Pt/Ti. The Pt dispersion on F-Pt/Ti reduced at 200, 500, and 600 $^{\circ}$C were 20.1, 24.1, and 22.0%, respectively whereas those of I-Pt/Ti were much lower ranging between 2.2-5.3%.

Since the Pt particle sizes observed from TEM were quite similar on both catalysts, the relatively low CO chemisorption on the impregnated catalysts may be due to the partial decoration of Pt metal surface by migrated TiO_2 support during the calcination/reduction processes. The higher thermal stability of flame-made catalysts was confirmed by both TEM and XRD results that the TiO_2 crystallite size and crystalline phase composition were not significantly changed upon reduction at 200-600°C. Reduction at 700 °C, however, caused dramatically decrease of Pt active sites on F-Pt/Ti catalyst to 5.4% and negligible for the impregnated one.

4.2.4 CO-IR

The FT-IR spectra of adsorbed CO on the Pt/TiO_2 catalysts reduced at different reduction temperatures are shown in Figure 31. The CO linearly adsorbed on low-coordination Pt atom on edge sites and bridged-type adsorbed CO were

characterized by adsorption bands at 2056 and 1825 cm^{-1}, respectively. It has been reported that bridge-type adsorbed CO formed mainly on large Pt particles while linear-type adsorbed CO dominated on small Pt particles [1]. In this study, the ratio of Pt on corner to terrace was high due to the presence of very small Pt particle size (≤ 2 nm). In addition, the fraction of Pt terrace was decreased by reduction at high temperature, while the number of Pt-TiO_x sites increased. However, the IR spectra could not be detected on the impregnated catalysts when they were reduced at 500 ^{o}C and higher, due probably to the excessive decoration of TiO_x on Pt surface. Such results were consistent to the CO chemisorption results that all the impregnated catalysts exhibited much lower Pt active sites than the F-Pt/Ti. For the FSP-made catalysts, the adsorption band at 2056 cm^{-1} was slightly shifted to 2062 cm-1 for those reduced at 500 ^{o}C and higher. Furthermore, the adsorption band at 2088 cm-1, which corresponded to the CO adsorbed on Pt terraces Pt (111) and Pt (100) decreased with increasing reduction temperature. The peaks became very small for the F-Pt/Ti-700, corresponding to the relatively low amount of active Pt surface present as confirmed by the CO chemisorption results.

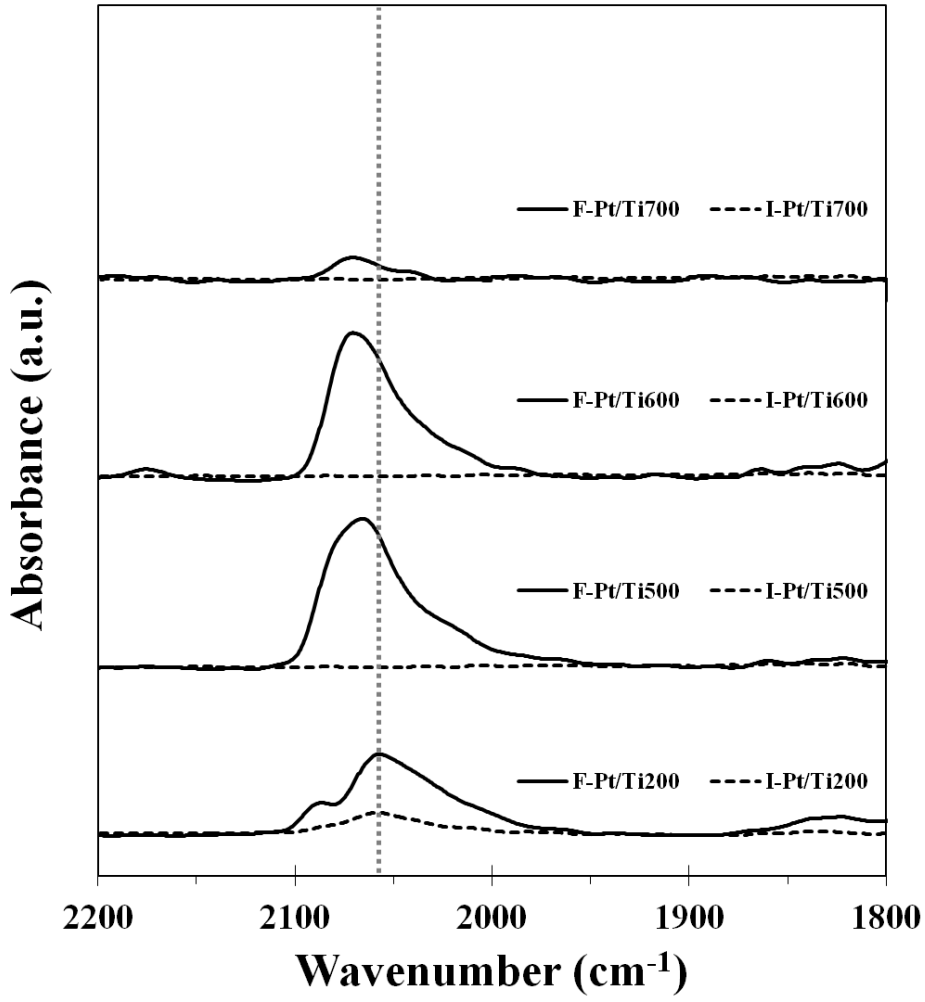

Figure 31 CO-IR results of the F-Pt/Ti and I-Pt/Ti catalysts

4.2.5 H_2-TPR

The reduction behaviors of the F-Pt/Ti and I-Pt/Ti catalysts were investigated by H_2-TPR and the results are shown in Figure 32. The I-Pt/Ti catalysts exhibited three hydrogen consumption peaks with a maximum at 220, 411, and 537 $^{\circ}$C whereas two hydrogen consumption peaks and a shoulder peak at 227, 419, and 651 °C were

observed on the F-Pt/Ti catalysts. The first peak was associated to the reduction of Pt oxide particles and the second peak was attributed to reduction of Pt species interacting with the TiO_2 support to form Pt-TiO_x interface sites [73, 74]. The hydrogen consumption above 500 °C was due to the reduction of surface capping oxygen of TiO_2. From the H_2-TPR results, the F-Pt/Ti catalyst exhibited stronger metal-support interaction than the I-Pt/Ti and lower H_2 consumption ratio of Pt/Pt-TiO_x.

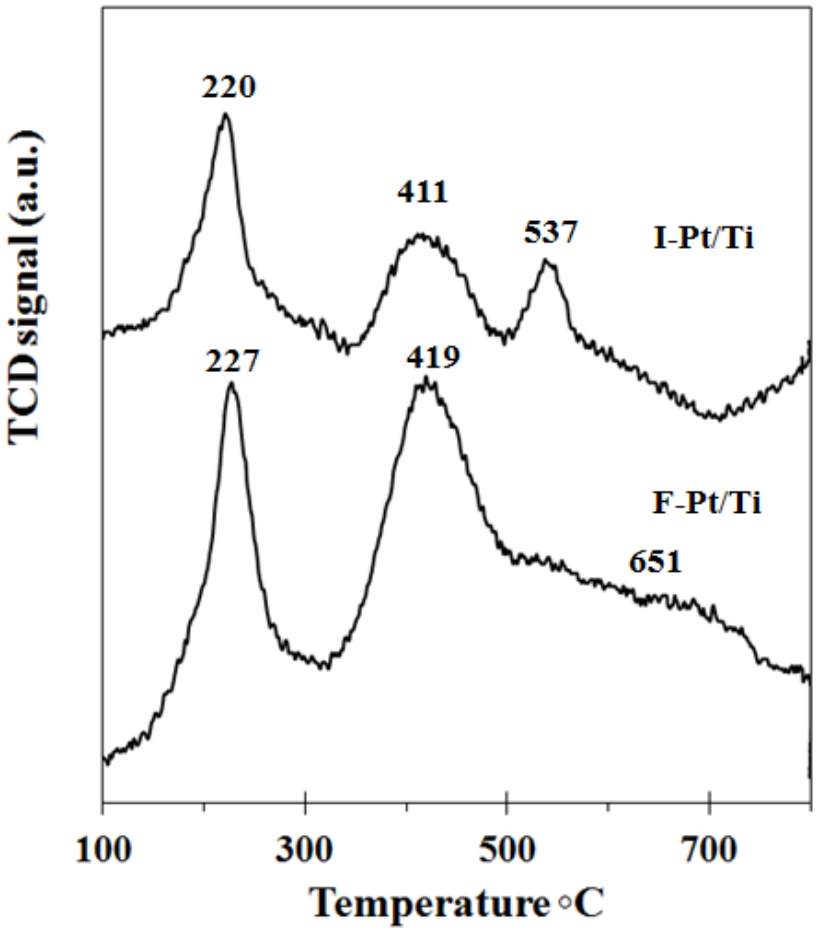

Figure 32 H_2-TPR profiles of the F-Pt/Ti and I-Pt/Ti catalysts

4.2.6 Evaluation of 3-nitrostyrene hydrogenation

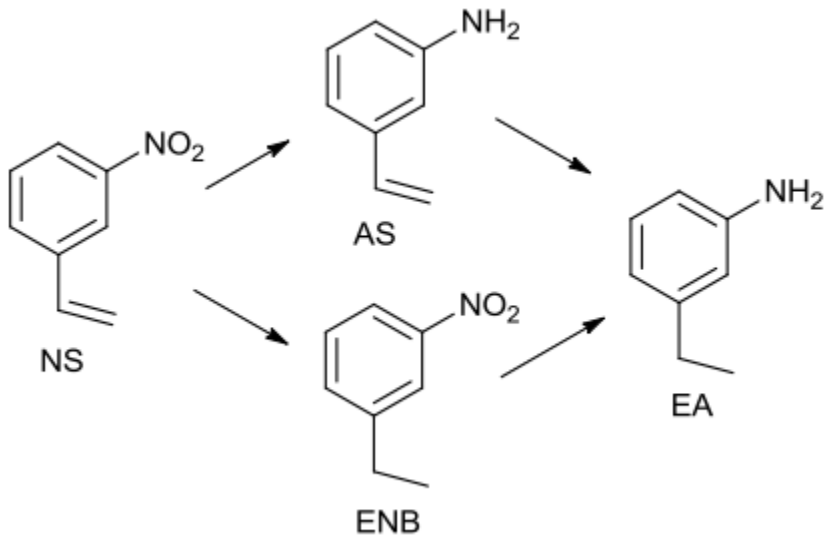

Figure 33 Hydrogenation of 3-nitrostyrene [2]

The catalytic behaviors of the Pt/TiO_2 catalysts in the liquid-phase selective hydrogenation of NS including NS conversion, product selectivity and TOF are summarized in Table 6. Under the reaction conditions used, the products of the hydrogenation of NS, as shows in Figure 33, were vinylanilene (VA), ethynitrobenzene (ENB) and ethyaniline (EA). Hydrogenation of NS is rather complex because of two major reaction pathways occurring from hydrogenation of a C=C double bond and a nitro group N=O. Figure 34 shows the possible reaction pathways for hydrogenation of nitro compounds to anilines which was proposed by Haber. He proposed two

main reaction routes as direction and condensation routes. In the direct route, nitrobenzene is hydrogenated to nitrobenzene (NB), then to phynylhydroxylamine (PHA) and to aniline (AN). In condensation route, the formation of azoxybenzene (AOB) is occurred from two intermediates azobenzene (AB) and hydrozobenzene (HAB). Another possible process for the formation of aniline is obtained from phynylhydroxylamine decomposition into nitrobenzene and aniline (as shown in step V). This diagram is based on the study of nitrobenzene hydrogenation on Ir/Carbon catalyst.

For any reduction temperature used, the F-Pt/Ti catalysts exhibited much higher catalytic activity than the I-Pt/Ti catalysts, which could be attributed to the higher Pt dispersion. However, for low reduction temperature, both Pt/TiO_2 catalysts had no favored selectivity for the possible product of the hydrogenation. The major hydrogenation products were ENB and VA without formation of intermediates hydrogenation products such as the hydroxylamine.

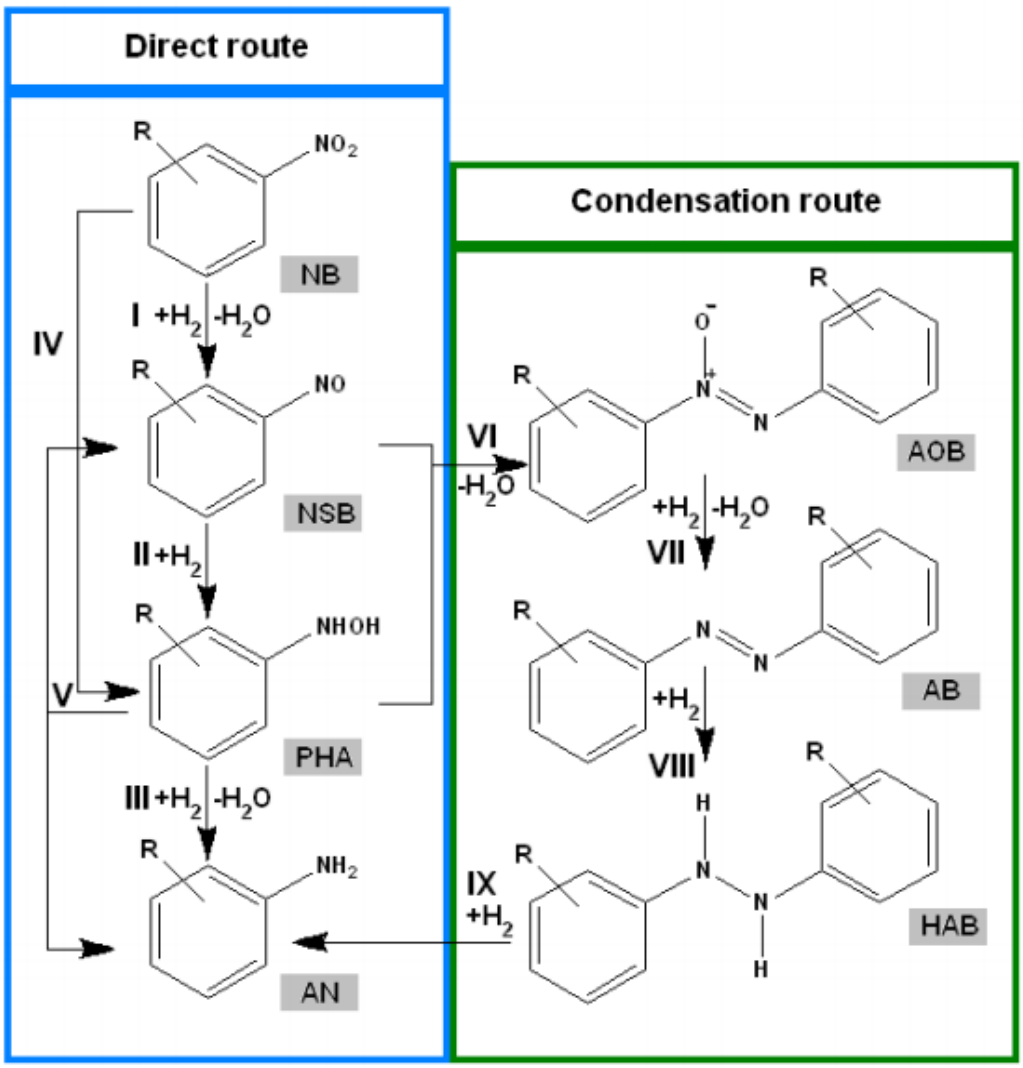

Figure 34 Shows the possible reaction pathways for hydrogenation of nitro compounds to anilines[75].

Table 6 CO chemisorption, XRD, and reaction results of the Pt/TiO_2 catalysts reduced at various

Catalyst	Red.T	CO chemisorption		XRD results		Time	Conv.	Selectivity [%]			TOF
	[℃]	D [%]	d_{Pt} [nm]	d_{xrd} [nm]	Anatase %	[min]	[%]	VA	ENB	EA	[s^{-1}]
F-Pt/Ti	200	20.1	5.6	21.0	81.0	20	61.2	39.7	47.6	12.7	34
						40	89.1	43.0	34.2	22.8	n.d.
	500	24.1	4.6	22.0	79.3	20	66.1	60.0	28.2	11.8	30
						25	73.0	64.0	22.5	13.5	n.d.
						30	99.4	53.1	10.5	36.4	n.d.
	600	22.0	4.9	22.1	73.1	20	66.2	73.3	16.0	10.4	33
						25	95.8	67.1	7.7	25.2	n.d.
	700	5.4	20.0	47.8	0.0	20	55.4	52.0	31.0	9.0	113
						30	60.0	57.4	31.8	10.8	n.d.

I-Pt/Ti	200	2.2	49.1	14.8	44.0	20	4.8	58.1	41.9	0.0	22
						120	20.3	50.0	46.6	3.4	n.d.
	500	5.3	20.4	14.8	44.0	20	49.5	72.0	19.9	8.1	96
						60	97.1	76.1	5.9	18.0	n.d.
	600	3.6	30.0	42.6	0.0	20	32.0	69.7	25.7	4.6	91
						60	91.9	72.0	9.4	18.5	n.d.
	700	n.d.	n.d.	50.3	0.0	20	26.0	70.1	22.9	7.2	n.d.

Reaction (3.4 mmol NS in 10 ml of ethanol) at 50 ^{o} C with 10 mg catalyst under 40 bar H_2 after 20 min

Determined by assuming that one molecule of CO adsorps on one molecule of Pt

Increasing reduction temperature to 500 and 600 $^{\circ}$C slightly increased the conversion of NS on F-Pt/Ti catalysts from 61 to 66%. In addition, the selectivity of VA also increased from 39 to 73%. It has been reported that the catalytic activity of Pt catalysts in the hydrogenation of NS relied on availability of Pt surface atoms but the selectivity of VA depended on the number of Pt-TiO_x interface sites [1]. The improvement of VA selectivity after reduction at higher temperature has also been reported by Fujita et al. [2]. They carried out the NS hydrogenation by using Pt/TiO_2 catalysts reduced at various reduction temperatures ranging between 200 to 450 $^{\circ}$C. However, in their observation the selectivity of VA was enhanced at the expense of activity when the reduction temperature increased. They explained that the decoration of TiO_x occurred on Pt crystalline terrace sites at high reduction temperature improved the VA selectivity. On the other hand, the growth of Pt metal size after reduction at high temperature resulted in the decreasing of the catalytic activity. In this study, both activity and selectivity of F-Pt/Ti catalyst increased with increasing reduction temperature from 200 to 600 $^{\circ}$C, while the TOF was similar at ranged in 30-33 s^{-1}. For the flame made catalysts, Pt dispersion and cluster size were not significantly changed after reduction at high temperature up to 600 $^{\circ}$C as confirmed by TEM and CO chemisorption. Higher thermal stability of the flame-made catalyst could be attributed to the higher interaction between metal and support occurred under high temperature flame environment, which has often found in the flame-made supported metal catalysts [2]. The results in this study, however,

suggest that strong interaction of Pt-TiO_x existed with little coverage of Pt active sites on the flame-made F-Pt/Ti catalysts. According to CO chemisorption and CO-IR, reduction at 500 and 600 ^{o}C not only increased the amount of Pt active sites but also lowered the Pt terrace sites. There-fore, the selectivity of VA was increased simultaneously with an increase in the NS conversion over the F-Pt/Ti-500 and F-Pt/Ti-600 catalysts. The coverage of Pt active sites appeared after reduction at 700 ^{o}C with a slight increase of Pt particle size and increase of TOF to 113 s^{-1}.

For the impregnated catalysts, the conversion of NS, selectivity of VA and TOF also increased to 49.5%, 72% and 96, respectively when the catalyst was reduced at 500 ^{o}C, com-pared to the one reduced at 200 °C (NS conversion 4.8%, VA selectivity 58% and TOF 22 s^{-1}). The CO chemisorption results showed twice Pt active sites on the I-Pt/Ti-500 compared to the I-Pt/Ti-200. The high reduction temperature seemed to be necessary to reduce the number of oxidized Pt metal and Pt terrace sites. Further increase of the reduction temperature to 600 and 700 ^{o}C, on the other hand, led to a significant catalytic activity dropped. Compared to the flame made F-Pt/Ti catalysts, the I-Pt/Ti catalysts showed lower thermal stability and an excessive coverage of Pt surface by TiO_x species which occurred at much lower temperature. The performance plot between the NS conversion and VA selectivity are shown in Figure 35. It was clearly seen that the VA selectivity did not depend on the NS conversion. The VA selectivities in NS hydrogenation were strongly determined by the

nature of Pt surface sites and the decreasing of Pt terrace atoms resulted in higher VA selectivities and the formation of Pt-TiO_x sites favored VA formation.

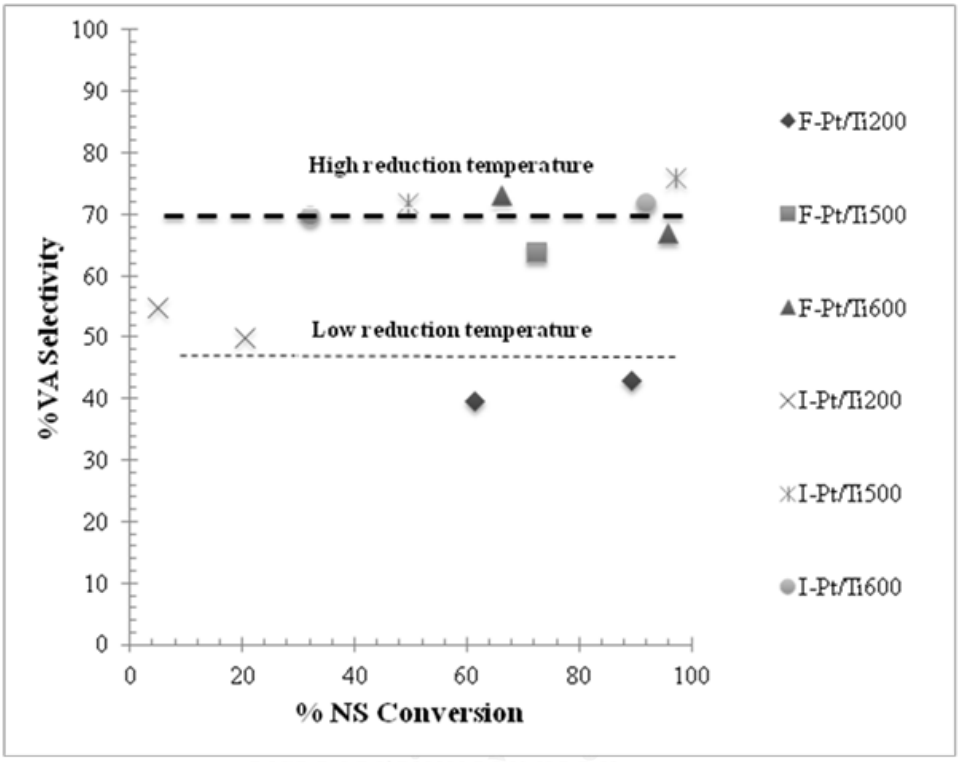

Figure 35 the performance plot between the NS conversion and VA selectivity

4.3 Influence of Co loading on Pt/TiO_2 catalyst synthesized by flame spray pyrolysis for the liquid-phase selective hydrogenation of 3-nitrostyrene

The purpose of this section is to investigate the properties of FSP-synthesized PtCo/TiO_2 in the hydrogenation of 3-nitrostyrene which was reported in this section. The catalytic performances were correlated with the physicochemical properties of the catalysts obtained by various characterization techniques such as X-ray diffraction

(XRD), N_2 Physisorption, CO pulse chemisorption, temperature program reduction (TPR), infrared spectroscopy of adsorbed CO (CO-IR), and transmission electron spectroscopy (TEM).

4.3.1 XRD and N_2 physisorption

Figure 36 shows XRD pattern of the as-prepared catalysts prepared by flame spray pyrolysis. All the synthesized samples exhibited the characteristic peaks of anatase TiO_2 at 2θ = 25° (major), 37°, 48°, 55°, 56°, 62°, 71°, and 75°. Small contaminations of rutile phase at 2θ = 28° (major), 36 °, 42°, and 57° were also observed on all flame-made catalysts. The characteristic peaks of platinum and cobalt species were not detected for all the catalysts due to low amount of metals present and/or high dispersion of these metals on the TiO_2 supports.

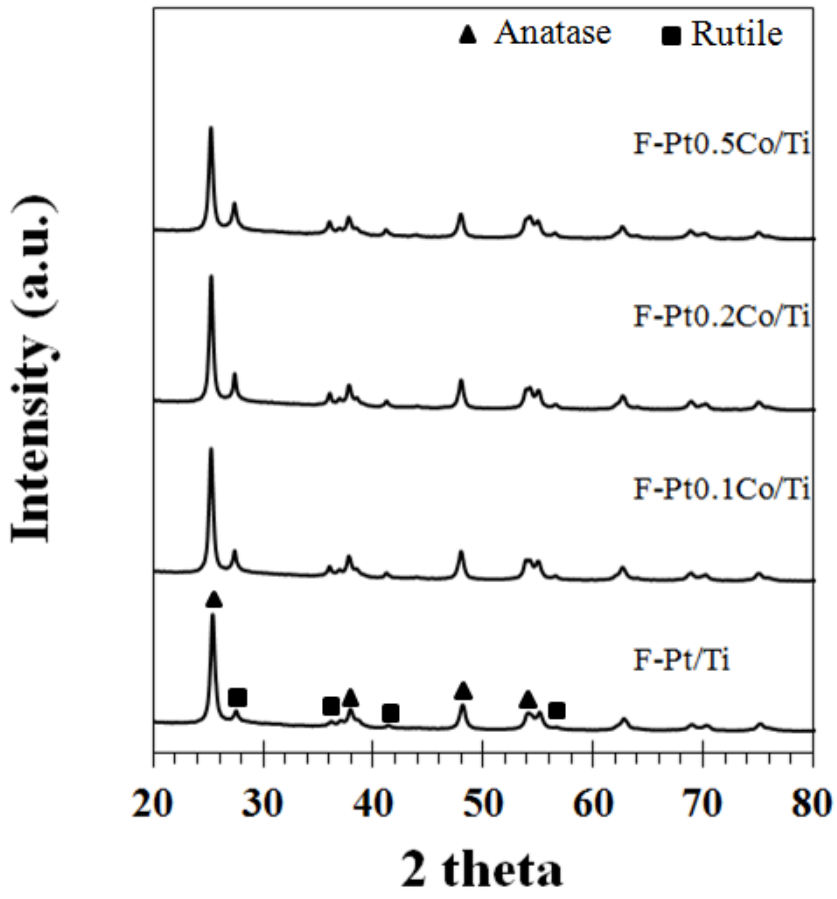

Figure 36 XRD patterns of the F-Pt/TiO_2 and F-PtCo/TiO_2 catalysts

The XRD patterns of F-Pt/Ti and F-Pt0.5Co/Ti catalysts reduced at 200 and 500 ^{o}C compared with the fresh ones. For the both catalysts, reduction at 200 and 500 ^{o}C exhibited little influence on the crystallite size and %anatase phase as shows in Figure 37 and 38.

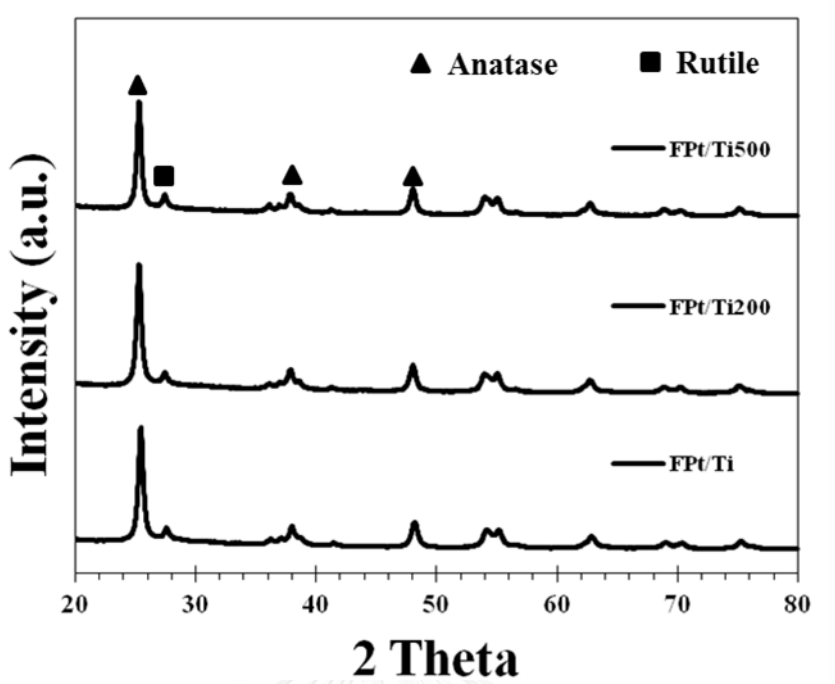

Figure 37 The XRD patterns of F-Pt/TiO_2 catalyst with various reduction temperatures

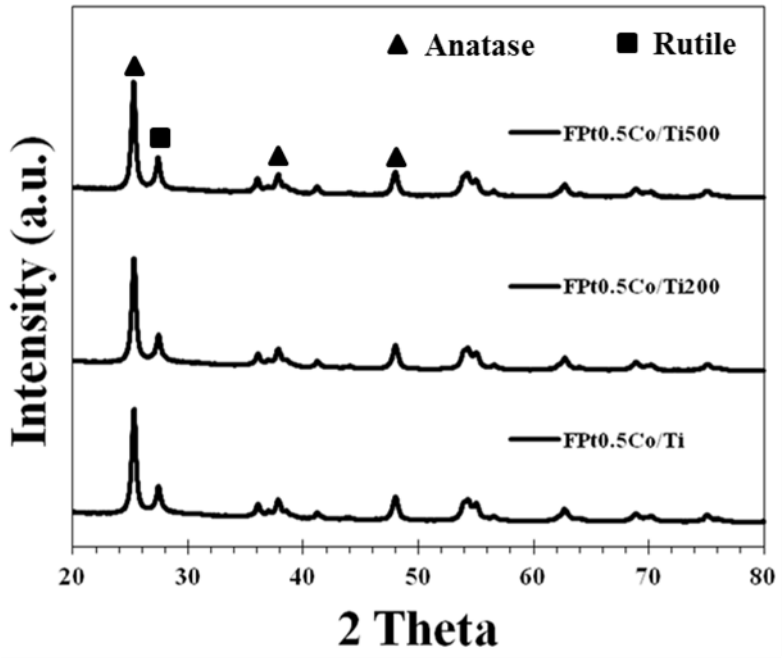

Figure 38 The XRD patterns of F-Pt0.5Co/TiO_2 catalyst with various reduction temperatures

The average crystallite size and crystalline phase composition of the TiO_2 were calculated from the XRD results according to the methods of Debye–Scherrer equation [76] and Spurr [77], respectively. The results are summarized in Table 7. Addition of Co resulted in a decrease of %anatase (%A) content of the flame-derived catalysts from 91 to 78% as Co loading contents increased from 0 to 0.3 wt%. In case of FPt/Ti and FPt0.5Co/Ti catalysts, reduction at 200 and 500 ^{o}C has little influence on the crystallite size, %anatase and surface area as shown in Table 6. The average crystallite size and BET surface area of all the catalysts were almost the same at around 20 to 23 nm and 54 to 58 m^2/g, respectively.

4.3.2 TEM

The TEM images of Pt/TiO_2 and $PtCo/TiO_2$ catalysts synthesized by FSP method are shown in Figure 39. Polyhedral particles with average size around 10 to 30 nm were found in all the samples. It was in good agreement with the crystallite size calculated from the XRD results, indicating that these TiO_2 particles were single crystalline. From the TEM micrographs, Pt/PtO or Co_xO_y metal clusters were not distinguishable from the TiO_2 in all the flame-made samples due probably to the poor contrast between the Pt, Co, and Ti atoms. It is also suggested that there was no significant influence of Co loading on the morphologies and particle size of the catalysts.

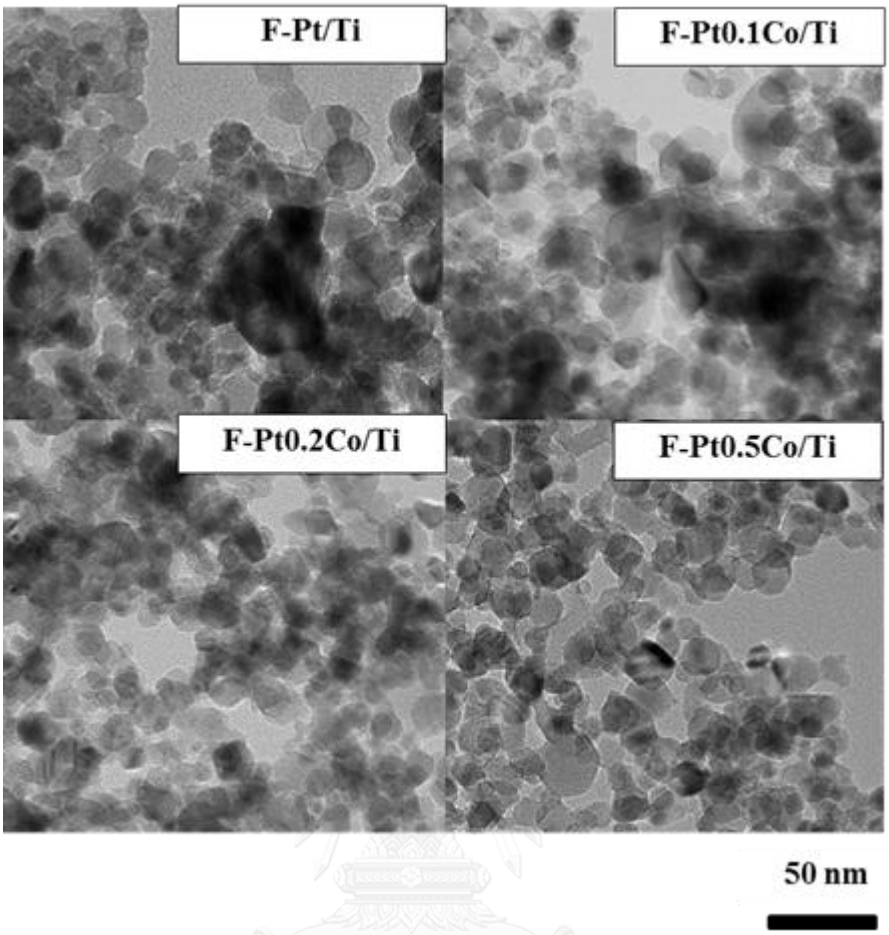

Figure 39 TEM micrographs of the all catalysts with various Co loading contents.

4.3.3 H_2-TPR

The reducibility of the flame-made Pt/TiO_2 and $PtCo/TiO_2$ catalysts were measured by TPR technique and the reduction profiles are presented in Figure 40. The mono- and bi-metallic catalysts exhibited two major peaks in the TPR profiles. The flame-made Pt/TiO_2 showed two reduction peaks at 225°C and 422°C, suggesting two types of platinum species with differences in the interaction between Pt species and the TiO_2 support. The first peak can be assigned to the reduction of Pt oxide

particles and the other peak was the reduction of Pt-TiO_x interface species interacting with the support. In the case of flame-made PtCo/TiO_2 catalysts, the reduction peaks in the TPR profiles became broader and shifted to higher reduction temperatures compared to those of Pt/TiO_2, indicating the stronger interaction between cobalt and the Pt base catalysts. Additionally, it is also possible that some cobalt particles migrated on the Pt surface, resulting in lower reducibility [78, 79].

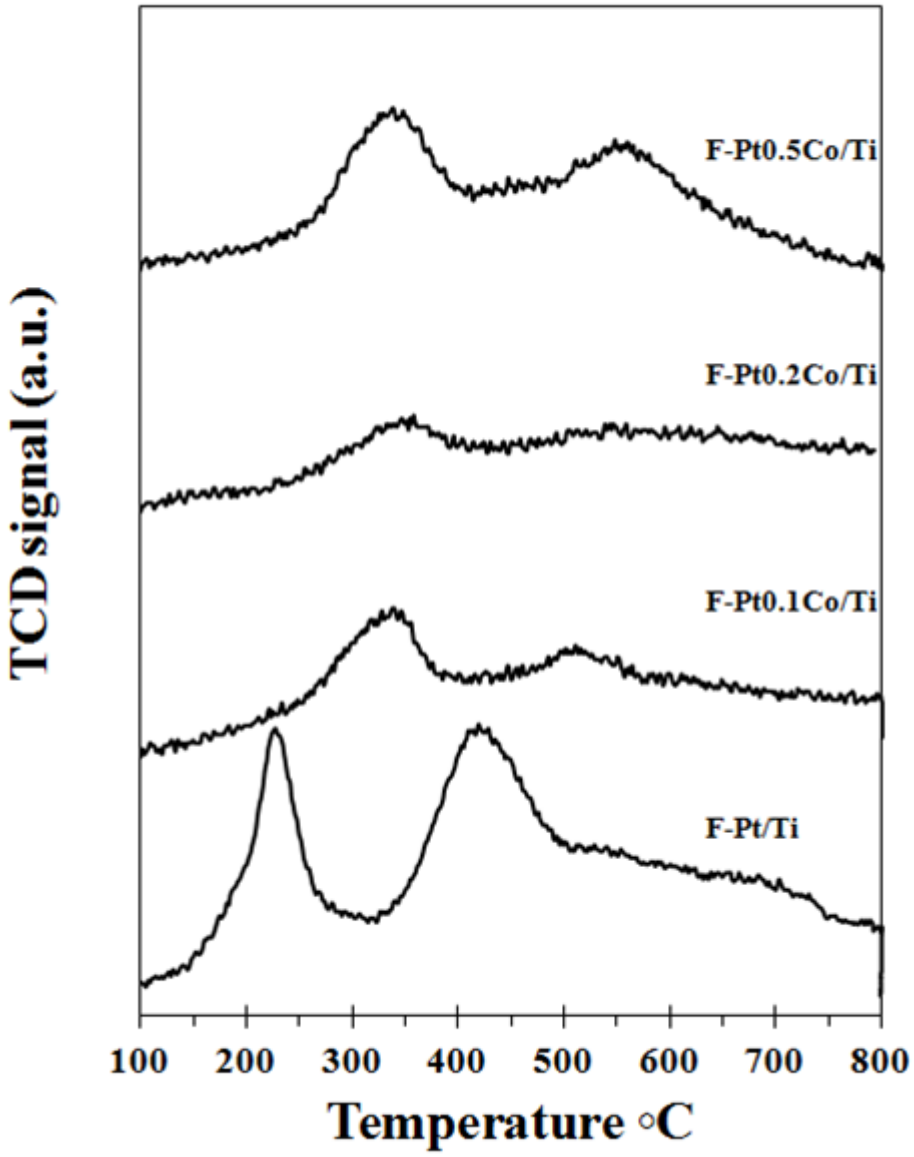

Figure 40 H_2-TPR profiles of the F-Pt/TiO_2 catalysts

4.3.4 CO-IR

The FT-IR spectra of adsorbed CO on the FPtCo/Ti and FPtCo/Ti catalysts reduced at different reduction temperatures are shown in Figure 41. The CO adsorption behaviors on Pt catalyst are shown in Figure 25 which consists of linear, Bridge and hollow CO adsorptions. Adsorption of CO on Pt catalysts can use for characterizing the Pt surface structure in nitrostyrene hydrogenation. The CO linearly adsorbed on low-coordination Pt atom on edge sites and bridged-type adsorbed CO were characterized by adsorption bands at 2056 and 1825 cm^{-1}, respectively. The IR spectra of adsorbed CO were performed to determine the relative amounts of Pt atoms located on the corners and terrace sites of the reduced flame-made Pt/TiO_2 and $PtCo/TiO_2$ catalysts at 200 and 500 ^{o}C. The results are shown in Figure 4.20. Intense CO adsorption bands corresponding to different adsorbed CO types were observed on all the catalysts. The band of bridged-type adsorbed CO was observed around 1825 cm^{-1} and the band of CO linearly adsorbed was observed at approximately 2000 - 2100 cm^{-1}. The monometallic $F\text{-}Pt/TiO_2$ catalysts mainly exhibited linear-type adsorbed CO.

The bands corresponding to the bridge-type adsorbed CO were observed from the $F\text{-}PtCo/TiO_2$ catalysts. These bands increased with increasing Co contents and reached the maximum at 0.2%wt Co. Furthermore, CO adsorbed on the low-

coordination Pt atom on surface and Pt terrace atoms were observed at 2066 cm^{-1} and 2090 cm^{-1}, respectively.

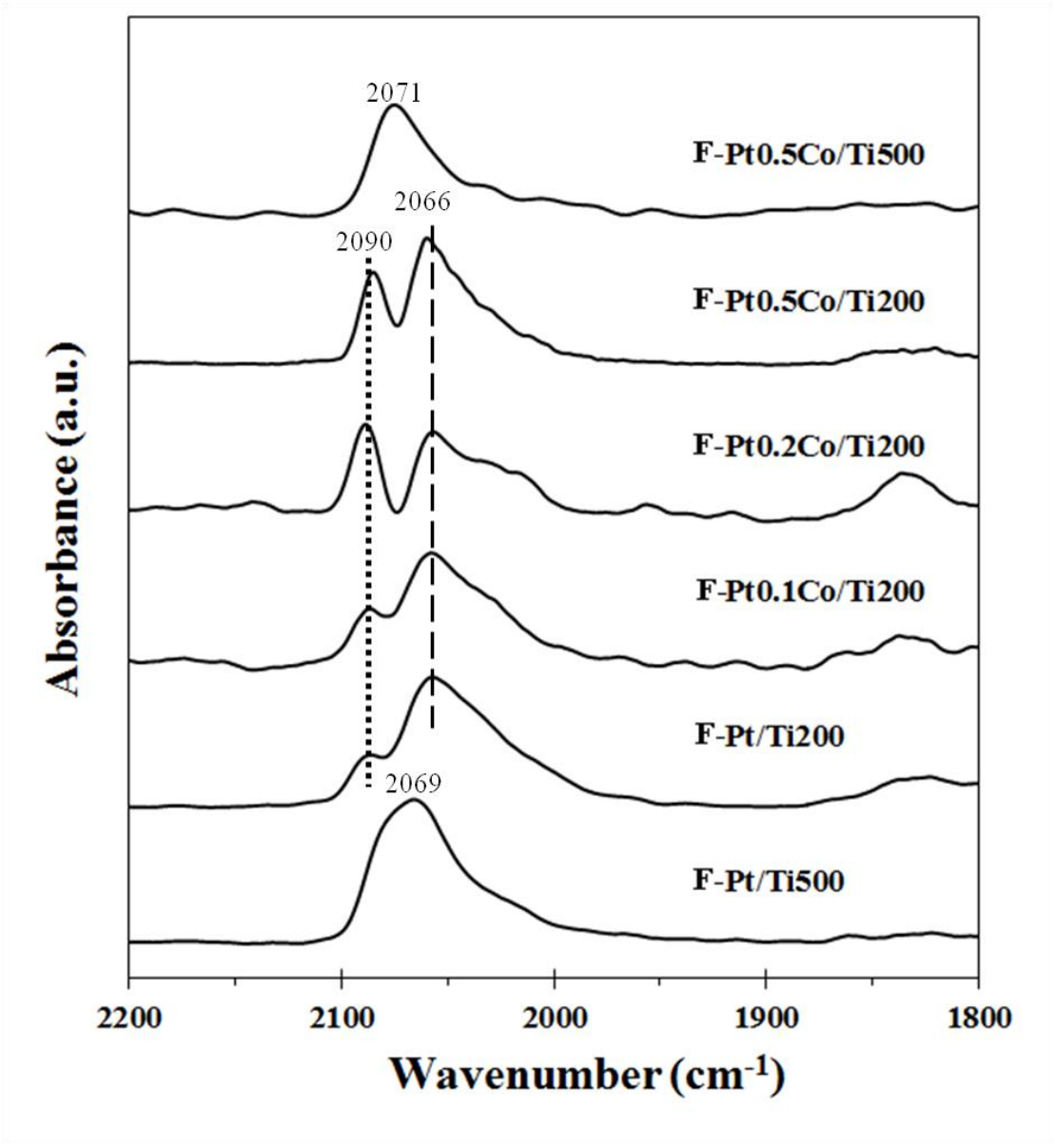

Figure 41 CO-IR results of the reduced F-Pt/TiO_2 catalysts with various Co loading contents.

It can be seen that the addition of Co facilitated the formation of Pt terrace atoms with the highest amount found over the F-Pt0.2Co/Ti catalyst. The IR adsorbed bands of F-Pt/Ti and F-Pt0.5Co/Ti catalysts were shown as a single peak at around 2071 cm^{-1} between the low-coordination Pt atoms on surface and Pt terraces due probably to the decoration of TiO_x species on these Pt species [1, 2].

4.3.5 Evaluation of 3-nitrostyrene hydrogenation

The schematic of 3-nitrostyrene hydrogenation is shown in Figure 1. Under reaction conditions used, nitrostyrene (NS) hydrogenation is an quite complex reaction, which has two main reaction pathways occurring from a hydrogenation of C=C double bond and a nitrogroup N=O. Hydrogenation of C=C double bond provides ethylnitrobenzene (ENB) and hydrogenation of a nitro group provides vinylaniline (VA). The both of hydrogenated products can be hydrogenated to be ethylaniline (EA). The catalytic behaviors of all the flame-made catalysts in the hydrogenation of 3-nitrostyrene are summarized in Table 6.

Table 7 Physiochemical and catalytic properties of the F-Pt/TiO_2 and F-PtCo/TiO_2 catalysts

Catalyst	Red. Temperature	XRD		BET	Conversion (%)	Selectivity (%)		
		% A	d_{XRD}(nm)	S (m^2/g)		VA	ENB	EA
F-Pt/Ti	200	81.0	21	58.7	61.0	39.4	47.3	13.3
	500	79.3	22	56.5	66.0	60.0	28.2	11.8
F-Pt0.1Co/Ti	200	84.8	21.4	56.8	35.7	36.6	54.3	9.1
F-Pt0.2Co/Ti	200	82.0	23.6	54.5	33.0	30.0	62.8	7.2
F-Pt0.5Co/Ti	200	78.0	21.7	54.2	33.4	33.3	59.7	7.0
	500	73.8	23.0	52.6	74.0	59.8	28.0	12.2

Reaction (3.4 mmol 3-nitrostyrene (NS) in 10 ml of ethanol) at 50 ^{o}C with 10 mg catalyst under 40 bar H_2 after 20 min

%A = weight% of anatase phase VA = vinylaniline, ENB = ethylnitrobenzene, EA = ethylaniline

It has been reported that a proper selection of the catalyst could enrich the catalytic performance while avoiding the formation of hydroxylamine intermediate [1, 34, 80]. This has been achieved over small Pt crystallites on TiO_2 support [1]. In the present study, all the flame-made catalysts showed high catalytic activity without producing hydroxylamine intermediates. However, the catalytic activity of Pt/TiO_2 catalysts was dropped by the presence of Co which could be due to the decreased reducibility of Pt oxides as supported by the H_2-TPR characterization. Over the monometallic F-Pt/Ti catalysts at low reduction temperature, the selectivity for VA was not favored (ENB/VA = 1.2). Despite their lower activities, the VA selectivity over $PtCo/TiO_2$ catalysts was not increased comparing to the monometallic Pt/TiO_2. In other words, the addition of cobalt on flame-made Pt/TiO_2 catalysts promoted the reduction of C=C double bond so that the ENB selectivity increased. The highest ENB selectivity was obtained /VA = 2.1). This behavior suggested that on the bimetallic catalysts the C=C reacted faster than the nitro group because of a preferential adsorption of C=C group on the Pt terrace atoms, as demonstrated by the CO-IR measurement in Figure 4.20.

It has been reported that an increasing of reduction temperature can increase the selectivity of VA by producing Pt-TiO_x interface sites but at the expense of catalytic activity [2]. However, in the present work higher selectivity of VA can be achieved over FSP-derived Pt/TiO_2 and $PtCo/TiO_2$ catalysts without activity drop

when the reduction temperature was increased to 500°C. The activity of both F-Pt/Ti and F-Pt0.5Co/Ti catalysts reduced at 500oC were increased by 8 and 55%, respectively comparing to those reduced at 200°C with essentially similar VA selectivities at around 60% (ENB/VA = 0.97). The catalyst reducibility would increase by higher reduction temperature, resulting in higher activities. However, a significant increase in hydrogenation activities of F-Pt0.5Co/Ti compared to F-Pt/Ti suggests an existence of strong interaction between Pt and Co atoms and/or electron transfer from Co^0 to Pt^0 on the F-Pt0.5Co/Ti catalyst [9]. It can be seen from the H_2-TPR results that addition of Co resulted in a stronger metal-support interaction as shown by a shift of reduction temperature towards higher temperature as Co loading increased. Thus, using low reduction temperature (200°C), the FSP-made bimetallic Pt-Co catalysts showed relatively low hydrogenation activities compared to the monometallic ones. When reduced at 500°C, the activity of F-Pt0.5Co/Ti surpassed that of F-Pt/Ti and those reduced at 200°C, suggesting the modification of electronic properties of Pt by Co. Higher activity of PtCo bimetallic catalysts compared to the monometallic Pt has also been reported in various hydrogenation reactions such as selective hydrogenation of citral [9], CO hydrogenation [81], and cinnamaldehyde hydrogenation [10, 12]. However, the preparation methods and reduction conditions were varied distinctively [9, 81, 82]. On the other hand, the product selectivities in NS hydrogenation were strongly determined by the nature of Pt surface sites as shown

by the CO-IR results. Increasing of Pt terrace atoms resulted in lower VA selectivities while the formation of Pt-TiO_x sites favored VA formation.

4.4 Influence of Ce loading on Pt/TiO_2 catalyst synthesized by flame spray pyrolysis and co-impregnation for the liquid-phase selective hydrogenation of 3-nitrostyrene

The purpose of this section is to investigate the properties of FSP-synthesized $PtCe/TiO_2$ in the hydrogenation of 3-nitrostyrene which was reported in this section. The catalytic performances were correlated with the physicochemical properties of the catalysts obtained by various characterization techniques such as X-ray diffraction (XRD), CO pulse chemisorption, temperature program reduction (TPR), and infrared spectroscopy of adsorbed CO (CO-IR).

4.4.1 XRD

The XRD patterns of the Pt/TiO_2 and $PtCe/TiO_2$ catalysts prepared by one-step FSP method are shown in Figure 42. The XRD patterns of the catalysts prepared by flame spray pyrolysis exhibited the characteristic peaks of anatase TiO_2 at 2θ = 25° (major), 37°, 48°, 55°, 56°, 62°, 71°, and 75°. Small contaminations of rutile phase at 2θ = 28° (major), 36°, 42°, and 57° were also observed on all flame-made catalysts. The characteristic peaks of platinum and cerium species were not detected for all the catalysts due to low amount of metals present and/or high dispersion of these metals on the TiO_2 supports.

The average crystallite size and crystalline phase composition of the TiO_2 were calculated from the XRD results according to the methods of Debye–Scherrer equation [76] and Spurr [77], respectively. The results are summarized in Table 4.4. Addition of cerium has litle effect on %anatase (%A) content and the crystallite size of the flame-derived catalysts as Co loading contents increased from 0 to 1.5 wt%.

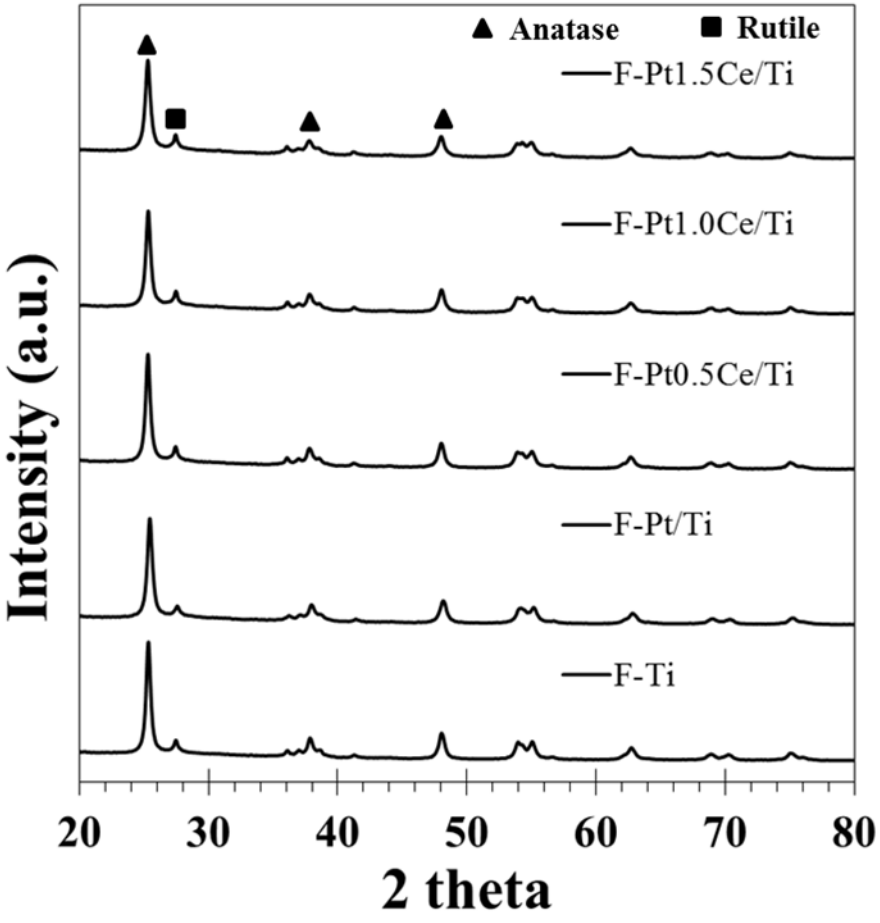

Figure 42 XRD patterns of the F-Pt/TiO_2 and F-PtCe/TiO_2 catalysts

4.4.2 H_2-TPR

The reducibility of the flame-made Pt/TiO_2 and $PtCe/TiO_2$ catalysts were measured by TPR technique and the reduction profiles are presented in Figure 43. The mono- and bi-metallic catalysts exhibited two major peaks in the TPR profiles. The flame-made Pt/TiO_2 showed two reduction peaks at 225°C and 422°C, suggesting two types of platinum species with differences in the interaction between Pt species and the TiO_2 support. The first peak can be assigned to the reduction of Pt oxide particles and the other peak was the reduction of Pt-TiO_x interface species interacting with the support. In the case of flame-made $PtCe/TiO_2$ catalysts, the reduction peaks in the TPR profiles shifted to lower reduction temperatures compared to those of F-Pt/Ti catalyst, indicating the stronger interaction between cerium and the Pt base catalysts.

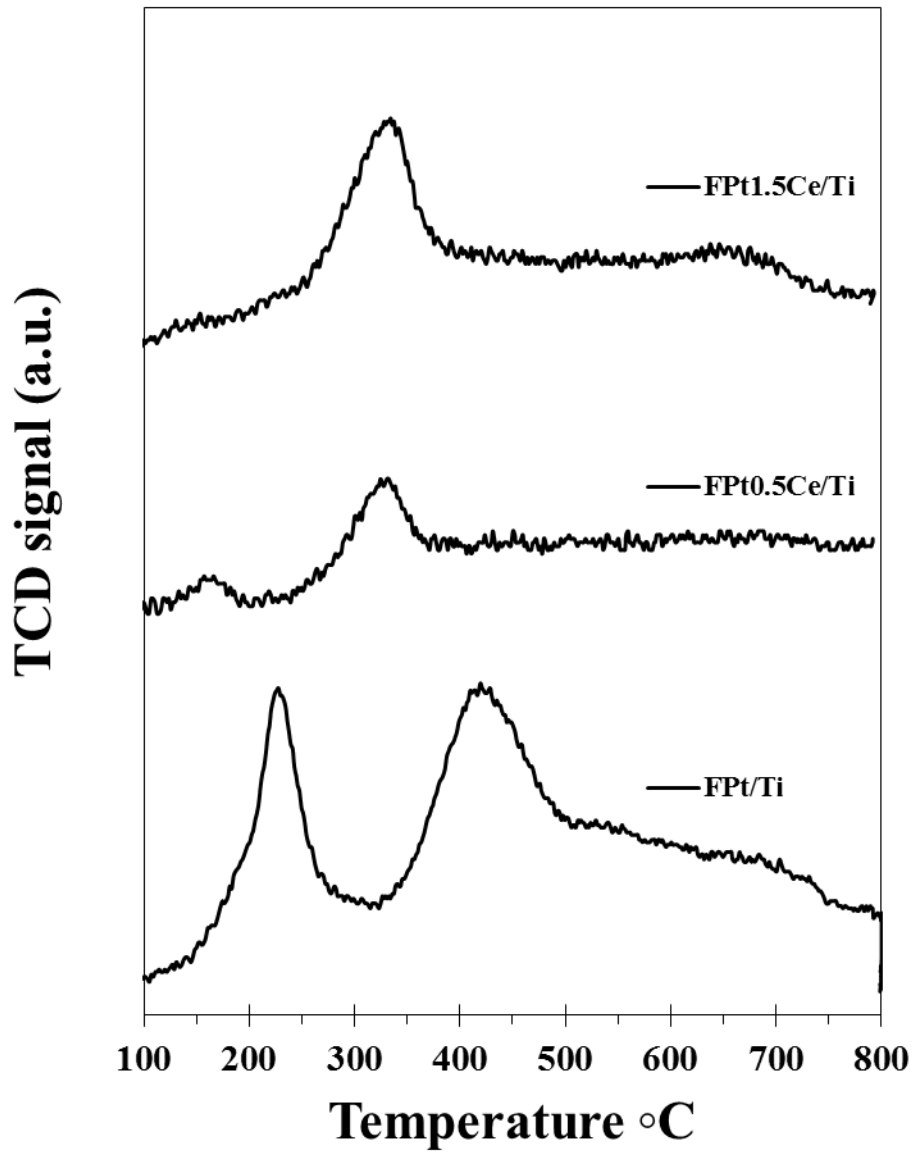

Figure 43 H_2-TPR profiles of the F-Pt/Ti and F-PtCe/Ti catalysts

4.4.3 CO-IR

The FT-IR spectra of adsorbed CO on the F-Pt/Ti and F-PtCe/Ti catalysts reduced at 200 $^{\circ}$C are shown in Figure 44. The CO adsorption behaviors on Pt

catalyst are shown in Figure 25 which consists of linear, Bridge and hollow CO adsorptions. Adsorption of CO on Pt catalysts can use for characterizing the Pt surface structure in nitrostyrene hydrogenation. The CO linearly adsorbed on low-coordination Pt atom on edge sites and bridged-type adsorbed CO were characterized by adsorption bands at 2056 and 1825 cm^{-1}, respectively. The IR spectra of adsorbed CO were performed to determine the relative amounts of Pt atoms located on the corners and terrace sites of the reduced flame-made Pt/TiO_2 and $PtCe/TiO_2$ catalysts at 200 ^{o}C. The results are shown in Figure 4.23. Intense CO adsorption bands corresponding to different adsorbed CO types were observed on all the catalysts. The band of bridged-type adsorbed CO was observed around 1825 cm^{-1} and the band of CO linearly adsorbed was observed at approximately 2000 - 2100 cm^{-1}. The monometallic F-Pt/Ti and F-PtCe/Ti catalysts mainly exhibited linear-type adsorbed CO.

The bands corresponding to the bridge-type adsorbed CO were observed from the F-PtCe/Ti catalysts. These bands decreased with increasing Ce contents that can indicated that the Pt dispersion over surface and are mostly isolated with high dispersion. The second peaks of CO adsorbed shifted to higher wavenumber by increasing of Ce content. These results indicated that the formation of Pt terrace sites increased with Ce loading.

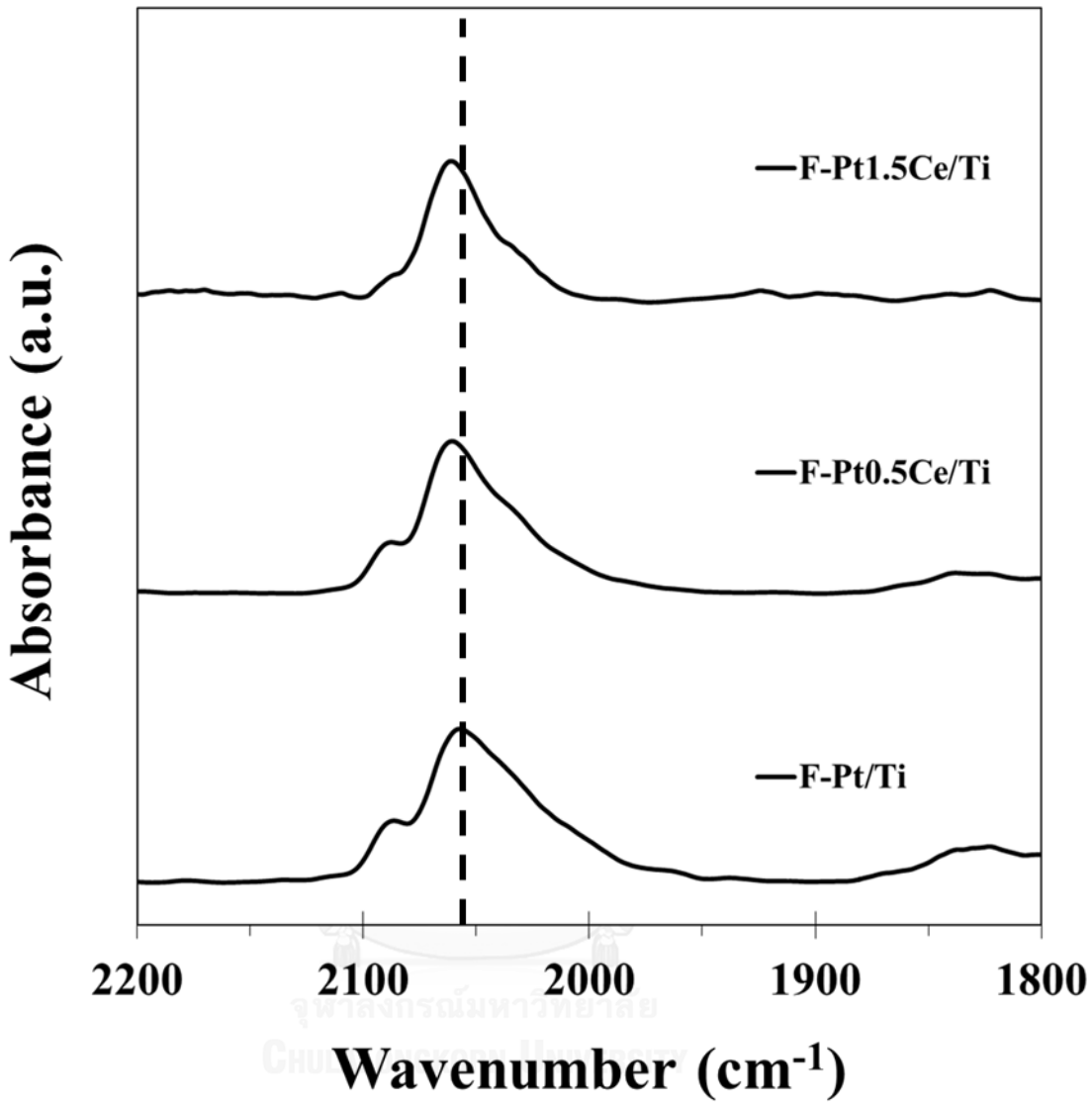

Figure 44 CO-IR results of the reduced F-Pt/TiO_2 catalysts at 200 °C with various Co loading contents.

4.4.4 CO chemisorption

CO pulse chemisorption is a powerful technique to indicate the relative amounts of active Pt metal surface on the catalyst. All catalysts samples were calculated from

CO chemisorption based on the assumption that one carbon monoxide molecule adsorbs on one Pt site and the results are shown in Table 8. The Pt dispersion on F-Pt/Ti reduced at 200 and 500 $^{\circ}$C were 20.1 and 24.1. It was found that Pt dispersion were much higher with increasing Ce content.

4.4.5 Evaluation of 3-nitrostyrene hydrogenation

Under reaction conditions used, nitrostyrene (NS) hydrogenation is a quite complex reaction, which has two main reaction pathways occurring from a hydrogenation of C=C double bond and a nitrogroup N=O. Hydrogenation of C=C double bond provides ethylnitrobenzene (ENB) and hydrogenation of a nitrogroup provides vinylaniline (VA). The both of hydrogenated products can be hydrogenated to be ethylaniline (EA). The catalytic behaviors of all the flame-made catalysts in the hydrogenation of 3-nitrostyrene are summarized in Table 7. In this study, all the flame-made catalysts showed high catalytic activity without producing hydroxylamine intermediates. However, the catalytic activity of Pt/TiO_2 catalysts was slightly decreased by the presence of Ce which could be due to the decreased H_2 consumption of Pt oxides as supported by the H_2-TPR characterization. Over the monometallic F-Pt/Ti and F-PtCe/Ti catalysts at low reduction temperature, the selectivity for VA was not favored. The ENB selectivity over PtCe/TiO_2 catalysts was increased comparing to the monometallic Pt/TiO_2. In other words, the addition of cerium on flame-made Pt/TiO_2 catalysts promoted the reduction of C=C double

bond so that the ENB selectivity increased. The highest ENB selectivity was found on F-Pt1.5Ce/Ti catalyst. This behavior suggested that on the bimetallic catalysts the C=C reacted faster than the nitro group because of a preferential adsorption of C=C group on the Pt terrace sites due to Ce metal suppressed the formation of Pt-TiO_x interface sites by forming $Ce_{1-x}T_xO_{2-y}$, determined by H_2-TPR technique [83].

It has been reported that an increasing of reduction temperature can increase the selectivity of VA by producing Pt-TiO_x interface sites but the excessive of TiO_2 decoration toward decreasing of catalytic activity [27]. However, in the present work higher selectivity of VA can be achieved on F-Pt/Ti and F-PtCe/Ti catalysts without decreasing of activity when the reduction temperature was increased to 500°C. The activity of both F-Pt/Ti and F-PtCe/Ti catalysts reduced at 500°C were increased comparing to those reduced at 200°C. On the other hand, the product selectivities in hydrogenation of nitrostyrene were strongly determined by the nature of Pt surface sites as shown by the CO-IR results. Increasing of Pt terrace atoms resulted in lower VA selectivities while the formation of Pt-TiO_x sites favored VA formation.

Table 8 Physiochemical and catalytic properties of the FSP-made Pt/TiO_2 and $PtCe/TiO_2$ catalysts

Catalyst	Red. Temperature	XRD		CO chem.	Conversion (%)	Selectivity (%)		
		% A	d_{XRD}(nm)	%D		VA	ENB	EA
F-Pt/Ti	200	81.0	21	20.1	61.0	39.4	47.3	13.3
	500	79.3	22	24.1	66.0	60.0	28.2	11.8
F-Pt0.5Ce/Ti	200	86.5	21.9	35.7	52.0	35.7	51.3	11.0
	500	n.d.	n.d.	n.d.	67.0	43.3	40.7	16.0
F-Pt1.5Ce/Ti	200	85.4	21.9	51.8	56.8	26.7	62.3	11.0
	500	n.d.	n.d.	n.d.	68.0	59.3	25.0	15.7

Reaction (3.4 mmol 3-nitrostyrene (NS) in 10 ml of ethanol) at 50 ^{o}C with 10 mg catalyst under 40 bar H_2 after 20 min

%A = weight% of anatase phase VA = vinylaniline, ENB = ethylnitrobenzene, EA = ethylaniline

CHAPTER V

Conclusions and Recommendations

5.1 Conclusion

5.1.1 Influence of preparation method on Pt/TiO_2 and catalysts for the liquid-phase selective hydrogenation of 3-nitrostyrene

The effect of preparation methods on the physicochemical and catalytic properties of Pt/TiO_2 catalysts were investigated in the hydrogenation of 3-nitrostyrene. The F-Pt/Ti catalysts showed higher Pt dispersion and catalytic activity for liquid phase hydrogenation of 3-nitrostyrene. The preparation of Pt/TiO_2 catalysts on I-Pt/STi showed higher selectivity of VA than I-Pt/FTi catalyst due to higher formation of Pt low coordination as show in CO-IR results. However, I-Pt/FTi catalyst exhibited higher activity than I-Pt/STi catalyst because of higher Pt dispersion.

5.1.2 Influence of reduction temperature on flame-made Pt/TiO_2 and impregnated catalysts for the liquid-phase selective hydrogenation of 3-nitrostyrene

The effect reduction temperatures on the physicochemical and catalytic properties of Pt/TiO_2 catalysts were investigated in the hydrogenation of 3-nitrostyrene. The F-Pt/Ti catalysts showed higher Pt dispersion and catalytic activity for liquid phase hydrogenation of 3-nitrostyrene. Reduction at high temperature (500-

600°C) resulted in higher Pt dispersion, higher Pt-Ti interface sites and, hence, higher hydrogenation activities and higher selectivity to VA. The reducing Pt terrace atoms with increasing of reduction temperature can improve the VA selectivity without activity drop. The preparation of Pt/TiO_2 catalysts by FSP method prevents an excessive coverage of Pt surface by TiO_x species. We proposed the mechanism on FPt/TiO_2 catalysts in Figure 45.

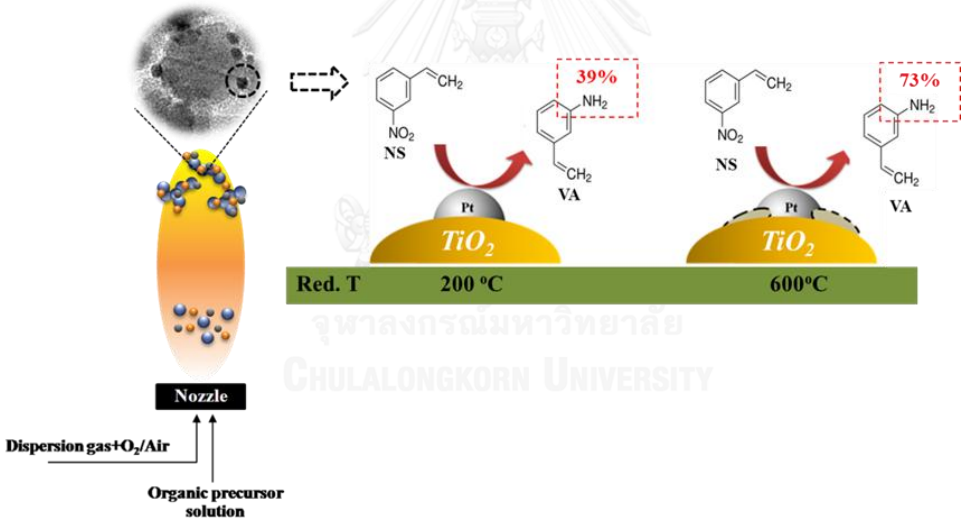

Figure 45 mechanism of 3-nitrostyrene hydrogenation over F-Pt/Ti catalyst.

5.1.3 Influence of Co loading on Pt/TiO_2 catalyst synthesized by flame spray pyrolysis for the liquid-phase selective hydrogenation of 3-nitrostyrene

The effect of cobalt on the physiochemical and catalytic properties of flame-synthesized Pt-Co/TiO_2 catalysts was investigated in the hydrogenation of 3-nitrostyrene. When reduced at 200°C, the addition of cobalt resulted in an increase ratio of CO adsorbed on Pt terrace to corner atoms, hence the ENB selectivity increased with the maximum at 0.2%wt Co (ENB/VA = 2.1). However, the NS conversion and VA selectivity of Pt-Co/TiO_2 was drastically increased and surpassed that of monometallic Pt/TiO_2 and the Pt-Co/TiO_2 reduced at 200°C, suggesting the modification of electronic properties of Pt by Co and the formation of Pt-TiO_x sites (as confirmed by CO-IR results). We proposed the mechanism on FPtCo/TiO_2 catalysts in Figure 46.

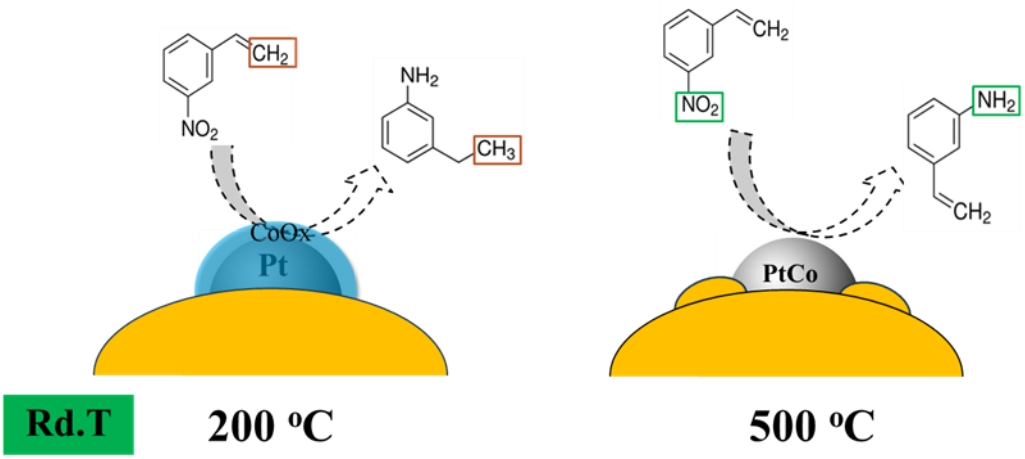

Figure 46 mechanism of 3-nitrostyrene hydrogenation over F-PtCo/Ti catalyst.

5.1.4 Influence of Ce loading on Pt/TiO_2 catalyst synthesized by flame spray pyrolysis and co-impregnation for the liquid-phase selective hydrogenation of 3-nitrostyrene

The effect of cerium on the physiochemical and catalytic properties of flame-synthesized Pt-Ce/TiO_2 catalysts was investigated in the hydrogenation of 3-nitrostyrene. When reduced at 200°C, the addition of cerium resulted in an decrease of CO adsorbed bridged type and decrease the formation of Pt terrace sites, but the ENB selectivity increased with the maximum at 1.5 %wt Ce. It should be noted that addition of Ce can lower interaction between Pt and TiO_2 resulting in the decreasing of catalytic performance. However, the VA selectivity of F-PtCe/Ti was increased with increasing of reduction temperature, suggesting the modification of Pt surface by the decoration of TiO_2. We proposed the mechanism on FPtCe/TiO_2 catalysts in Figure 47.

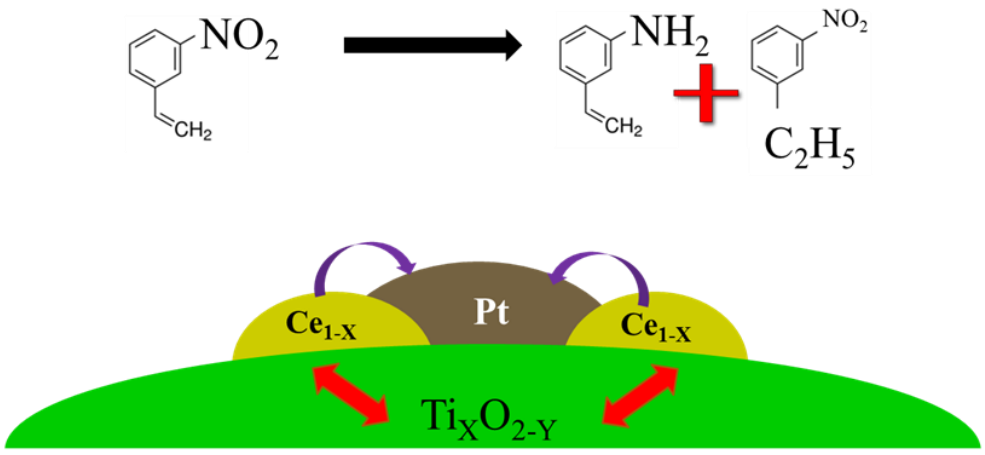

Possible formation: $Pt/Ce_{1-x}T_xO_{2-y}$

Figure 47 mechanism of 3-nitrostyrene hydrogenation over F-PtCe/Ti catalyst.

5.2 Recommendation

The formation of PtCo and PtCe alloy in $PtCo/TiO_2$ and $PtCe/TiO_2$ catalysts should be confirmed by STEM technique. According to the study by Stobel et al [27]. The Selection of promoter for Pt/TiO_2 catalyst in hydrogenation of 3-nitrostyrene should be the elements which have higher electronegativity than Pt such as Pb or N.

REFERENCES

[1] A. Corma, P. Serna, P. Concepción, J.J. Calvino, Transforming Nonselective into Chemoselective Metal Catalysts for the Hydrogenation of Substituted Nitroaromatics, Journal of the American Chemical Society, 130 (2008) 8748-8753.

[2] S.-i. Fujita, H. Yoshida, K. Asai, X. Meng, M. Arai, Selective hydrogenation of nitrostyrene to aminostyrene over Pt/TiO2 catalysts: Effects of pressurized carbon dioxide and catalyst preparation conditions, The Journal of Supercritical Fluids, 60 (2011) 106-112.

[3] M. Makosch, W.-I. Lin, V. Bumbálek, J. Sá, J.W. Medlin, K. Hungerbühler, J.A. van Bokhoven, Organic Thiol Modified Pt/TiO2 Catalysts to Control Chemoselective Hydrogenation of Substituted Nitroarenes, ACS Catalysis, 2 (2012) 2079-2081.

[4] H.-U. Blaser, H. Steiner, M. Studer, Selective Catalytic Hydrogenation of Functionalized Nitroarenes: An Update, ChemCatChem, 1 (2009) 210-221.

[5] R.M. Deshpande, A.N. Mahajan, M.M. Diwakar, P.S. Ozarde, R.V. Chaudhari, Chemoselective Hydrogenation of Substituted Nitroaromatics Using Novel Water-Soluble Iron Complex Catalysts, The Journal of Organic Chemistry, 69 (2004) 4835-4838.

[6] G.S. Samuelsen, V.L. Garik, G.B.L. Smith, The Hydrogenation of Nitro Compounds with Raney Nickel Treated with Chloroplatinic Acid and with Alkali1, Journal of the American Chemical Society, 72 (1950) 3872-3874.

[7] M.J. Beier, J.-M. Andanson, A. Baiker, Tuning the Chemoselective Hydrogenation of Nitrostyrenes Catalyzed by Ionic Liquid-Supported Platinum Nanoparticles, ACS Catalysis, 2 (2012) 2587-2595.

[8] U.B. Siegrist, Peter; Blaser, Hans-Ulrich; Studer, Martin, The selective hydrogenation of functionalized nitroarenes: new catalytic systems, Chemical Industries 75 (1998) 207-219.

[9] N.M. Bertero, A.F. Trasarti, B. Moraweck, A. Borgna, A.J. Marchi, Selective liquid-phase hydrogenation of citral over supported bimetallic Pt–Co catalysts, Applied Catalysis A: General, 358 (2009) 32-41.

[10] Y. Li, Z.-G. Li, R.-X. Zhou, Bimetallic Pt-Co catalysis on carbon nanotubes for the selective hydrogenation of cinnamaldehyde to cinnamyl alcohol: Preparation and characterization, Journal of Molecular Catalysis A: Chemical, 279 (2008) 140-146.
[11] A. Borgna, B.G. Anderson, A.M. Saib, H. Bluhm, M. Hävecker, A. Knop-Gericke, A.E.T. Kuiper, Y. Tamminga, J.W. Niemantsverdriet, Pt–Co/SiO2 Bimetallic Planar Model Catalysts for Selective Hydrogenation of Crotonaldehyde, The Journal of Physical Chemistry B, 108 (2004) 17905-17914.
[12] W. Yu, Y. Wang, H. Liu, W. Zheng, Preparation and characterization of polymer-protected PtCo bimetallic colloids and their catalytic properties in the selective hydrogenation of cinnamaldehyde, Journal of Molecular Catalysis A: Chemical, 112 (1996) 105-113.
[13] N. Mahata, F. Gonçalves, M.F.R. Pereira, J.L. Figueiredo, Selective hydrogenation of cinnamaldehyde to cinnamyl alcohol over mesoporous carbon supported Fe and Zn promoted Pt catalyst, Applied Catalysis A: General, 339 (2008) 159-168.
[14] H. Vu, F. Gonçalves, R. Philippe, E. Lamouroux, M. Corrias, Y. Kihn, D. Plee, P. Kalck, P. Serp, Bimetallic catalysis on carbon nanotubes for the selective hydrogenation of cinnamaldehyde, Journal of Catalysis, 240 (2006) 18-22.
[15] F. Zhao, Y. Ikushima, M. Chatterjee, O. Sato, M. Arai, Hydrogenation of an α,β-unsaturated aldehyde catalyzed with ruthenium complexes with different fluorinated phosphine compounds in supercritical carbon dioxide and conventional organic solvents, The Journal of Supercritical Fluids, 27 (2003) 65-72.
[16] A.B. Merlo, B.F. Machado, V. Vetere, J.L. Faria, M.L. Casella, PtSn/SiO2 catalysts prepared by surface controlled reactions for the selective hydrogenation of cinnamaldehyde, Applied Catalysis A: General, 383 (2010) 43-49.
[17] S. Pisduangdaw, J. Panpranot, C. Chaisuk, K. Faungnawakij, O. Mekasuwandumrong, Flame sprayed tri-metallic Pt–Sn–X/Al2O3 catalysts (X = Ce, Zn, and K) for propane dehydration, Catalysis Communications, 12 (2011) 1161-1165.
[18] S. Bhogeswararao, D. Srinivas, Intramolecular selective hydrogenation of cinnamaldehyde over CeO2–ZrO2-supported Pt catalysts, Journal of Catalysis, 285 (2012) 31-40.

[19] B. Bachiller-Baeza, I. Rodríguez-Ramos, A. Guerrero-Ruiz, Influence of Mg and Ce addition to ruthenium based catalysts used in the selective hydrogenation of α,β-unsaturated aldehydes, Applied Catalysis A: General, 205 (2001) 227-237.
[20] R. Zheng, M.D. Porosoff, J.L. Weiner, S. Lu, Y. Zhu, J.G. Chen, Controlling hydrogenation of CO and CC bonds in cinnamaldehyde using silica supported Co-Pt and Cu-Pt bimetallic catalysts, Applied Catalysis A: General, 419–420 (2012) 126-132.
[21] B. Moraweck, R. Fréty, G. Pecchi, M. Morales, P. Reyes, Characterization and catalytic activity of Al2O3-supported Pt-Co catalysts, Catalysis Letters, 43 (1997) 85-89.
[22] S. Pisduangdaw, J. Panpranot, C. Methastidsook, C. Chaisuk, K. Faungnawakij, P. Praserthdam, O. Mekasuwandumrong, Characteristics and catalytic properties of Pt–Sn/Al2O3 nanoparticles synthesized by one-step flame spray pyrolysis in the dehydrogenation of propane, Applied Catalysis A: General, 370 (2009) 1-6.
[23] C. Chaisuk, P. Boonpitak, J. Panpranot, O. Mekasuwandumrong, Effects of Co dopants and flame conditions on the formation of Co/ZrO2 nanoparticles by flame spray pyrolysis and their catalytic properties in CO hydrogenation, Catalysis Communications, 12 (2011) 917-922.
[24] G.L. Chiarello, I. Rossetti, L. Forni, Flame-spray pyrolysis preparation of perovskites for methane catalytic combustion, Journal of Catalysis, 236 (2005) 251-261.
[25] G. Liu, J. Li, K. Yang, W. Tang, H. Liu, J. Yang, R. Yue, Y. Chen, Effects of cerium incorporation on the catalytic oxidation of benzene over flame-made perovskite La1−xCexMnO3 catalysts, Particuology.
[26] C. Chaisuk, A. Wehatoranawee, S. Preampiyawat, S. Netiphat, A. Shotipruk, O. Mekasuwandumrong, Preparation and characterization of CeO2/TiO2 nanoparticles by flame spray pyrolysis, Ceramics International, 37 (2011) 1459-1463.
[27] R. Strobel, F. Krumeich, W.J. Stark, S.E. Pratsinis, A. Baiker, Flame spray synthesis of Pd/Al2O3 catalysts and their behavior in enantioselective hydrogenation, Journal of Catalysis, 222 (2004) 307-314.

[28] R. Strobel, W.J. Stark, L. Mädler, S.E. Pratsinis, A. Baiker, Flame-made platinum/alumina: structural properties and catalytic behaviour in enantioselective hydrogenation, Journal of Catalysis, 213 (2003) 296-304.
[29] R. Kavitha, S. Meghani, V. Jayaram, Synthesis of titania films by combustion flame spray pyrolysis technique and its characterization for photocatalysis, Materials Science and Engineering: B, 139 (2007) 134-140.
[30] M.O. Symalla, A. Drochner, H. Vogel, R. Büchel, S.E. Pratsinis, A. Baiker, Structure and NOx storage behaviour of flame-made BaCO3 and Pt/BaCO3 nanoparticles, Applied Catalysis B: Environmental, 89 (2009) 41-48.
[31] H. Debus, XXXI.-On the conversion of prussic acid into methylamine, Journal of the Chemical Society, 16 (1863) 249-260.
[32] K.-i. Shimizu, Y. Miyamoto, T. Kawasaki, T. Tanji, Y. Tai, A. Satsuma, Chemoselective Hydrogenation of Nitroaromatics by Supported Gold Catalysts: Mechanistic Reasons of Size- and Support-Dependent Activity and Selectivity, The Journal of Physical Chemistry C, 113 (2009) 17803-17810.
[33] M. Boronat, P. Concepción, A. Corma, S. González, F. Illas, P. Serna, A Molecular Mechanism for the Chemoselective Hydrogenation of Substituted Nitroaromatics with Nanoparticles of Gold on TiO2 Catalysts: A Cooperative Effect between Gold and the Support, Journal of the American Chemical Society, 129 (2007) 16230-16237.
[34] A. Corma, P. Serna, Chemoselective Hydrogenation of Nitro Compounds with Supported Gold Catalysts, Science, 313 (2006) 332-334.
[35] H. Yoshida, K. Kato, J. Wang, X. Meng, S. Narisawa, S.-i. Fujita, Z. Wu, F. Zhao, M. Arai, Hydrogenation of Nitrostyrene with a Pt/TiO2 Catalyst in CO2-Dissolved Expanded Polar and Nonpolar Organic Liquids: Their Macroscopic and Microscopic Features, The Journal of Physical Chemistry C, 115 (2011) 2257-2267.
[36] R.M. Rioux, H. Song, M. Grass, S. Habas, K. Niesz, J.D. Hoefelmeyer, P. Yang, G.A. Somorjai, Monodisperse platinum nanoparticles of well-defined shape: synthesis, characterization, catalytic properties and future prospects, Top Catal, 39 (2006) 167-174.

[37] T. Wang, G. Mpourmpakis, W.W. Lonergan, D.G. Vlachos, J.G. Chen, Effect of oxide supports in stabilizing desirable Pt-Ni bimetallic structures for hydrogenation and reforming reactions, Physical Chemistry Chemical Physics, 15 (2013) 12156-12164.
[38] O.I. Arabi-Katbi, K. Wegner, S.E. Pratsinis, Aerosol synthesis of titania nanoparticles: Effect of flame orientation and configuration, Annales de Chimie Science des Matériaux, 27 (2002) 37-46.
[39] H.S. Hoffmann, P.B. Staudt, T.M.H. Costa, C.C. Moro, E.V. Benvenutti, FTIR study of the electronic metal–support interactions on platinum dispersed on silica modified with titania, Surface and Interface Analysis, 33 (2002) 631-634.
[40] T. Chafik, O. Dulaurent, J.L. Gass, D. Bianchi, Heat of adsorption of carbon monoxide on a Pt/Rh/CeO2/Al2O3 three-way catalyst using in-situ infrared spectroscopy at high temperatures, Journal of Catalysis, 179 (1998) 503-514.
[41] O. Dulaurent, D. Bianchi, Adsorption isobars for CO on a Pt/Al2O3 catalyst at high temperatures using FTIR spectroscopy: isosteric heat of adsorption and adsorption model, Applied Catalysis A: General, 196 (2000) 271-280.
[42] H.K.a.J.W. G. Ertl, Handbook of Heterogeneous Catalysis, 1 (1997).
[43] J.A. Schwarz, C. Contescu, A. Contescu, Methods for Preparation of Catalytic Materials, Chemical Reviews, 95 (1995) 477-510.
[44] R. Strobel, A. Alfons, S.E. Pratsinis, Aerosol flame synthesis of catalysts, Advanced Powder Technology, 17 (2006) 457-480.
[45] G.D. Ulrich, Flame synthesis of fine particles, Chemical and Engineering News, 62 (1984) 22–29
[46] P. Kathirvel, J. Chandrasekaran, D. Manoharan, S. Kumar, Preparation and characterization of alpha alumina nanoparticles by in-flight oxidation of flame synthesis, Journal of Alloys and Compounds, 590 (2014) 341-345.
[47] B. Guo, H. Yim, Z.-P. Luo, Formation of alumina nanofibers in carbon-containing coflow laminar diffusion flames, Journal of Aerosol Science, 40 (2009) 379-384.
[48] M. Aromaa, A. Arffman, H. Suhonen, J. Haapanen, J. Keskinen, M. Honkanen, J.-P. Nikkanen, E. Levänen, M.E. Messing, K. Deppert, H. Teisala, M. Tuominen, J. Kuusipalo, M. Stepien, J.J. Saarinen, M. Toivakka, J.M. Mäkelä, Atmospheric synthesis of

superhydrophobic TiO2 nanoparticle deposits in a single step using Liquid Flame Spray, Journal of Aerosol Science, 52 (2012) 57-68.
[49] T. Johannessen, S.E. Pratsinis, H. Livbjerg, Computational fluid-particle dynamics for the flame synthesis of alumina particles, Chemical Engineering Science, 55 (2000) 177-191.
[50] O. Mekasuwandumrong, S. Phothakwanpracha, B. Jongsomjit, A. Shotipruk, J. Panpranot, Influence of flame conditions on the dispersion of Pd on the flame spray-derived Pd/TiO2 nanoparticles, Powder Technology, 210 (2011) 328-331.
[51] B. Pongthawornsakun, S.-i. Fujita, M. Arai, O. Mekasuwandumrong, J. Panpranot, Mono- and bi-metallic Au–Pd/TiO2 catalysts synthesized by one-step flame spray pyrolysis for liquid-phase hydrogenation of 1-heptyne, Applied Catalysis A: General, 467 (2013) 132-141.
[52] N. Tamaekong, C. Liewhiran, A. Wisitsoraat, S. Phanichphant, Acetylene sensor based on Pt/ZnO thick films as prepared by flame spray pyrolysis, Sensors and Actuators B: Chemical, 152 (2011) 155-161.
[53] P. Pawinrat, O. Mekasuwandumrong, J. Panpranot, Synthesis of Au–ZnO and Pt–ZnO nanocomposites by one-step flame spray pyrolysis and its application for photocatalytic degradation of dyes, Catalysis Communications, 10 (2009) 1380-1385.
[54] G.L. Chiarello, I. Rossetti, L. Forni, P. Lopinto, G. Migliavacca, Solvent nature effect in preparation of perovskites by flame pyrolysis: 2. Alcohols and alcohols + propionic acid mixtures, Applied Catalysis B: Environmental, 72 (2007) 227-232.
[55] Y. Zhai, J. Xiong, C. Li, X. Xu, G. Luo, Influence of preparation method on performance of a metal supported perovskite catalyst for combustion of methane, Journal of Rare Earths, 28 (2010) 54-58.
[56] R. Mueller, L. Mädler, S.E. Pratsinis, Nanoparticle synthesis at high production rates by flame spray pyrolysis, Chemical Engineering Science, 58 (2003) 1969-1976.
[57] L. Mädler, W.J. Stark, S.E. Pratsinis, Flame-made ceria nanoparticles, Journal of Materials Research, 17 (2002) 1356-1362.
[58] L. Mädler, H.K. Kammler, R. Mueller, S.E. Pratsinis, Controlled synthesis of nanostructured particles by flame spray pyrolysis, Journal of Aerosol Science, 33 (2002) 369-389.

[59] H.K. Kammler, R. Mueller, O. Senn, S.E. Pratsinis, Synthesis of silica-carbon particles in a turbulent H2-air flame aerosol reactor, AIChE Journal, 47 (2001) 1533-1543.

[60] R. Mueller, H.K. Kammler, K. Wegner, S.E. Pratsinis, OH surface density of SiO2 and TiO2 by thermogravimetric analysis, Langmuir, 19 (2003) 160-165.

[61] G. Liu, R. Yue, Y. Jia, Y. Ni, J. Yang, H. Liu, Z. Wang, X. Wu, Y. Chen, Catalytic oxidation of benzene over Ce–Mn oxides synthesized by flame spray pyrolysis, Particuology, 11 (2013) 454-459.

[62] N. van Vegten, T. Baidya, F. Krumeich, W. Kleist, A. Baiker, Flame-made MgAl2−xMxO4 (M = Mn, Fe, Co) mixed oxides: Structural properties and catalytic behavior in methane combustion, Applied Catalysis B: Environmental, 97 (2010) 398-406.

[63] B. Schimmoeller, R. Delaigle, D.P. Debecker, E.M. Gaigneaux, Flame-made vs. wet-impregnated vanadia/titania in the total oxidation of chlorobenzene: Possible role of VOx species, Catalysis Today, 157 (2010) 198-203.

[64] F. Hoxha, E. Schmidt, T. Mallat, B. Schimmoeller, S.E. Pratsinis, A. Baiker, Hydrogenation of acetophenone derivatives: Tuning the enantioselectivity via the metal–support interaction, Journal of Catalysis, 278 (2011) 94-101.

[65] D. Channei, B. Inceesungvorn, N. Wetchakun, S. Phanichphant, A. Nakaruk, P. Koshy, C.C. Sorrell, Photocatalytic activity under visible light of Fe-doped CeO2 nanoparticles synthesized by flame spray pyrolysis, Ceramics International, 39 (2013) 3129-3134.

[66] C.-Y. Chiang, K. Aroh, N. Franson, V.R. Satsangi, S. Dass, S. Ehrman, Copper oxide nanoparticle made by flame spray pyrolysis for photoelectrochemical water splitting – Part II. Photoelectrochemical study, International Journal of Hydrogen Energy, 36 (2011) 15519-15526.

[67] M. Piacentini, R. Strobel, M. Maciejewski, S.E. Pratsinis, A. Baiker, Flame-made Pt–Ba/Al2O3 catalysts: Structural properties and behavior in lean-NOx storage-reduction, Journal of Catalysis, 243 (2006) 43-56.

[68] S. Hannemann, J.-D. Grunwaldt, P. Lienemann, D. Günther, F. Krumeich, S.E. Pratsinis, A. Baiker, Combination of flame synthesis and high-throughput

experimentation: The preparation of alumina-supported noble metal particles and their application in the partial oxidation of methane, Applied Catalysis A: General, 316 (2007) 226-239.

[69] J. Huang, Y. Jiang, N. van Vegten, M. Hunger, A. Baiker, Tuning the support acidity of flame-made Pd/SiO2–Al2O3 catalysts for chemoselective hydrogenation, Journal of Catalysis, 281 (2011) 352-360.

[70] B. Schimmoeller, Y. Jiang, S.E. Pratsinis, A. Baiker, Structure of flame-made vanadia/silica and catalytic behavior in the oxidative dehydrogenation of propane, Journal of Catalysis, 274 (2010) 64-75.

[71] P. Weerachawanasak, P. Praserthdam, M. Arai, J. Panpranot, A comparative study of strong metal–support interaction and catalytic behavior of Pd catalysts supported on micron- and nano-sized TiO2 in liquid-phase selective hydrogenation of phenylacetylene, Journal of Molecular Catalysis A: Chemical, 279 (2008) 133-139.

[72] H. Zhang, J.F. Banfield, Phase transformation of nanocrystalline anatase-to-rutile via combined interface and surface nucleation, Journal of Materials Research, 15 (2000) 437-448.

[73] Z. Rui, S. Wu, C. Peng, H. Ji, Comparison of TiO2 Degussa P25 with anatase and rutile crystalline phases for methane combustion, Chemical Engineering Journal, 243 (2014) 254-264.

[74] P. Claus, S. Schimpf, R. Schödel, P. Kraak, W. Mörke, D. Hönicke, Hydrogenation of crotonaldehyde on Pt/TiO2 catalysts: Influence of the phase composition of titania on activity and intramolecular selectivity, Applied Catalysis A: General, 165 (1997) 429-441.

[75] F.Z. Haber, Elektrochem, 22 (1898) 506.

[76] U. Holzwarth, N. Gibson, The Scherrer equation versus the 'Debye-Scherrer equation', Nat Nano, 6 (2011) 534-534.

[77] R.A. Spurr, H. Myers, Quantitative Analysis of Anatase-Rutile Mixtures with an X-Ray Diffractometer, Analytical Chemistry, 29 (1957) 760-762.

[78] V. Papaefthimiou, T. Dintzer, V.r. Dupuis, A. Tamion, F. Tournus, D. Teschner, M. Havecker, A. Knop-Gericke, R. Schlogl, S. Zafeiratos, When a Metastable Oxide

Stabilizes at the Nanoscale: Wurtzite CoO Formation upon Dealloying of PtCo Nanoparticles, The Journal of Physical Chemistry Letters, 2 (2011) 900-904.
[79] S. Zafeiratos, F. Paloukis, G. Papakonstantinou, D. Teschner, M. Hävecker, E. Vass, P. Schnörch, A. Knop-Gericke, R. Schlögl, B. Moreno, E. Chinarro, J.R. Jurado, S.G. Neophytides, A comparative in situ XPS study of PtRuCo catalyst in methanol steam reforming and water gas shift reactions, Catalysis Today, 157 (2010) 250-256.
[80] G. Richner, J.A. van Bokhoven, Y.-M. Neuhold, M. Makosch, K. Hungerbuhler, In situ infrared monitoring of the solid/liquid catalyst interface during the three-phase hydrogenation of nitrobenzene over nanosized Au on TiO2, Physical Chemistry Chemical Physics, 13 (2011) 12463-12471.
[81] G. Lu, T. Hoffer, L. Guczi, Reducibility and CO hydrogenation over Pt and Pt-Co bimetallic catalysts encaged in NaY-zeolite, Catalysis Letters, 14 (1992) 207-220.
[82] Z. Rong, Z. Sun, Y. Wang, J. Lv, Y. Wang, Selective Hydrogenation of Cinnamaldehyde to Cinnamyl Alcohol over Graphene Supported Pt–Co Bimetallic Catalysts, Catalysis Letters, 144 (2014) 980-986.
[83] K.C. Petallidou, K. Polychronopoulou, S. Boghosian, S. Garcia-Rodriguez, A.M. Efstathiou, Water–Gas Shift Reaction on Pt/Ce1–xTixO2–δ: The Effect of Ce/Ti Ratio, The Journal of Physical Chemistry C, 117 (2013) 25467-25477.

APPENDIX

Appendix A

Calculation for catalyst preparation

Table A.1 Chemicals Properties

Metal or Metal oxide	MW of metal	Metal Precursor	MW of Metal Precursor	Density (g/cm^3)	Metal content (%)
Pt	58.93	Platinum(II) acetyl-acetonate 99.99%	195.23	0.92	0.3
Al_2O_3	123.22	Aluminium-tri-sec-butoxide 97%	101.96	1.05	99.79

Calculation of catalyst

Preparation of catalysts is shown as follows:

Reagent: 0.3 wt% Pt of Platinum(II)acetyl-acetonate 99.99%

Support: Al_2O_3

Example Calculation for the preparation of Pt/Al_2O_3 catalyst with Platinum(II)acetyl-acetonate 99.99% as Pt precursor (Pt/Al_2O_3)

Based on 500 ml total solution

Calculation for Pt (mol) : $\frac{[0.3gPt]\times 1molPt}{195.23Pt} = 1.5366\times 10^{-3} molPt$ - (1)

Calculation for Al (mol) : $\frac{[99.79gAl_2O_3\times 1molAl_2O_3]\times 2molAl}{101.96gAl_2O_3\times 1molAl_2O_3} = 1.9557molAl$ - (2)

Where, $\frac{molPt}{molAl} = \frac{(1)}{(2)} = \frac{1.5366\times 10^{-3}}{1.9557} = 7.8570\times 10^{-3}$

Thus, mol metal = 1 + (7.8570×10^{-3}) = 1.0007857 mol

Calculation for Pt precursor :

$$\frac{[1.1776\times 10^{-4} molPt]\times[1molPt(precursor)]\times[393.299Pt(precursor)]}{[1molPt]\times[1molPt(precursor)]\times[0.9999]}$$
$$= 0.046318gPt(precursor)$$

Calculation for Al precursor :

$$\frac{[0.1499molAl]\times[1molAl(precursor)]\times[246.33gAl(precursor)]}{[1molAl]\times[1molAl(precursor)]\times[0.97]}$$
$$= 38.06gAl(precursor)$$

Appendix B

Calculation of crystallite size

Calculation of the crystallite size by Debye-Scherrer equation

The crystallite size was calculated from the half-height width of the diffraction peak of XRD pattern using the Debye-Scherrer equation.

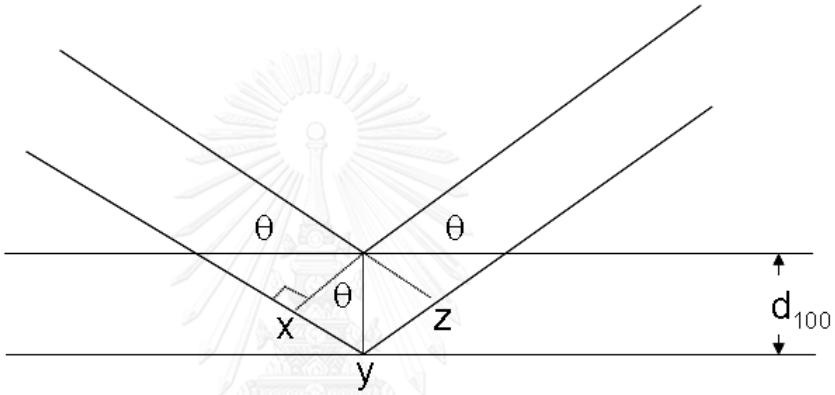

Figure B.1 Derivation of Bragg's Law for X-ray diffraction

$$xy = yz = d\sin\theta$$

Thus

$$xyz = 2d\sin\theta$$

But

$$xyz = n\lambda$$

$$2d\sin e\theta = n\lambda$$

Therefore $2d\sin\theta = n\lambda$ *Bragg's Law*

$$d = \frac{n\lambda}{2sin\theta}$$

The Bragg's Law was derive to C.1

From Scherrer equation:

$$D = \frac{K\lambda}{\beta cos\theta}$$

Where D = Crystallite size, Å, *K* = Crystallite-shape factor = 0.9

λ = X-ray wavelength, 1.5418 Å for Cu$K\alpha$

θ = Observed peak angle, degree

β = X-ray diffraction broadening, radian

The X-ray diffraction broadening (β) is the pure width of powder diffraction free from all broadening due to the experimental equipment. α-Alumina is used as a standard sample to observe the instrumental broadening since its crystallite size is larger than 2000 Å. The X-ray diffraction broadening (β) can be obtained by using Warren's formula.

From Warren's formula:

$$\beta = \sqrt{B_M^2 - B_S^2}$$

Where B_M = The measured peak width in radians at half peak height.

B_S = The corresponding width of the standard material.

Calculation of phase composition

Phase composition of all catalysts was calculated from:

Weight of anatase as function of

$$\mathbf{f} = \frac{\mathbf{1}}{\mathbf{1 + 1.26}\frac{\boldsymbol{Ir}}{\boldsymbol{Ia}}}$$

Where Ir = Intensity of rutile TiO_2 phase

Ia = Intensity of anatase TiO_2 phase

Appendix C

Calculation for catalytic performance

Calculation of NS conversion and selectivity of the catalyst are shown in this section. We use decane as a standard for calibration in reactant and product in hydrogenation of 3- nitrostyrene and plot the molar ratio vs. area ratio and then the relation of decane and the obtained-product were written in the equation for calculation the catalytic performance. The calibrations are exhibited below

Calibration of 3-nitrostyrene

NS								Date	110127
Decane			Substrate			Decane	NS	area ratio	moler ratio
[ml]	[g]	[mmol]	[ml]	[g]	[mmol]	2.8	11.9		
0.2	0.1446	1.006	0.2	0.2675	1.722	3523	5496	1.560	1.711
0.2	0.1446	1.006	0.2	0.2675	1.722	3475	7508	2.161	1.711
0.2	0.1446	1.006	0.2	0.2675	1.722	5014	8601	1.715	1.711
0.2	0.1446	1.006	0.2	0.2675	1.722	5082	8214	1.616	1.711
0.2	0.1446	1.006	0.2	0.2675	1.722	5401	8931	1.654	1.711
0.2	0.1445	1.005	0.4	0.4878	3.140	4714	13825	2.933	3.123
0.2	0.1445	1.005	0.4	0.4878	3.140	5045	14761	2.926	3.123
0.2	0.1445	1.005	0.4	0.4878	3.140	4738	12354	2.607	3.123
0.2	0.1445	1.005	0.4	0.4878	3.140	4530	14459	3.192	3.123
0.2	0.1445	1.005	0.4	0.4878	3.140	4527	13929	3.077	3.123
0.2	0.1445	1.005	0.4	0.4878	3.140	5334	16080	3.015	3.123

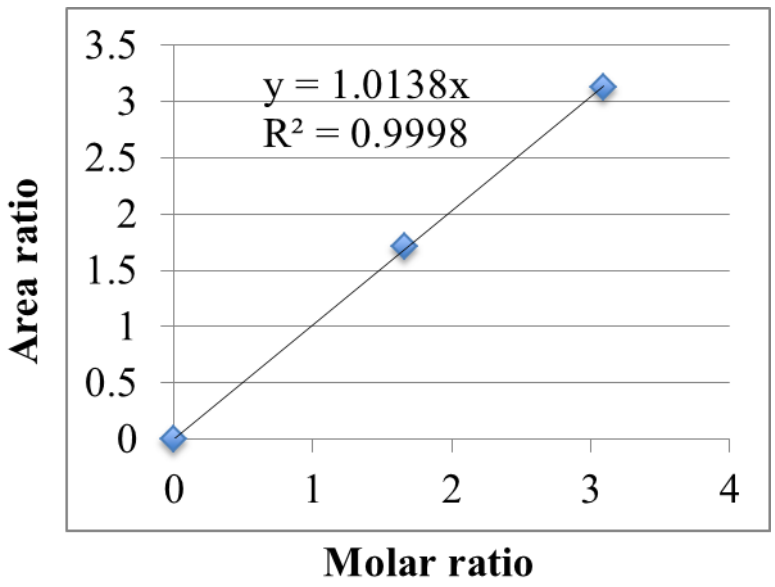

From this data we get the relation of decane and 3-nitrostyrene as:

$$\text{Mole ratio of } \left(\frac{\text{NS}}{\text{De}}\right) = 1.0138 \times \text{ Area ratio of } \left(\frac{\text{NS}}{\text{De}}\right)$$

$$\text{Mole NS } = \left(\frac{Mole_{De}}{Area_{De}}\right) 1.0138 \times \text{Area NS} \quad (1)$$

Calibration of Vinylaniline

VA								Date	110127
Decane			Substrate			Decane	VA	area ratio	moler ratio
[ml]	[g]	[mmol]	[ml]	[g]	[mmol]	2.8	8.7		
0.2	0.1472	1.024	0.2	0.2318	1.887	4966	8172	1.646	1.842
0.2	0.1472	1.024	0.2	0.2318	1.887	4792	8638	1.803	1.842
0.2	0.1472	1.024	0.2	0.2318	1.887	5214	8327	1.597	1.842
0.2	0.1472	1.024	0.2	0.2318	1.887	5516	8920	1.617	1.842
0.2	0.1472	1.024	0.2	0.2318	1.887	5115	9286	1.815	1.842
0.2	0.1472	1.024	0.2	0.2318	1.887	4922	9048	1.838	1.842
0.2	0.1445	1.005	0.4	0.4369	3.556	4714	14646	3.107	3.537
0.2	0.1445	1.005	0.4	0.4369	3.556	5045	15716	3.115	3.537
0.2	0.1445	1.005	0.4	0.4369	3.556	4738	17013	3.591	3.537
0.2	0.1445	1.005	0.4	0.4369	3.556	4530	14904	3.290	3.537
0.2	0.1445	1.005	0.4	0.4369	3.556	4527	14527	3.209	3.537
0.2	0.1445	1.005	0.4	0.4369	3.556	5334	16793	3.148	3.537

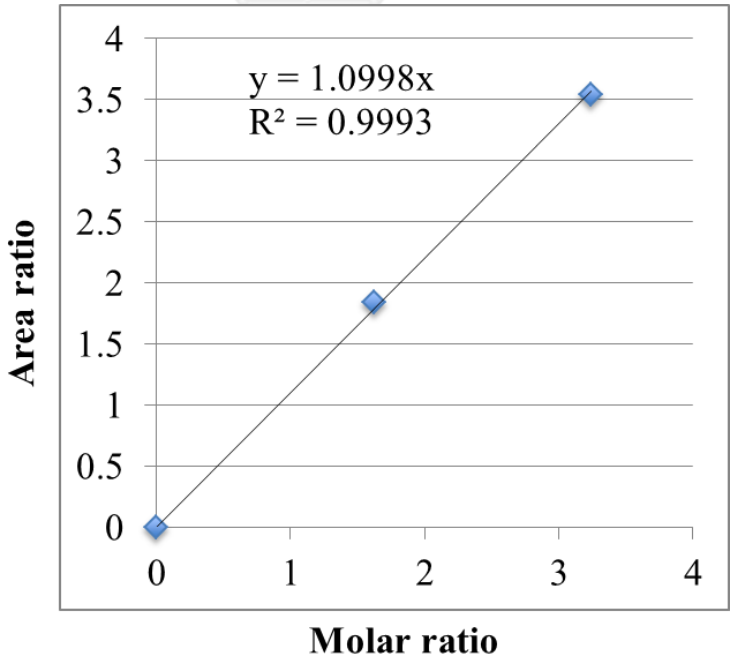

From this data we get the relation of decane and vinylaniline as:

$$\text{Mole ratio of } \left(\frac{\text{VA}}{\text{De}}\right) = 1.099 \times \text{ Area ratio of } \left(\frac{\text{VA}}{\text{De}}\right)$$

$$\text{Mole VA } = \left(\frac{Mole_{De}}{Area_{De}}\right) 1.099 \times \text{Area VA} \quad (2)$$

Calibration of Ethynitrobenzene

ENB								Date	110127
Decane			Substrate			Decane	ENB	area ratio	moler ratio
[ml]	[g]	[mmol]	[ml]	[g]	[mmol]	2.8	10.7		
0.2	0.1472	1.024	0.2	0.2506	1.658	4966	7479	1.506	1.619
0.2	0.1472	1.024	0.2	0.2506	1.658	4792	7955	1.660	1.619
0.2	0.1472	1.024	0.2	0.2506	1.658	5214	7582	1.454	1.619
0.2	0.1472	1.024	0.2	0.2506	1.658	5516	7985	1.448	1.619
0.2	0.1472	1.024	0.2	0.2506	1.658	5115	8456	1.653	1.619
0.2	0.1472	1.024	0.2	0.2506	1.658	4922	8318	1.690	1.619
0.2	0.1445	1.005	0.4	0.4737	3.134	4714	13187	2.797	3.117
0.2	0.1445	1.005	0.4	0.4737	3.134	5045	13554	2.687	3.117
0.2	0.1445	1.005	0.4	0.4737	3.134	4530	13868	3.061	3.117
0.2	0.1445	1.005	0.4	0.4737	3.134	4527	13533	2.989	3.117
0.2	0.1445	1.005	0.4	0.4737	3.134	5334	15016	2.815	3.117

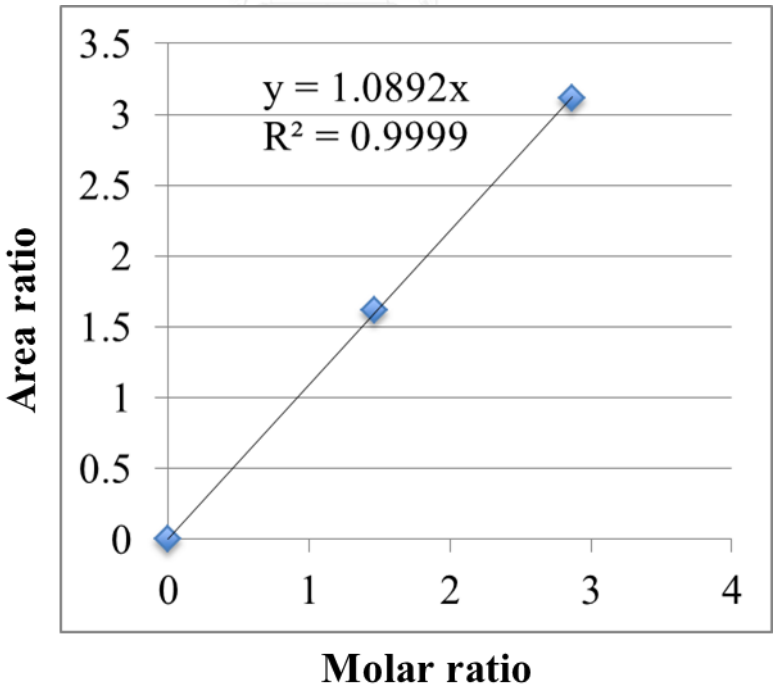

From this data we get the relation of decane and ethynitrobenzene as:

$$\text{Mole ratio of } \left(\frac{\text{ENB}}{\text{De}}\right) = 1.089 \times \text{ Area ratio of } \left(\frac{\text{ENB}}{\text{De}}\right)$$

$$\text{Mole ENB} = \left(\frac{Mole_{De}}{Area_{De}}\right) 1.089 \times \text{Area ENB} \quad (3)$$

Calibration of Ethyanilene

EA								Date	110127
Decane			Substrate			Decane	EA	area ratio	moler ratio
[ml]	[g]	[mmol]	[ml]	[g]	[mmol]	2.8	6.5		
0.2	0.1472	1.024	0.2	0.2192	1.773	4966	7547	1.520	1.731
0.2	0.1472	1.024	0.2	0.2192	1.773	4792	7991	1.668	1.731
0.2	0.1472	1.024	0.2	0.2192	1.773	5214	7694	1.476	1.731
0.2	0.1472	1.024	0.2	0.2192	1.773	5516	8328	1.510	1.731
0.2	0.1472	1.024	0.2	0.2192	1.773	5115	8541	1.670	1.731
0.2	0.1472	1.024	0.2	0.2192	1.773	4922	8253	1.677	1.731
0.2	0.1445	1.005	0.4	0.4148	3.355	4714	13665	2.899	3.336
0.2	0.1445	1.005	0.4	0.4148	3.355	5045	14687	2.911	3.336
0.2	0.1445	1.005	0.4	0.4148	3.355	4738	15642	3.301	3.336
0.2	0.1445	1.005	0.4	0.4148	3.355	4530	13764	3.038	3.336
0.2	0.1445	1.005	0.4	0.4148	3.355	4527	13459	2.973	3.336
0.2	0.1445	1.005	0.4	0.4148	3.355	5334	15664	2.937	3.336

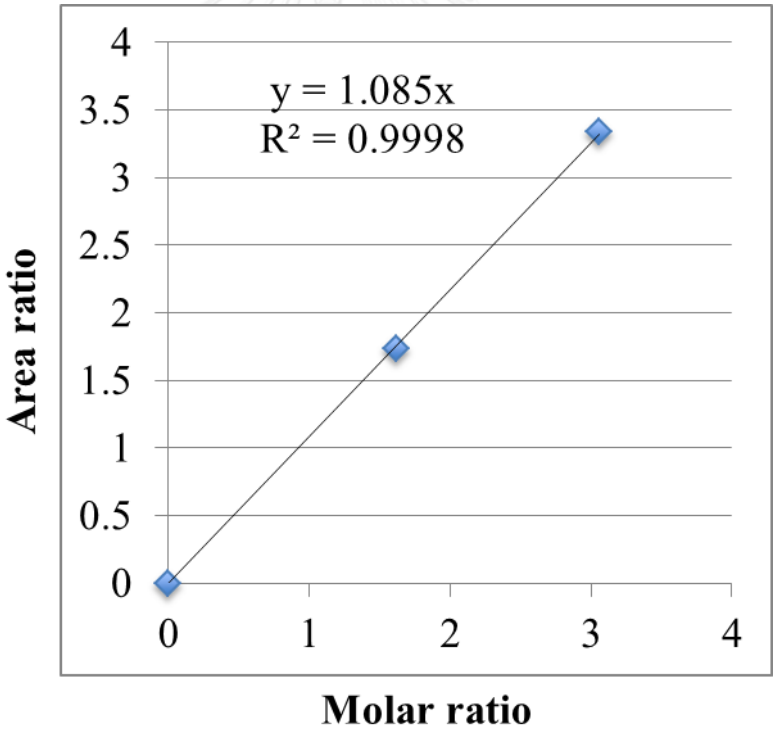

From this data we get the relation of decane and ethyaniline as:

$$\text{Mole ratio of } \left(\frac{\text{EA}}{\text{De}}\right) = 1.085 \times \text{ Area ratio of } \left(\frac{EA}{\text{De}}\right)$$

$$\text{Mole EA} = \left(\frac{Mole_{De}}{Area_{De}}\right) 1.085 \times \text{Area EA} \quad (4)$$

Calculation of mass balance

Mole balance:

$$\text{Mole}_{\text{in}} = \text{Mole}_{\text{out}}$$

$$1 = \frac{\text{Mole}_{\text{in}}}{\text{Mole}_{\text{out}}}$$

$$1 = \frac{\text{Mole}_{\text{NS}}}{\text{Mole}_{\text{NS}} + \text{Mole}_{\text{VA}} + \text{Mole}_{\text{ENB}} + \text{Mole}_{\text{EA}}}$$

Insert the equation (1), (2), (3) and (4) then,

$$1 = \left(\frac{\text{Mole}_{\text{De}}}{\text{Area}_{\text{De}}}\right)(1.0138 \times \text{Area}_{\text{NS}} + 1.099 \times \text{Area}_{\text{VA}} + 1.089 \times \text{Area}_{\text{ENB}} + 1.085 \times \text{Area}_{\text{EA}})$$

Calculation of NS conversion

$$\%\ \text{NS Conversion} = \frac{\text{Mole}_{\text{in}} - \text{Mole}_{out}}{\text{Mole}_{\text{in}}} \times 100$$

$$\%\text{NS Conversion} = \frac{\text{Mole NS}_{\text{in}} - \text{Mole NS}_{out}}{\text{Mole NS}_{\text{in}}} \times 100$$

Calculation of VA selectivity

$$\%\ \text{Selectivity of VA} = \frac{\text{VA product}}{\text{Mole of all products}} \times 100$$

$$\%\text{Selectivity of VA} = \frac{\text{Mole VA}}{\text{Mole VA} + \text{Mole ENB} + \text{Mole EA}} \times 100$$

Calculation of TOF

$$\text{TOF} = \frac{\text{Rate of reaction}}{\text{Active sites}}$$

$$\text{TOF} = \frac{\text{Mole NS}_{\text{in}} \times \text{NS Conversion/time} \times \text{g. catalyst}}{\text{Active sites/g. catalyst}}$$

Appendix D

Calculation for total CO chemisorption and dispersion

Calculation of the CO chemisorption a metal dispersion of the catalyst, a stoichiometry of CO:Pt = 1 is assumed. The calculation procedure is as follows:

Let the weight of catalyst used = W g

Integral area of CO peak after adsorption = A unit

Integral area of 50 μl of standard CO peak = B unit

Amounts of CO adsorbed on catalyst = B-A unit

Concentration of Pt = 0.5 wt%

Volume of CO adsorbed on catalyst = $\frac{B-A}{B} \times 50\ \mu l$

Volume of 1 mol of Pt at 25 ^{o}C = 24.46 l

Mole of CO adsorbed on catalyst = $\frac{\frac{B-A}{B}\times 50}{24.46}\ \mu mol$

Total CO chemisorption = $\frac{\frac{B-A}{B}\times 50}{24.46} \times \frac{1}{W}\ \mu mol/g.$

= N μmol/g catalyst

Pt dispersion calculation:

$$\%D = \frac{\text{Amount of Pt equivalent to CO adsorption on catalyst after reduction}}{\text{Total amount of Pt active sites expected after reduction}} \times 100$$

Molecular weight of Pt = 195.078 g/mol

$$\text{Metal dispersion} = \frac{CO_{total} \times 100}{\text{No. } \mu\text{mol}Pt_{total}}$$

$$\text{Metal dispersion} = \frac{N \times 100}{\text{No. } \mu\text{mol}Pt_{total}}$$

$$\text{Metal dispersion} = \frac{N \times 100}{(\%\text{reducibility}/100) \times 0.005 \times (W/195.078) \times 10^6}$$

$$\text{Metal dispersion} = \frac{N \times 3.90}{(\%\text{reducibility}) \times W}$$